FINITE ELEMENT ANALYSIS OF POST-TENSIONED CONCRETE WIND TURBINE TOWERS

A THESIS
SUBMITTED TO THE FACULTY OF THE
UNIVERSITY OF MINNESOTA
BY

JOSHUA STEPHEN TOMCZAK

IN PARTIAL FULFILLMENT OF THE REQUIREMENTS
FOR THE DEGREE OF
MASTER OF SCIENCE

DR. ANDREA SCHOKKER

AUGUST 2021

Acknowledgements

I would like to open this thesis by thanking my advisor Dr. Andrea Schokker for giving me the opportunity to work on this research project and for all the advice and guidance throughout. I would like to thank members of my committee, Dr. Brock Hedegaard and Dr. Micheal Greminger for reviewing and improving my work. Not to mention all the ANSYS troubleshooting!

I would like to thank the University of Minnesota Grant in Aid program for funding this research. I would also like to thank all of those before me for putting out research on wind turbine towers.

Dedication

This thesis is dedicated to my supportive family, who encouraged me to go into Civil Engineering.

Abstract

Wind turbines have seen a global increase in production by countries and energy developers trying to achieve renewable energy goals. Market demands have resulted in the development of larger turbines to produce more energy. Energy developers have been able to increase the energy production with two approaches. 1) Increasing the turbine blade length, which captures more wind, and 2) increasing the tower height which places the turbine blades higher into the atmosphere where there is stronger, more consistent wind.

Wind turbines have been predominantly constructed with steel towers, which have been optimized to provide the most energy for the lowest possible cost. However, increasing the loading and height will require a larger turbine support structure. The current method of erecting a steel turbine tower is to fabricate the tower off-site and ship the pieces to the job site for assembly. With an increase in tower size to accommodate taller turbine towers, some tower sections may need to be split in half to meet shipping regulations. With the increase in tower height there is an increased difficulty in field fabrication and shipping, increasing the overall cost of the turbine tower. At around a tower height of 80 m (263 ft), concrete turbine towers start to become cost competitive with steel turbine towers [7].

The objective of this research is to analyze three post-tensioned concrete wind turbine towers in ANSYS to evaluate feasibility for use in towers above 100m. The towers evaluated will be 100 m (328 ft), 150 m (492 ft) and 200 m (656 ft) in height. Tower loading, geometry and material properties were obtained from a study published by NREL. The results of this study are meant to provide a basis for future wind turbine analysis in ANSYS of post-tensioned towers with specific design parameters.

Table of Contents

List of Tables

List of Figures

1.0 Introduction and Background

Wind energy is the second largest renewable energy source, after hydropower, and has been growing exponentially over the last decade [31]. The Global Wind Energy Council predicts that by 2035, renewable energy will generate more than 25% of the world's electricity needs, with a quarter of it coming from wind energy [10]. The worldwide movement to generate large amounts of electricity with wind turbines has led to a significant increase in the generating capacity of wind turbines [31].

The wind energy industry generation is expected to continue to grow with countries around the world working towards 100% renewable energy goals. In the United States, since 2000, wind energy production has increased from 40,000 MW to 432,419 MW in 2015 [18]. Another example is South Africa as they have devised a plan to add 9000 MW of wind energy capacity by 2030 [31]. Multiple European countries have made significant progress towards producing renewable and clean energy. The wind energy market is a growing industry around the world because of the global interest in renewable energy. The wind energy market has shown little sign of slowing down and will continue to grow as energy production becomes more economical; and as countries continue to push towards renewable energy goals.

Wind turbine components are categorized into the following: hub, nacelle, turbine blades, support tower and foundation, as can be seen below in Figure 1.1. The hub connects the turbine blades to the nacelle. The generators, drive train and the control system are housed within the nacelle, and this is where the energy is generated. Wind turbines use the force of the wind to spin the turbine blades to produce energy. The turbine tower supports the turbine assembly and nacelle. Turbine towers have been traditionally made of steel. The scope of this research is focused on structural considerations; specifically, the tower portion of the wind turbine system.

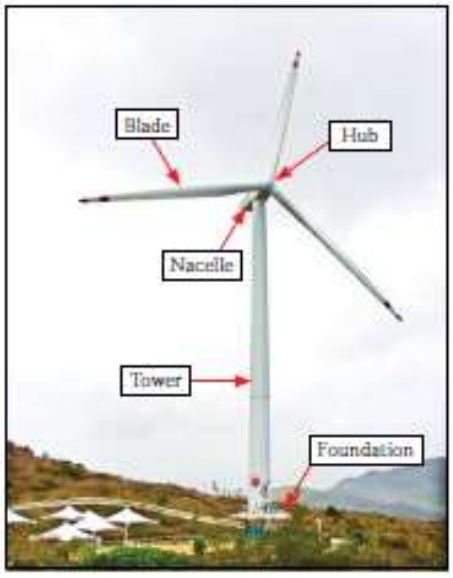

Figure 0.1 Components of a Windmill Tower [31].

Historically, wind turbine research has been focused primarily on the development of composite materials for the turbine blades. Turbine blades have become lighter and longer, contributing to an increase in the wind turbine power output. Research and development of tower materials have been less common with tubular steel sections being the most prevalent material used in industry. The use of post-tensioned concrete in wind turbine towers has gained some traction in European markets [7] because of distinct advantages of a concrete tower in comparison to a steel tower, particularly at greater tower heights. These advantages will be discussed in more detail later in this Chapter.

Wind turbines are operational for their intended service life, around 20 to 30 years. At the end of the turbines service life the original structural components of the turbine are usually not able to support the weight of the more modern turbine components during an upgrade. Similar to planning for future traffic lanes in a bridge to extend service life, designing the tower and foundation of a wind turbine for future loads would be beneficial for developers to future-proof concrete towers with a larger wall thickness and additional post-tensioning ducts, so that the concrete towers may allow for the installation of the next generation of wind turbines onto the existing towers [7].

Energy developers have been able to increase wind capacity by using two methods: 1) increasing the turbine blade length, which captures more wind; and 2) increasing the tower height, which places the turbine blades higher into the atmosphere where wind is stronger and more consistent [7, 14, 18, 27, 31]. Figure 1.2 shows that over time windmills have increased in height and rotor diameter. Wind resource maps produced by NREL (National Renewable Energy Laboratory) show the wind speed at an elevation above surface level and can be a good resource for those looking for areas to add wind energy. Wind resource maps can be seen in Figures 1.4 and 1.5, the average wind speeds at 200 m (656 ft) above surface level are almost two times the wind speed at 100 m (328 ft) above surface level. To reach the larger wind resource, wind turbine tower heights have increased from an average of 55 m in 1999 to 85 m in 2014 as shown in Figure 1.6 [24]. In 2019, the average turbine tower height in the United States was reported to be 142 m (466 ft) tall, shown in Figure 1.6. This average will keep increasing with innovations in materials and design [22]. To provide a sense of scale, Figure 1.3 shows a comparison between modern structures and various wind turbine heights. Currently, the world's most powerful offshore wind turbine is GE's Haliade-X, with a 220 m (722 ft) diameter rotor and a 248 m (853 ft) hub height [28].

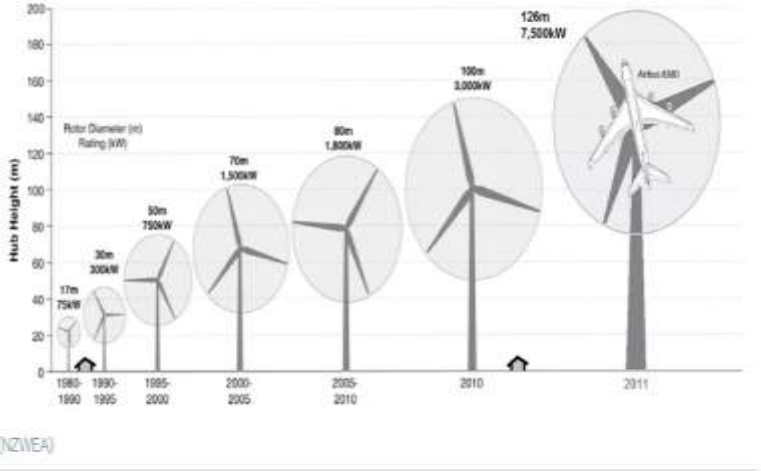

Figure 1.2. Hub heights over time [28].

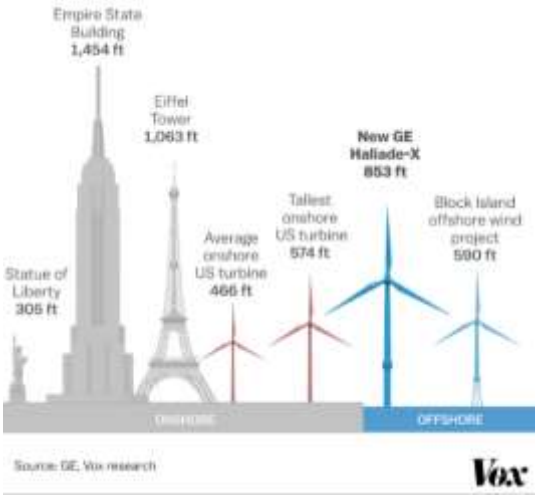

Figure 1.3. Average Wind turbine height [28].

Figure 1.4. Average wind speed 100m (328ft) above surface level [24].

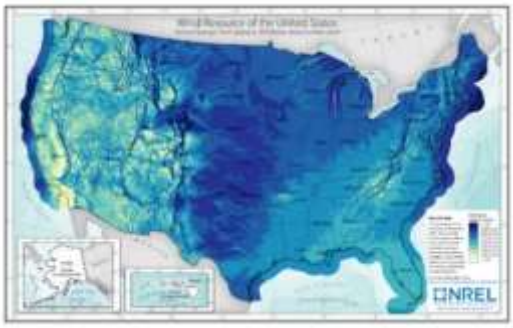

Figure 1.5. Average wind speed 200m (656ft) above surface level [30].

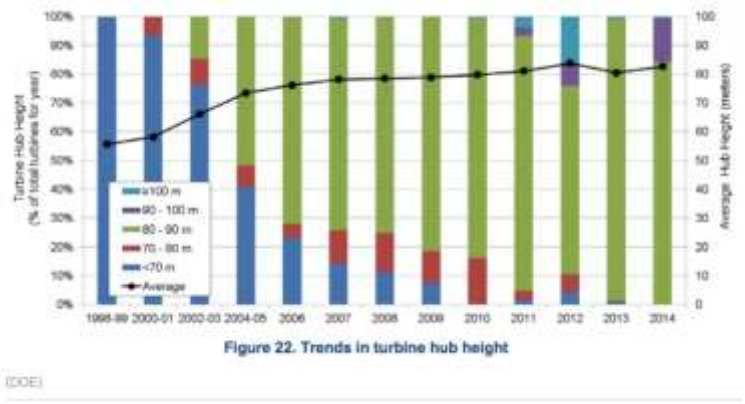

Figure 1.6. Trends in turbine height [28].

Increasing tower heights is especially interesting in areas of low wind potential at standard turbine tower heights. States that have higher wind speeds like the plain's states of Iowa, Minnesota, North Dakota, South Dakota, Kansas, Colorado, Texas, Oklahoma, and Colorado, have been able to install wind capacity at lower hub heights due to the abundant wind supply. These states have been leaders in installed wind power. States that have lower wind speeds, such as states in the south-eastern United States, would need to construct taller towers and harness the winds that are higher off the ground to produce wind energy. Increasing turbine tower heights will allow areas that have little wind potential to install wind turbines and produce renewable energy. Using taller towers in the southeast United States or other moderate wind areas significantly increases the capacity potential for wind energy, particularly for 1-2.5 MW towers [7].

Modern wind turbines require higher and more robust support structures to support longer turbine blade lengths (increased turbine diameters), where higher and more consistent wind speeds are used to produce more energy [14, 31]. Tubular steel tower construction cost increases exponentially as tower height increases due to additional material requirements, logistics and other complexities. These variables are the major contributing factors to challenges such as the stiffness controlling design [18]. For the previously stated reasons, concrete towers have been shown to start to become an economical solution at approximately 80 m [18].

Concrete is a material that can be sourced locally in most areas, reducing the need for shipping large tower components over long distances. If the tower is made of precast segments at a casting yard on site or near the site, shipping costs will drastically decrease the cost of the tower. Concrete also has the following material advantages over steel towers: inherent stiffness, no local buckling issues, and better fatigue resistance. To maximize design and construction efficiency for tall towers, prestressed concrete becomes the optimal solution. Because of limitations with individual pretensioned concrete sections, post-tensioning provides the more feasible option. In fact, tall post-tensioned piers for bridges have been successfully used for decades. A post-tensioned concrete tower has better fatigue properties than steel and does not have the local buckling issues of tubular steel sections [18]. Material costs for concrete for a 100 m (328 ft) tower is less than that of an identical steel tower [7].

1.1 Project Objective

The objective of this project is to evaluate the feasibility of using post-tensioned (PT) concrete in wind turbine towers with heights more than 100 meters (328 feet). This will be achieved by using a Finite Element Analysis (FEA) software, ANSYS, to evaluate PT towers of varying heights to determine stress levels, required amount of post-tensioning and section sizes. This work forms the basis of initial design of PT towers over 100m.

The following tasks are included:

- Model a baseline steel tower using ANSYS to validate model parameters. The baseline steel tower used matches the geometry and loading obtained from Wang et. al. [37].
- Model concrete towers at heights of 100 m, 150 m and 200 m using ANSYS. Tower geometries, wall thickness, and tower loading is similar to concrete towers obtained from LaNier [18].

2.0 Literature Review

2.1 Post-Tensioned Towers

Toronto's CN Tower (Fig. 2.1) at 553 m (1815 ft) is one of the tallest free-standing structures ever built [17]. The structure was originally built in 1975 as a communications and observation tower. An interesting feature of this tower is that it was constructed of a prestressed concrete shaft that was slip formed [17]. The tower was designed to be fully post tensioned, with no tensile stress under the expected 50-year maximum wind effects. Post-tensioned concrete has historically existed in towers of great heights as well as in bridge piers; for example, the sunshine skyway bridge (Fig. 2.2) was built in 1982 with a height of 122+ m (400+ ft) [33]. Applying this mature technology to wind turbine towers is of great interest and would result in a more economically feasible and durable solution.

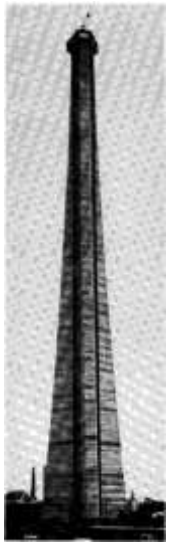

Figure 2.1 Slip forming CN Tower [17].

Figure 2.2. Sunshine Skyway Bridge [33].

2.2 Wind Turbine Tower Trends

As tower heights begin to reach over approximately 90 m (295 ft), concrete towers become more attractive as a way to improve tower dynamic properties and ease transportation difficulties associated with steel towers [15]. Steel towers are limited to a height of approximately 80-90 m (263-295 ft) before becoming uneconomical due to the transportation difficulties by larger tower diameters [30, 31]. Modern turbine tower

construction has implemented the use of concrete or hybrid concrete/steel towers that has allowed towers to reach hub heights of 120 m (394 ft) or more [24]. The materials used in the tower have become a popular topic for research in recent years to optimize cost, dynamic response, and service life. Wind turbines in the 5-10 MW range use 100 m (325 ft) or larger rotor diameters [7]. At this height, steel is no longer economically feasible due to its larger required diameter and the logistic problems that arise as a result. With a hub height of 125 m (410 ft), it's possible to save up to 30% on tower costs when using concrete compared to steel [7]. The economics of the project will be affected by the concrete tower type and the crane capacity needed [7].

Concrete towers are used more commonly in Europe, while not many have been used in North America [7]. The American Concrete Institute (ACI) cites the reasons for this are likely misunderstanding the length of time to construct concrete towers, lack of familiarity with fatigue properties of concrete, lack of industry standards for concrete tower designs and the lack of historical cost data of concrete towers [7]. Concrete has been a competitive material for designing towers, tall chimneys, poles and bridge piers as construction methods have improved [22]. Concrete allows for more flexibility in construction, design, fabrication/prefabrication process, and transportation logistics (the precast plant can be set up on-site to avoid any transportation of tower segments) [22]. An additional benefit of using concrete is that it is a more globally available product and has relatively stable worldwide prices as opposed to steel [5]. As the industry continues to grow and towers increase height, post-tensioned concrete can provide a solution to issues such as transportation and the dynamic response of the tower when the wind turbine is in operation.

As mentioned, previously, an increase in tower size will require larger tower bases which creates problems with transportation of components that are fabricated off site (such as steel or composites). Complete tubular tower sections can be transported up to 4.5 m (15 ft) in diameter on most highway systems [5, 22, 31]. For towers greater than 80-90 m (263-295 ft), the base diameter will likely exceed shipping limits. Shipping regulations

constrain how large a single shell unit can be made, as can be seen in Figure 2.3. The optimum size of the tower cross section will be governed by shipping size limits for steel. The real economic benefits for concrete towers come as shipping limits are reached on the steel shell since shell components would need to be broken down into pieces smaller than the full tower diameter, triggering further design and construction complications.

As tower height increases, the effect of stiffness on deflections and dynamic response becomes the primary design limitation. As the demands for tower heights increase, towers need to be sufficiently strong and stiff which leads to higher construction costs for towers made of steel [22]. Hollow steel sections have low stiffness and natural frequency values [15], making them less than ideal for tall towers. For use in turbine towers, concrete has better dynamic properties of stiffness and natural frequency [15, 22] in comparison to steel. When tower heights reach above 100 m (328 ft), it is even more important to design the tower stiffness to carefully avoid excitation and damage from resonant oscillations due to wind, earthquakes and turbine operations [14].

In recent years the industry has also developed a concept using both steel and concrete in wind turbine towers, Figure 2.3. These hybrid towers that are composed with a concrete tower base with an upper steel section are typically designed to optimize economics of the steel tower for off-site fabrication and on-site erection [7].

Figure 2.3. Optimal tower size vs. transportable tower size [28].

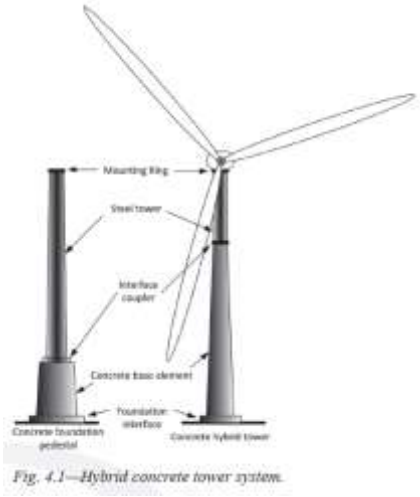

Figure 2.4. Hybrid concrete tower [31].

2.2.1 Concrete Wind Turbine Tower Geometry

As mentioned previously, China and several European countries have started to use concrete wind turbine towers as an alternative to steel more frequently [7]. Concrete towers are not used as widely in North America because of perceived limitations. This includes the lack of understanding construction time of concrete towers, familiarity with fatigue properties of concrete, industry standards for concrete tower design and historical cost data [7]. Post-tensioning tends to be a specialized type of design and construction with multi-strand tendon units most commonly used in bridge design. Without code details, design examples, or industry data, designers are less likely to choose post-tensioning due to risk associated with the unknown despite the potential advantages. The work in this thesis provides a first step by presenting the advantages in the behavior of post-tensioned towers and the feasibility of design as related to known design and construction practices for bridge piers.

Research has spurred different cross section layouts and designs for turbine towers. Concrete towers can either be full height concrete or used as a pedestal for a steel tower, acting in a hybrid capacity. The cross sections for concrete towers are usually circular or octagonal, as seen in Figures 2.5 and 2.6. The design of the concrete tower can also vary

based on the construction method. The construction method will be described in more depth in section 2.2.2.

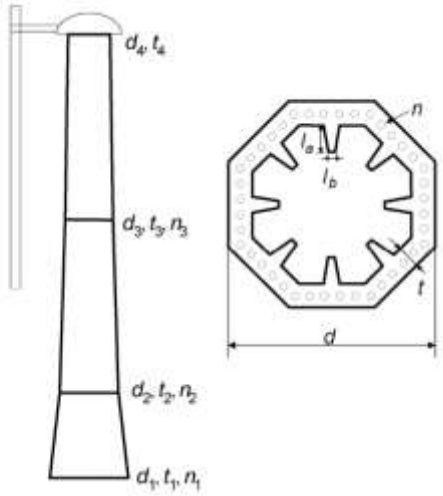

Figure 2.5. Concrete Tower design [22].

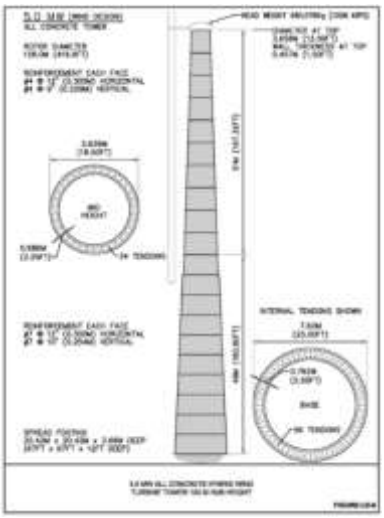

Figure 2.6. Tapered Concrete Tower [18].

Tapered cross sections have been implemented in both full-height concrete towers and steel towers. Tapering the tower cross section is useful to decrease weight or strength as loads decrease [22, 31]. The bending moment and shear forces are maximum at the base of the tower, requiring a larger cross section at the base in comparison to the top of the tower [26]. A full height concrete tower of 100-150 m (328-492 ft) will typically require a base diameter between 8-10 m (28-33 ft) [7]. The turbine tower base dimension can affect the segmentation, transportation, and assembly costs in the tower portions of the tower [7].

Similar considerations are needed for hybrid towers which utilize both concrete and steel in the turbine support structure. Concrete is used for the base (forming a pedestal for the steel tower to sit on), while the upper portion of the tower is steel. The height of concrete and height of steel segments varies based on optimizing tower economics and dynamic response. Example hybrid towers are shown in Figures 2.7-8. As shown below, a

hexagonal section of concrete (in this case, a patented system called Hexcrete) is used as a tower base for the first 31 m, where the steel tower is placed on top of the concrete.

Figure 2.7. MidAmerican hybrid tower [28].

Figure 2.8. Tindall Titan hybrid tower (Hexcrete) [26].

While concrete towers have been more widely used in Europe and China, there have been prototypes constructed in the U.S. In 2016, MidAmerican Energy installed a 116 m (379 ft), 2.4MW concrete wind turbine in Adams County, Iowa. Measuring to the blade tips, the turbine reaches to 170 m (557 ft). This concrete tower was constructed of 24 segments [8]. Figure 2.7. shows an image of the completed hybrid concrete wind turbine tower, developed, and constructed by MidAmerican Energy. In another instance, a precast system was used to construct a wind turbine tower to a height of 135 m (440 ft) [7]. This tower was made of 35 precast segments with a base diameter of 14.5 m (48 ft). The base of the tower was made with two segments. The location of this tower was not provided in the reference.

2.2.2 Concrete Wind Tower Construction

ACI committee 378, *Report on Design of Concrete Wind Turbine Towers* presents four types of concrete construction that could be used in different tower situations: precast, cast-in-place, shotcrete and spin-cast concrete [7]. Precast elements can either be made of circular segments or panels as shown in Figure 2.9. Cast in place concrete is placed using either a jump form or a slip form. Jump forms are fastened to the previously cured concrete and can be seen in Figure 2.10. Reinforcing steel is extended from the previously poured segment and the new concrete is placed, this process repeats until the full tower height is reached. Jump form construction is dependent on the strength of the most recently cast concrete. The placement of the next segment is delayed until the previous concrete gains enough strength to support the concrete tower segments above. Standard height for segments is 3-6 m (10-20 ft). Forms can be "jumped" or advanced around once per week depending on the concrete mixture design. In one instance, a 100 m (325 ft) tower was completed with jump forms in 25 days with a daily 13 ft jump [7]. Slip forming has been predominantly used in grain silo construction, as seen in Figure 2.11., and the same technology can be applied to concrete wind turbine towers. Slip forming is a process that involves continuous concrete placement with low slump concrete. Once slip forming starts, the process of placing concrete does not stop until the forms reach the full tower height. Slip forms advance using hydraulic jacks that grip reinforcing steel to gradually move the form upwards as concrete is being placed. Typical casting rates are 178-305 mm/hour, (7-12 in/hr) for a 1.22-1.98 m (4-6.5 ft) tall form [7]. For instance, a 100m tower could be fabricated in 20 days (6.5 ft or 2 m a day) at this rate. Offshore oil platforms, such as the Troll A gas platform, have been constructed using slip forms [7].

(a) Circular elements

(b) Advanced tower systems

Figure 2.9. (a) Precast circular cross section, (b) Precast panel construction [7].

Figure 2.10. Jump forms used in concrete tower construction [7].

Figure 2.11. Slip forms used in grain silo construction [7].

2.3 Design Documents

A uniform standard for the design of concrete wind turbine towers in the U.S is not currently available [5]. However, the industry is pushing to regulate codes jointly by the American Society of Civil Engineers with the American Wind Energy Association (ASCE/AWEA) and ACI. Both have referenced the International Electrotechnical Committee Wind Energy Generation Systems Design requirements (IEC61400-1) for design loads [13]. Throughout the literature review process, it was determined that different sources used different codes to calculate wind loading. The American-based research has used the ASCE 7 and the ACI 307 code (Code Requirements for Reinforced Concrete Chimneys), while the research that focused more on international standards used the IEC 61400-1 [2, 13]. Other research used the OEM (Original Equipment Manufacturer) turbine manufacturer load tables produced in accordance with IEC 61400-1. The large wind turbines available have been reviewed and certified by the international certification body through a series of testing, evaluating, manufacturing quality assurance [3]. When these turbines are brought into the United States, they must also pass the U.S. standards. ASCE, AWEA and ACI have begun to review the international standard (IEC 61400-1) to develop a code for use in the United States market to clarify structural requirements. It should be noted that IEC has published a code for Wind Turbine Tower and Foundation Requirements (IEC 61400-6) [13]. This code was not considered for this research as it was not published at the start of this project. Nonetheless the IEC 61400-6 provides guidance on tower loading and other structural considerations.

2.3.1 IEC61400

Design standard IEC61400 is an international standard published by International Electrotechnical Commission specific to wind turbines. The IEC61400 set of design documents have provisions to ensure wind turbines are designed for safety and serviceability during their design life. The first certification document from IEC was in 1995 with the first standard was published in 2001. The IEC standards are intended for global use and the National Renewable Energy Laboratory (NREL) in the United States

participates in the development of this set of standards. The focus of most of the standards relates to the energy generation components. The updated standard for tower and foundation design was not yet available (originally scheduled for 2020 publication) at the time of writing this thesis.

The full set of IEC61400-Wind Energy Generation Systems [13]-is broken down as follows:

IEC 61400-1, Part 1: Design requirements

IEC 61400-3, Part 3-1: Design requirements for fixed offshore wind turbines

IEC 61400-3, Part 3-2: Design requirements for floating offshore wind turbines

IEC 61400-5, Wind turbine blades

IEC 61400-6, Tower and foundation design requirements

IEC 61400-12-1, Power Performance measurements of electricity producing wind turbines

IEC 61400-12-4, Numerical site calibration for power performance testing of wind turbines

IEC 61400-21-1, Measurement and assessment of electrical characteristics-wind turbines

IEC 61400-21-3, Measurement and assessment of electrical characteristics-wind turbine harmonic model and its application

IEC 61400-24, Lightning protection

IEC 61400-25-1, Communications for monitoring and control of wind power plants – Overall description of principles and model

IEC 61400-25-4, Communications for monitoring and control of wind power plants – Mapping to communication profile

IEC 61400-25-5, Communications for monitoring and control of wind power plants – Compliance testing

IEC 61400-25-6, Communications for monitoring and control of wind power plants – Logic node classes and data classes for condition monitoring

IEC 61400-25-71, Communications for monitoring and control of wind power plants – Configuration descriptive language

IEC 61400-26-1, Availability for wind energy generation systems

IEC 61400-27-1, Electrical simulation models – Generic models

IEC 61400-27-1, Electrical simulation models – Model validation

2.3.2 ASCE/AWEA Recommended Practice for compliance of large land-based wind turbine support structures

The ASCE/AWEA on wind turbine support structures details recommendations for the design and approval process to promote engineering integrity of wind turbines in the U.S. [3]. This recommendation report focuses mostly on the design of tubular steel wind turbine towers. The goal of the report is to clarify structural requirements for wind turbines for the authority holding jurisdiction (AHJ) and the developers (who design the turbines to meet local codes and manage construction) [3]. The role of the recommendation report is to provide guidance when the U.S. practice (ASCE 7) and the international practice (IEC 61400-1) differ [3]. The wind loading demand is of particular interest. The ASCE/AWEA recommendation report suggests the use of the following models to determine wind speed profiles: Normal Turbulence Model (NTM), Extreme Wind speed Model (EWM), the Extreme Operating Gust (EOG), the Extreme Turbulence Model (ETM), the Extreme Direction Change (EDC), the Extreme coherent gust with direction change (ECD) and the Extreme wind shear (EWS). The above stated models were adopted from the IEC 61400-1 and discussed in ASCE/AWEA in comparison to standard ASCE. The ASCE/AWEA committee investigated the use of the ASCE to calculate wind loading and compared to the IEC method with mixed results on how each model predicted wind loads.

2.3.3 Report on Design of Concrete Wind Turbine Towers

ACI created an Innovation Task Group to write a report on the design of concrete wind turbine towers in 2016. The task group has since been disbanded and replaced by ACI Committee 378, Concrete Windmill Towers. The Report on Design of Concrete Wind Turbine Towers [7] examines the benefits of concrete towers for land-based wind turbines with heights greater than 325 ft (100m) in comparison to steel tubular towers.

ACI ITG-9R-16 discusses wind farm development and certification, types of concrete towers, tower design regarding tower frequency, prestressing, fatigue and modeling. Design loads and load combinations are also detailed.

2.4 Design Loading

Design loading is broken up into turbine forces and modal considerations. As stated previously, the lack of a design code has led designers to use a mix of codes from similar structures such as concrete tower construction. Dolan et. al. [7] has recommended to use IEC61400-1 as the governing code for concrete wind turbine design/construction at this time. In practice, towers are typically designed for the extreme operating and non-operating 50-year high speed wind. Wind turbine manufacturers provide a design loads matrix based on the rated turbine power and location specific design wind speeds [18].

Design loads to consider on a turbine tower can be divided into four categories: gravitational and inertial loads including power production, braking and seismic effects; aerodynamic loads; actuation loads including blade startup; and loadings such as ice, rain, and nonoperational conditions such as high wind on a parked turbine [7].

2.4.1 Forces on Turbine

The main forces acting on a wind turbine tower come from the wind turbine. The forces that act on the turbine blades are transferred to the tower and eventually the foundation. A stationary wind load from the wind turbines is located at the top of the tower, (thrust force). An overturning “thrust” moment is also associated with the wind turbine loading and applied at the top of the tower, causing bending in the same direction as the thrust force; this is also known as the turbine moment. Turbine weight is applied to the tower top in the downward direction as a compression load on the top of the tower. Direct wind pressure on the tower increases parabolically with height. Direct wind pressure may also be simplied into equivalent rectantular distributions to simplify calculations as was done

reference [22]. Figure 2.12 shows the thrust force, turbine moment, turbine weight, wind pressure and torsional component.

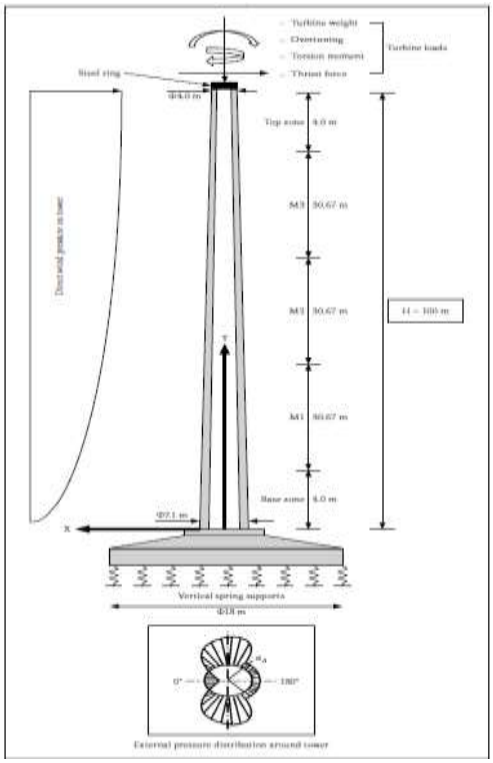

Figure 2.12. Forces acting on a wind turbine tower [30].

Due to the lack of a uniform code, there has not been a set method for calculating wind loading. Multiple sources have used a mix and match of IEC vs. ASCE load factors. Reference [18] has used the wind pressure approach using ASCE 7. LaNier [18] describes in depth his method for calculating loads on the tower. LaNier [18] also attached a WindPACT load analysis that details the wind loading for 1.5, 3.6 and 5.0 MW wind turbine towers. LaNier scaled up the 3.6 MW and 5.0 MW from the provided 1.5 and 3.0 MW loading provided, based on the rotor area. LaNier describes the Equivalent Static Lateral Wind Load, described in ASCE 7-98 that has been used for the wind load analysis of large industrial chimneys. This was determined to be applicable to structures of similar size, like a wind turbine tower. The turbine loads were applied as a static load to the top of the tower and was considered slightly conservative.

2.4.2 Modal Considerations

Wind turbines have strict constraints on tower fundamental frequency to avoid resonance [31]. Resonance occurs when an external force acts on a structure at the same frequency of the structure's natural frequency. This can cause large displacements and immediate failure or longer-term fatigue failure [31]. To ensure that the tower's frequency does not coincide with the forcing natural frequencies, two methods are considered. The first is to design the tower with a natural frequency that is not in the range of anticipated frequencies of the external forces. The other method applies mass damping to decrease dynamic amplification of an external vibrational force. The natural frequency of a tower is affected by the geometry and the material properties of the tower [22, 15]. The preferred method is to design the tower to be outside of the force natural frequencies. Although, designers have employed the use of large volumes of concrete at the top of towers as a tuned mass damper to control wind induced vibrations [7].

Frequencies acting on a tower are divided between the blade rotational frequency (1P frequency, caused by the unbalanced weight of the rotor, wind shear and tower shadow) and the blade passing frequency (3P frequency) as shown in Figure 2.13. [31] where the y-axis is unitless and the x-axis is in Hertz. Due to the variable operational wind speeds in today's modern variable wind turbines, the 1P and 3P frequencies are reported as a range of values.

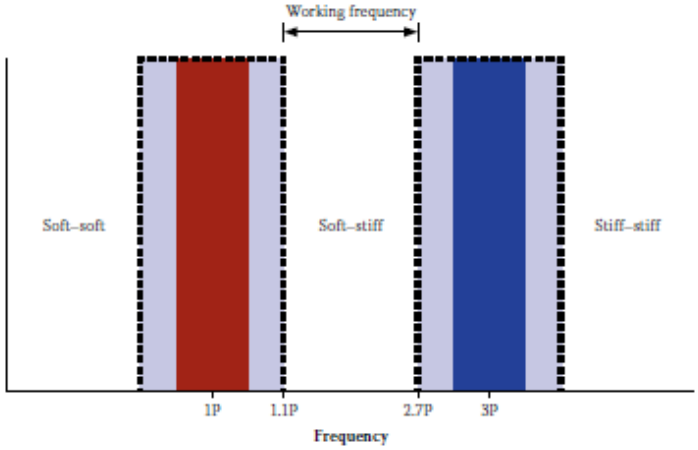

Figure 2.13. Excitation frequencies [31].

There are three methods to design a tower to have a frequency outside of the 1P and 3P frequencies. The first method is to design the fundamental frequency of the tower to be higher than the 3P frequency, considered a stiff-stiff structure. The second method is to design a structure to be between the 1P and 3P frequencies, considered a soft-stiff structure. It has been shown that the soft-stiff structure is the most economical wind turbine tower [11]. The third method is to design a structure with a fundamental frequency below the 1P frequency, considered a soft-soft structure. At the design stage it is difficult to calculate the fundamental frequency. After an applied safety factor of +/- 10%, the working frequency of the tower should be between 1.1P and 2.7P, as indicated in Figure 2.13. [32].

Stiff towers (where the tower natural frequency is higher than the blade passing frequency(3P)) require thick walls and are typically uneconomical due to the increase in material quantity. Soft (flexible) towers (where the tower natural frequency is lower than the rotor frequency(1P)) result in large deflections at the hub. This creates an interference between the blade and the tower. Soft tower designs have been used on smaller towers, but is uncommon on taller towers [7]. Stiff/flexible towers (where the tower natural frequency is between the 1P and 3P frequenies) are the preferred method of design because they are typically the most economical.

Controlling a concrete tower's natural frequency can be done by modifying the tower dimensions or the concrete elastic modulus [7]. Concrete cracking can lead to a reduced stiffness and natural frequency, possibly causing a shift into an undesirable range of 1P or 3P frequencies [7]. Post-tensioned tower design includes limiting stresses to control cracking at service loads while also providing an active force to close cracks after an overload.

It is important to note that setting the boundary conditions for the foundation to fully fixed in a FEM model could result in up to a 20% change in the fundamental frequency of the tower [32]. Researchers generally use elastic springs for the foundation to simulate

soil stiffness [3, 18]. In the model that is used in this work, the base was assumed as fixed since a specific site was not being modeled and comparisons at varying heights were intended to be relative. For a specific site, this refinement would be added to the base condition.

2.5 Finite Element Analysis

Finite element analysis (FEA) uses a computerized method to predict how a structure or solid reacts to forces [9]. FEA breaks down objects into finite elements (thousands to hundreds of thousands of elements) and mathematical equations predict the behaviors of each element [9]. Finite element analysis software can be used to approximate stress, deflections, fatigue, buckling, and many other solutions of interest in a complex structure. Common FEA software products include ANSYS and ABAQUS. FEA software for wind turbines includes: SOWFA, FAST, BModes, Modes, HAWC2 and GH Bladed. These are made available by National Renewable Energy Laboratory (NREL). The BModes and Modes codes are used to derive free-vibration properties of towers or blades based on modeling these components as a series of Bernoulli-Euler beam elements. FAST, HAWC2 and GH Bladed software can model complete wind turbine assemblies. This allows interaction between vibrating blades, hub, and the tower by a way of coupled equations of motion.

Structural modeling of concrete wind turbine towers can be completed using 1-Dimensional beam models or 3-Dimensional Finite Element Analysis software [36]. Wind turbine towers have generally used a 1D beam model due to its overall efficiency and reasonable accuracy. Although, 3D FEA software (ANSYS) to evaluate towers can provide more accurate results and detailed stress distribution. Research involving wind turbine towers in 3D FEA software has used shell elements to model towers because the thin-walled characteristics of a wind turbine tower can be effectively and accurately modeled using shell elements [37].

Research to date has focused mainly on optimizing tower designs. Researchers have used genetic algorithms in ANSYS and ABAQUS, respectively, to optimize tower tapers and segment thickness to minimize cost and optimize performance [37, 22].

2.5.1 Finite Element Analysis-Baseline Steel Model

The European Academy of Wind Energy (EAWE) performed a structural optimization of wind turbine towers based on finite element analysis and a genetic algorithm [37]. This study used a genetic algorithm in ANSYS to determine optimal tower base and top diameters and segment thickness. The constraints considered were deformation, ultimate stress, buckling and vibration. This paper was used as a baseline model to verify that our FEA model was working properly. The dimensions and loading given in Wang et al. [37] information was used to reproduce their model in ANSYS. More information on the baseline tower will be given in the results section.

Wang et. al. [37] also performed a parametric mesh sensitivity study on the first 6 modal frequencies of the baseline steel tower model and concluded that a 0.5 m quadrilateral mesh converged with minimal convergence errors. A fixed tower base was used in the analysis, though as mentioned above, it is more accurate to model the base with elastic springs to model soil stiffness. Modeling the tower base with elastic springs will simulate soil stiffness and produce more accurate results [3, 18].

2.5.2 Finite Element Analysis-Concrete Wind Turbine

Ma and Meng [22] performed an optimization of a concrete wind turbine tower using ABAQUS. The process towards optimization involved first optimizing the geometry of the tower cross section and the tower system variables (diameters, thickness, number of prestressing strands, rib height and width). Genetic algorithms were used to optimize the above variables, where the objective functions were selected to minimize cost and constrain natural frequency, stresses, deflections, geometric constraints. Wind loading and seismic loading are considered.

Kenna et. al. [15] proposed a concrete wind turbine tower model that took account of both material and geometric non-linearity. The paper models the concrete tower with shell elements and uses 4-node, 2D Reisser-Mindlin elements to model the concrete. The

unbonded prestressing tendons are modeled as 1D bar elements with an imposed prestress force. This model was used to analyze the dynamic behavior of a prestressed or post tensioned concrete wind turbine towers. Tendon stiffness was superimposed onto the concrete shell elements. Van Zyl and Van Zij also embed the steel into the finite element concrete shell to increase stiffness [31].

3.0 Experimental Plan

The literature review shows that the driving factor for increasing the size of wind turbines is the demand for more energy production. Wind turbines have been increasing in turbine blade lengths and turbine tower height to meet this goal. Given the lack of previous research in towers above 100m and with materials other than steel, this work focuses on the first steps in developing a post-tensioned concrete tower model.

The experimental plan includes the following:

- Model a baseline steel tower in ANSYS as a verification study to match Wang et. al. [37].
- Model three post-tensioned concrete towers at 100 m, 150 m and 200 m in height.
- Evaluate the model output and consider feasibility of a post-tensioned design in the proposed cross-sections.

Details of these steps are given in the next sections.

3.1 Steel Baseline Model Verification Study

The EAWE published a paper from Wang et al. [37] that illustrated the structural optimization of wind turbine towers based on finite element analysis and genetic algorithm. To learn how to use the software and verify a working model, reproducing the optimized steel tower was the first step in this research project. The ANSYS analyses used in this paper were Static Structural: Von-mises stress, total deformation; Eigenvalue Buckling: load multiplier (safety factor); and Modal: natural frequency. Results produced from ANSYS were then compared to the original study in the Results section.

The baseline steel tower with geometries and loading was obtained from Wang et al [37]. Since windmill towers are thin-walled structures even when designed in post-tensioned concrete, they can be modeled accurately with shell elements. In the reproduction model Shell 281 were used for the mesh elements in ANSYS. Shell 281 has eight nodes with six degrees of freedom at each node, making it suitable for linear, large rotation and/or large

strain nonlinear applications. The parametric study in Wang et al. [37] determine the optimum shell mesh size to be 0.5 m for the structure they model. This mesh size was used for the reproduced steel tower model.

Material properties are listed in Table 3.1. The density of the steel was increased to 8500 kg/m^3 to account for the additional paint, welds, bolts, and flanges that were not accounted for in the tower thickness data [37].

Table 3.1. Baseline steel model material properties [37].

Properties	Values
Tower height (m)	80
Density (kg/m^3)	8500
Young's Modulus (GPa)	210
Poisson's ratio	0.3

The tower is considered to have a fixed base. Wang et al. [37] obtained tower loading from a research paper by LaNier [18] and are listed in Table 3.2. F_x was applied to the top of the tower cross section as a horizontal point load and is the thrust force from the wind force on the rotor. An additional vertical load is placed on the tower to account for the weight of the nacelle and turbine components. Overturning moment M_x was also applied to the top of the tower. Tower loading is shown in Figure 3.1. Gravity is applied to the tower in this model to consider the tower self-weight. It is also important to note that LaNier [18] also listed a torsional force and vertical load that was not mentioned in Wang et al. [37]. Torsional moment was not applied to the steel tower model because a torsional moment was not given by Wang et. al [37].

Table 3.2. Baseline steel model loading conditions [18, 37].

Items	Factored aerodynamic loads (safety factor:1.35)
F_x (kN)	780
M_x (kN*m)	38,567
Wind turbine weight (kg)	480,076

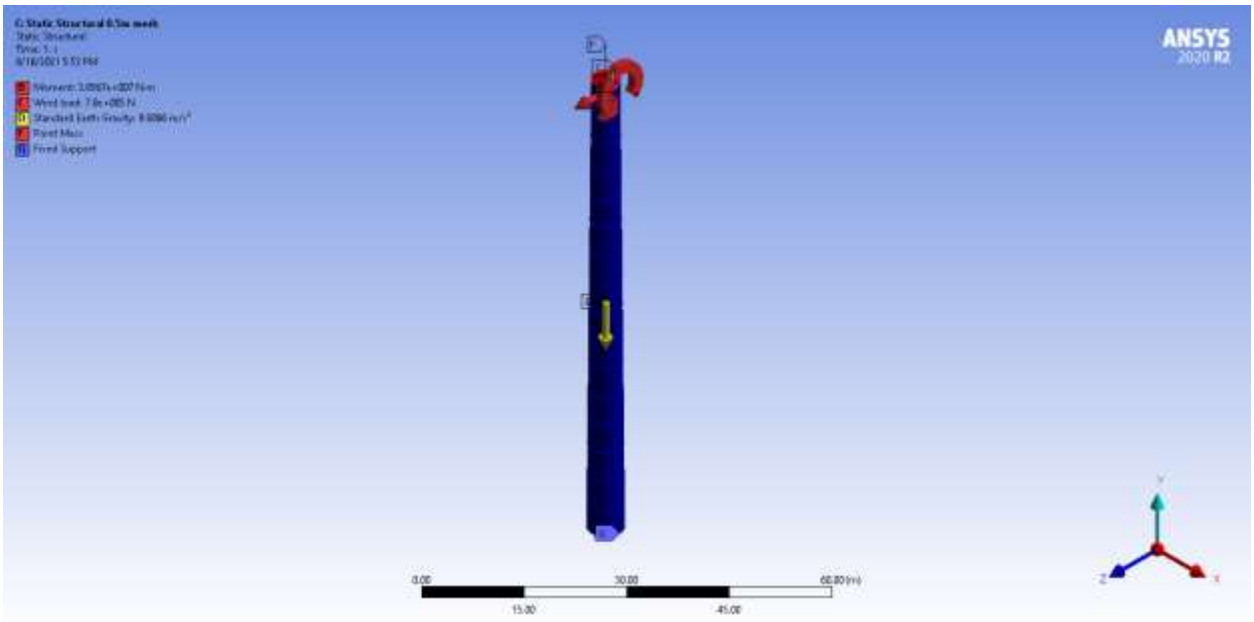

Figure 3.1. Loading on FEM steel baseline model.

Figure 3.1. shows the forces applied to the tower. The nacelle weight was applied as a mass at the top of tower. The turbine thrust force was applied as a horizontal point load applied over the tower cross section in the z-axis direction. The overturning moment was also applied at the top of the tower cross section about the x-axis.

Tower geometry is listed below in Table 3.3. The shell was drawn in AutoCAD Inventor as a shell loft and imported to ANSYS SpaceClaim as a .step file, as illustrated in Figure 3.2. Within ANSYS, the material properties and thickness were assigned from SpaceClaim. Shared topography was also used to bond the segments together in ANSYS.

Table 3.3. Baseline steel model geometry [37].

	Value
Height	80 m
Segments	16
Height of segments	5 m
Tower Top Diameter	4.268 m
Tower Bottom Diameter	5.650 m
Thickness	
Segment 1	0.037 m
Segment 2	0.036 m
Segment 3	0.032 m
Segment 4	0.028 m
Segment 5	0.026 m
Segment 6	0.025 m
Segment 7	0.025 m
Segment 8	0.023 m
Segment 9	0.022 m
Segment 10	0.021 m
Segment 11	0.020 m
Segment 12	0.019 m
Segment 13	0.019 m
Segment 14	0.018 m
Segment 15	0.017 m
Segment 16	0.016 m

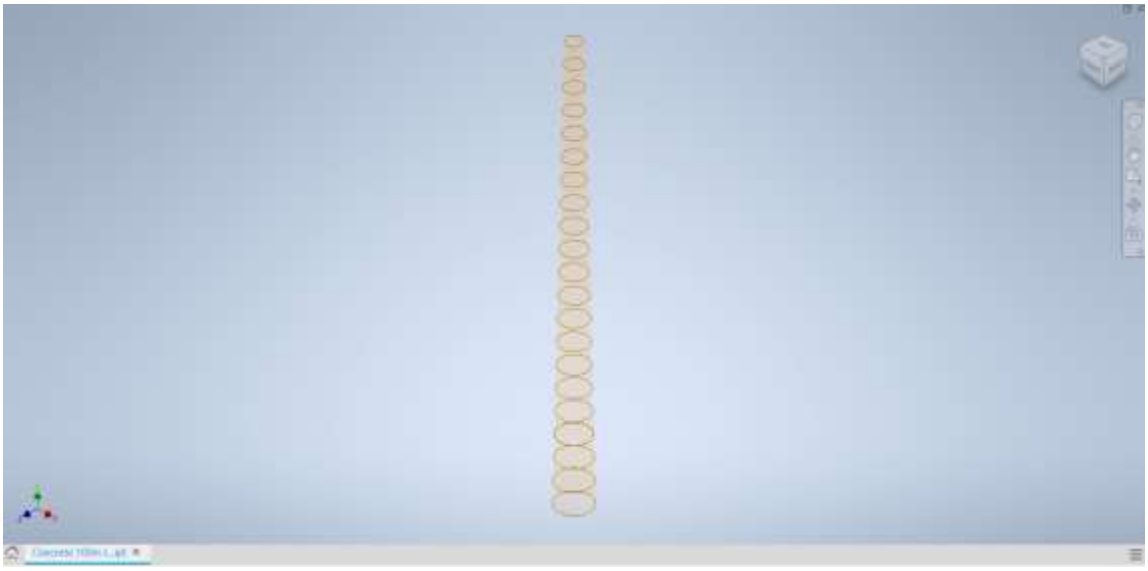

Figure 3.2. Steel tower .step file.

The results from ANSYS: Static Structural, Eigenvalue Buckling and Modal analyses are compared to the results reported by Wang et al. [37] in section 4.0 Results.

3.2 Concrete Tower Models

Three post-tensioned concrete towers were analyzed with heights of 100 m (328 ft), 150 m (492 ft) and 200 m (656 ft). Additionally, three 150 m towers were analyzed with a reduced post-tension force (90%, 80% and 70% PT force). The towers have the same taper as obtained from LaNier [18]. The concrete material properties used in this study are listed below in Table 3.4.

Loading parameters are consistent between the three concrete towers. Turbine loading was obtained from LaNier [18]; The forcing is from a WindPACT rotor study that is referenced in Wang et al. [37] and is summarized in Table 3.5. Calculating the design loading for a wind turbine is a complex process and is site specific. In this study, wind pressure along the height of the tower was not applied to the steel or concrete tower models as site specific wind speeds were not defined. For this preliminary investigation, the site is not a variable in the scope of the project.

Table 3.4. Concrete Material Properties.

Properties	Values
f_c' (psi)	8000
Density (kg/m^3) [1]	2392
Young's Modulus (MPa) [1]	37089.7
Poisson's ratio [38]	0.1414

Table 3.5. Concrete Tower Loading [37].

Vertical Post-Tensioning forces	See Table 3.8 & Table 3.9
Point Mass (weight of turbine blades and generator)	4.8008E+05 kg
Forces on Nacelle	-
Vertical (N)	6.747E+06
Thrust Force (N)	7.81E+05
Thrust Moment (N*m)	3.8567E+07
Torsional Moment (N*m)	7.876E+06

The application of loading to the concrete tower is shown below in Figure 3.3. The post tensioning forces are applied as point loads in 50 m increments shown below as forces F, G and H. See Table 3.9 and Table 3.10 for post tensioning forces.

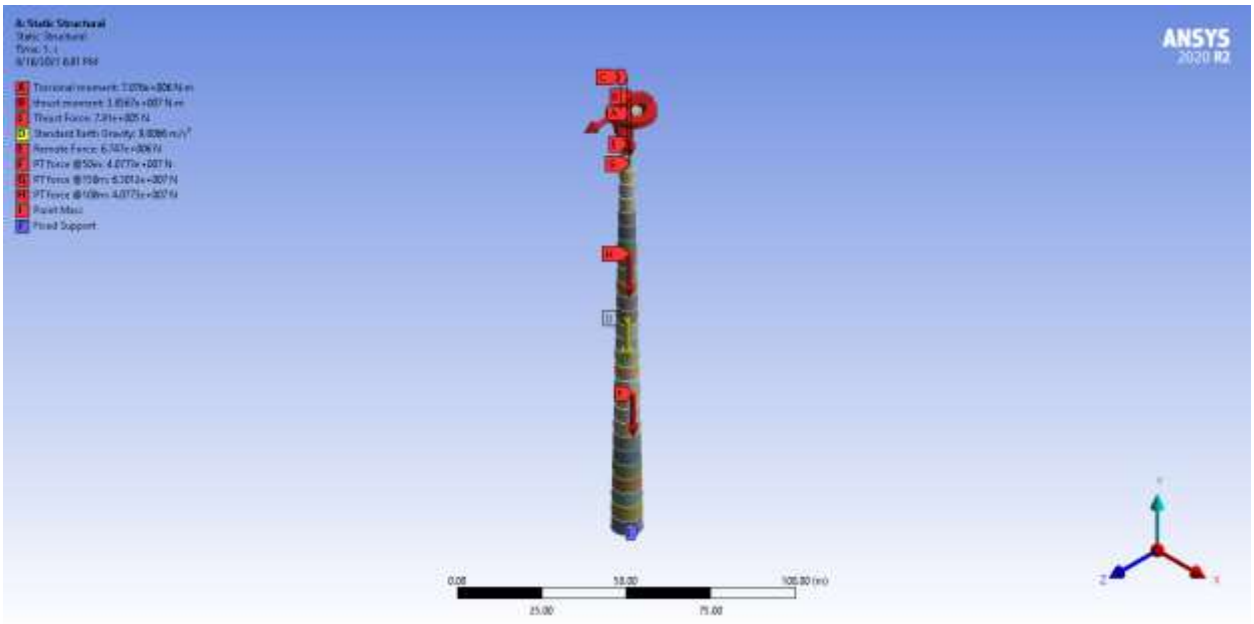

Figure 3.3. Loading applied to 150 m concrete tower.

Wall thickness is consistent between the tops of all three towers. Tower thickness increases towards the base with uniform wall thickness in 50 m intervals. The towers were divided into 5 m tall segments. Base diameters and thicknesses for the 150 and 200 m were extrapolated from LaNier [18], 5 MW 100 m concrete tower. Listed below in Table 3.6. is a summary of the tower dimensions used in the ANSYS model. Example calculations are shown below: equation 1 and 2.

Table 3.6. Concrete Tower Dimensions.

Height (m (ft))	**100 (328)**	**150 (492)**	**200 (656)**
Diameter			
Base	7.6 (25)	9.601 (31.5)	11.582 (38)
50m (m (ft))	5.639 (18.5)	7.62 (25)	9.601 (31.5)
100m (m (ft))	3.658 (12)	5.639 (18.5)	7.62 (25)
150m (m (ft))	-	3.658 (12)	5.639 (18.5)
200m (m (ft))	-	-	3.658 (12)
Thickness			
0-50 m (m (ft))	0.724 (2.38)	0.9525 (3.125)	1.3335 (4.375)
50-100 m (m (ft))	0.5715 (1.875)	0.724 (2.38)	0.9525 (3.125)
100-150 m (m (ft))	-	0.5715 (1.875)	0.724 (2.38)
150-200 m (m (ft))	-	-	0.5715 (1.875)

Tower Dimension Extrapolation (Table 3.6.) (see Figure 3.4. below)
For tower height=150m

Φ_{100}=Tower Diameter at 100m (for 100 m tower height)=3.658 m (Ref [15].)
Φ_0=Tower Diameter at 0m (for 100 m tower height)=7.62 m (Ref [15].)
L=length for similar triangles=100 m
H=extrapolation length=50 m (in this case)
X_2=length at tower base
Φ_e=Extrapolated base diameter (m)
X_1=length at 100 m tower base for extrapolating

$X_1=\Phi_0/2- \Phi_{100}/2$=7.62 m/2-3.658 m/2=1.981 m

$X_2=\frac{L+H}{L} * X_1=\frac{100\ m+50\ m}{100\ m} * 1.981\ m$=2.9715 m
$\Phi_e=2(X_2)+ \Phi_{100}$
Φe=2(2.9715 m)+3.658 m=9.601 m
(Equation 1)

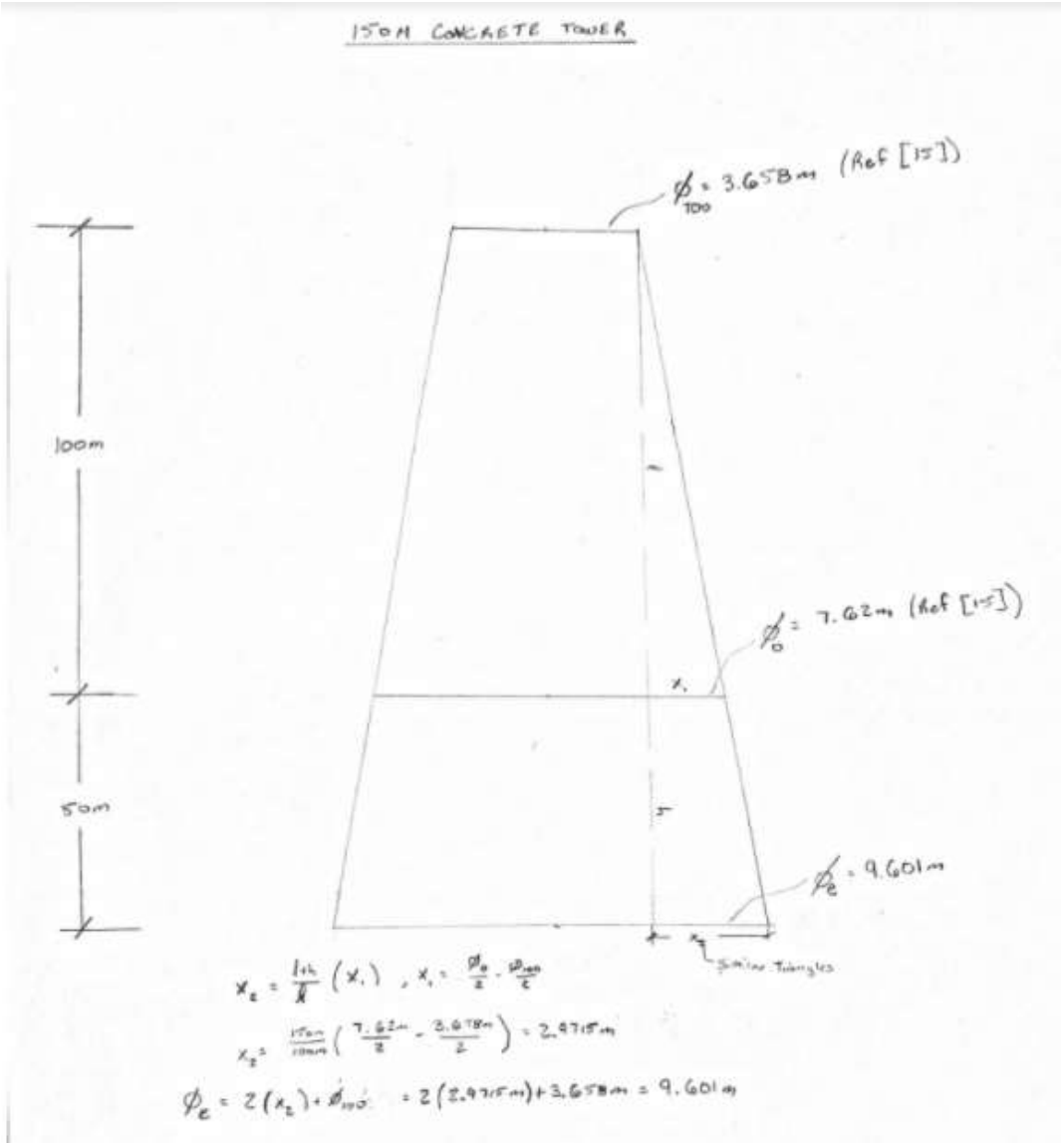

Figure 3.4. Tower base Diameter extrapolation for 150m and 200m Concrete Towers.

Wall thickness Extrapolation (Table 3.6.)
Thickness extrapolation at the base of the 150 m tall concrete tower.

$$\frac{t_0}{l+h} = \frac{t_{100}}{l} \qquad \text{(Equation 2)}$$

t_0=thickness at tower base (0 of 150 m)
t_{100}=thickness at tower base of 100 m tall tower (0.762 m [18])
l=height of original 100 m tower=100 m
h=tower height extension (total new tower height-initial tower height) =150m-100m=50m

$t_0=\frac{0.762\ m}{100\ m} * 150\ m$=1.143 m

The number of post tensioning tendons differs based on the heights of the towers. Unbonded, 0.6 in, 7-wire, low-relaxation strands are assumed for the post tensioning with an ultimate strength of 270 ksi. The concrete strength used in the study is 7 ksi [18]. The effective stress in prestressing (f_{se}, after short-term and long-term losses) used was assumed to be 160 ksi ($1.103(10^9)$ Pa) per LaNier [18]. A duct size of 6-27 was used (Table 3.8 [34]) in tower evaluation, with 24 strands per duct. Duct size is used to determine feasible duct spacing and available cover within the tower cross-section, as shown below in Table 3.7. (Equation 3). LaNier [18] listed the number of post-tensioning tendons in the 100 m concrete tower design. In this study, the post tensioning used in the 150 m and 200 m towers were extrapolated from the 100 m post-tensioned concrete tower design. All tower diameters and ducts were extrapolated from the 100 m base tower design, this resulted in the towers to have similar diameters, tapers and PT loading (including the number of ducts, PT force and the number of PT strands). See Table 3.9. for the number of strands/ducts and PT forces applied for each tower.

Table 3.7. Clear Spacing Between Ducts.

Section (m)	# Ducts	Tower Diameter (m)	Duct Diameter (m) (Ref [28])	Distance Between Ducts (m) (Fig 2.4-11)	Minimum Allowable Spacing 0.7*d (Ref [28])
50	50	9.601	0.121	0.603248621	0.0847
100	39	7.62	0.121	0.613818872	0.0847
150	28	5.639	0.121	0.63269432	0.0847
200	17	3.658	0.121	0.675996819	0.0847

Required minimum spacing between ducts (Ref [33]):
S_{min}=0.7*d
(Equation 3)
S_{min}=.7*0.121m=0.0847m < Spacing provided = 0.603m
Spacing provided is adequate in all sections.

Cross sections for the 200 m concrete tower are shown below in Figures 3.5-3.12 at heights of 0, 50, 100, 150 and 200 m. All 50 post tensioning tendons were anchored at the

base of the tower. Anchorage points occur in 50 m increments with alternating post tensioning tendons. For example, in the 200 m tower, 17 post tensioning ducts were continuous over the full height of the tower. 11 post tensioning tendons are continuous from 0-50 m of the tower, 11 post tensioning tendons are continuous over 0-100 m and 11 post tensioning tendons are continuous over 0-150 m of the tower height. The lengths of the tendons range from 50 m, 100 m, 150 m and 200m. There is a total of 50 post tensioning ducts in the 200 m tower per Table 3.9.

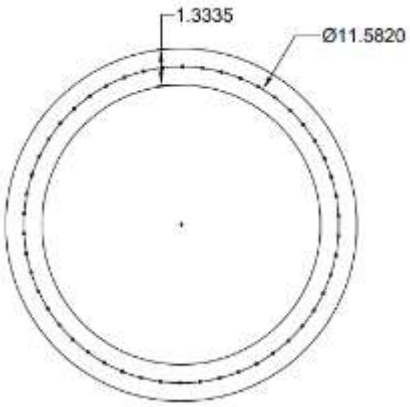

Figure 3.5. 200 m cross section at 0 m, 50 ducts.

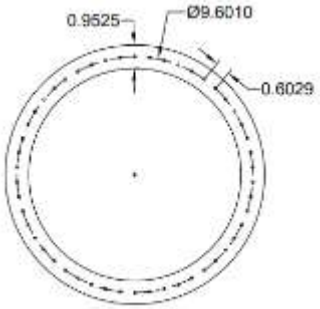

Figure 3.6. 200 m cross section at 50 m, 50 ducts

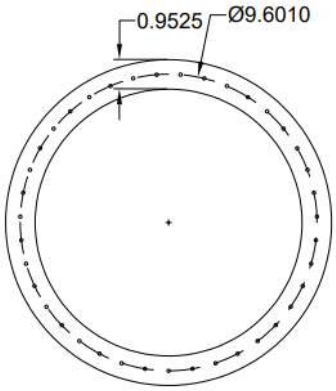

Figure 3.7. 200 m cross section at 50 m, 39 ducts.

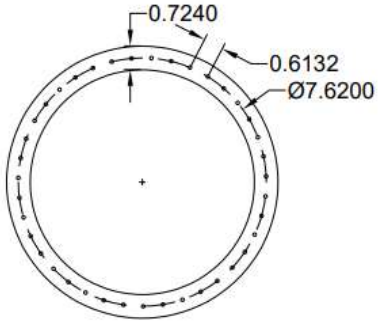

Figure 3.8. 200 m cross section at 100 m, 39 ducts.

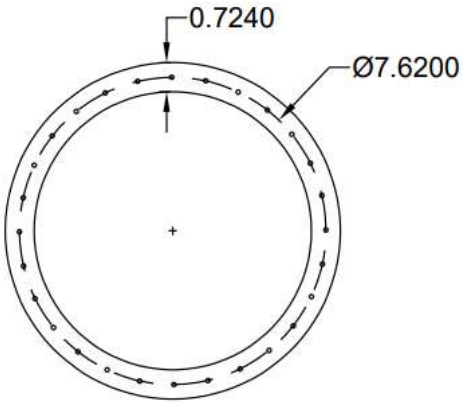

Figure 3.9. 200 m cross section at 100 m, 28 ducts.

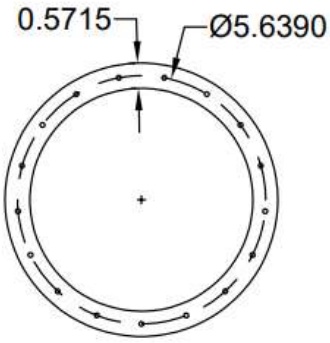

Figure 3.11. 200 m cross section at 150 m, 17 ducts.

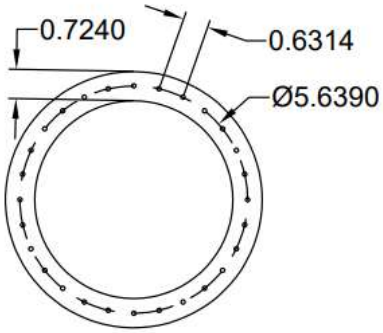

Figure 3.10. 200 m cross section at 150 m, 28 ducts.

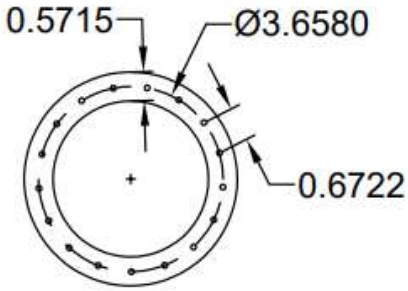

Figure 3.12. 200 m cross section at 200 m, 17 ducts.

Table 3.8. VSL Post Tensioning Data [34].

1.4 - TENDON PROPERTIES 15mm (0.6")

Unit	Strands numbers	Steel area			Breaking load			Corrugated steel duct[3] (recommended)		Corrugated plastic duct VSL PT-PLUS®		Steel pipes
		A_P acc. to prEN		ASTM	Y1860S7 (prEN)		Grade 270 (ASTM)	$Ø_i$ / $Ø_e$	e	$Ø_i$ / $Ø_e$	e	Ø ext. x t
		d=15.3 mm A_P=140 mm²	d=15.7 mm A_P=150 mm²	d=15.24 mm A_P=140 mm²	d=15.3 mm A_P=140 mm²	d=15.7 mm A_P=150 mm²	d=15.24 mm A_P=140 mm²					
		[mm²]	[mm²]	[mm²]	[kN]	[kN]	[kN]	[mm]	[mm]	[mm]	[mm]	[mm]
6-1	1	140	150	140	260	279	260.7	25/30	5	22/25	4	25.0 x 2.0
6-2	2	280	300	280	520	558	521	40/45	9	76/25[2]	-	42.4 x 2.0/2.5/3.0
6-3	3	420	450	420	780	837	782	40/45	6	76/25[2]	-	42.4 x 2.0/2.5/3.0
6-4	4	560	600	560	1040	1116	1043	45/50[1]	7	76/25[2]	-	48.3 x 2.0/2.5/3.0
6-7	5	700	750	700	1300	1395	1304	50/57	8	58/63	13	76.1 x 2.0/2.5/3.0
|	6	840	900	840	1560	1674	1564	55/62	9	58/63	11	|
6-7	7	980	1050	980	1820	1953	1825	55/62	7	58/63	9	76.1 x 2.0/2.5/3.0
6-12	8	1120	1200	1120	2080	2232	2086	65/72	11	76/81	18	80.0 x 2.0/.2.5
|	9	1260	1350	1260	2340	2511	2346	65/72	9	76/81	16	|
|	10	1400	1500	1400	2600	2790	2607	70/77	11	76/81	15	|
|	11	1540	1650	1540	2860	3069	2868	70/77	9	76/81	13	|
6-12	12	1680	1800	1680	3120	3348	3128	75/82	11	76/81	12	80.0 x 2.0/.2.5
6-15	13	1820	1950	1820	3380	3627	3389	80/87	13	100/106	25	101.6 x 3.0/4.0/5.0
|	14	1960	2100	1960	3640	3906	3650	80/87	11	100/106	24	|
6-15	15	2100	2250	2100	3900	4185	3911	80/87	10	100/106	23	101.6 x 3.0/4.0/5.0
6-19	16	2240	2400	2240	4160	4464	4171	85/92	12	100/106	22	101.6 x 3.0/4.0/5.0
|	17	2380	2550	2380	4420	4743	4432	85/92	11	100/106	20	|
|	18	2520	2700	2520	4680	5022	4693	90/97	13	100/106	19	|
6-19	19	2660	2850	2660	4940	5301	4953	90/97	12	100/106	18	101.6 x 3.0/4.0/5.0
6-22	20	2800	3000	2800	5200	5580	5214	100/107	17	100/106	17	114.3 x 3.0/4.0/5.0
|	21	2940	3150	2940	5460	5859	5475	100/107	16	100/106	16	|
6-22	22	3080	3300	3080	5720	6138	5735	100/107	15	100/106	15	114.3 x 3.0/4.0/5.0
6-27	23	3220	3450	3220	5980	6417	5996	100/107	14	115/121	22	114.3 x 3.0/4.0/5.0
|	24	3360	3600	3360	6240	6696	6257	100/107	13	115/121	22	|
|	25	3500	3750	3500	6500	6975	6518	110/117	18	115/121	21	|
|	26	3640	3900	3640	6760	7254	6778	110/117	17	115/121	21	|
6-27	27	3780	4050	3780	7020	7533	7039	110/117	16	115/121	20	114.3 x 3.0/4.0/5.0
6-31	*28*	*3920*	*4200*	*3920*	*7280*	*7812*	*7300*	*110/117*	*15*	*130/136*	*27*	*127.0 x 3.0/4.0/5.0*
|	29	4060	4350	4060	7540	8091	7560	120/127	21	130/136	27	|
|	30	4200	4500	4200	7800	8370	7821	120/127	20	130/136	26	|
6-31	31	4340	4650	4340	8060	8649	8082	120/127	19	130/136	25	127.0 x 3.0/4.0/5.0
6-37	32	4480	4800	4480	8320	8928	8342	120/127	18	130/136	24	139.7 x 3.0/4.0
|	33	4620	4950	4620	8580	9207	8603	120/127	17	130/136	23	|
|	34	4760	5100	4760	8840	9486	8864	120/127	16	130/136	22	|
|	35	4900	5250	4900	9100	9765	9125	130/137	22	130/136	22	|
|	36	5040	5400	5040	9360	10044	9385	130/137	21	130/136	21	|
6-37	37	5180	5550	5180	9620	10323	9646	130137	20	130/136	20	139.7 x 3.0/4.0
6-43	43	6020	6450	6020	11180	11997	11210	140/147	21	150/157	27	152.4 x 3.0/4.0/5.0
6-55	55	7700	8250	7700	14300	15345	14339	160/167	26	150/157	21	168.3 x 3.0/4.0

1) Flat ducts possible as well

2) Flat duct PT-PLUS® with rectangular slab anchorages, for PT-PLUS® see also under 3.1.3.

3) If flat ducts (steel or PT PLUS®) to be used with square type castings please contact your VSL representative. In plan view, tendons with slab type anchorages must be straight between anchorages or have only unidirectional turns with min. radii of > 6 m. Strands must always be pushed-in prior to concreting. Eccentricity e: negligible

4) Given values may slightly vary depending on local availability of ducts. They are minimal for most applications. For special cases (long tendons, many curvatures, small radii etc.) greater size duct is recommended – please verify with VSL. In any case the filling ratio (cross-section steel / duct) must not exceed 0.5 (EN523).

5) Please check with the nearest VSL office for the complete anchorage list.

Table 3.9. Post Tensioning.

Height (m (ft))	**100 (328)**	**150 (492)**	**200 (656)**
Post-Tensioning Tendons			
0-50m	28	39	50
50-100m	17	28	39
100-150m	-	17	28
150-200m	-	-	17
Total Post-Tensioning Force (kN (k))			
0-50m	40773 (9166)	40773 (9166)	40773 (9166)
50-100m	63012 (14166)	40773 (9166)	40773 (9166)
100-150m	-	63012 (14166)	40773 (9166)
150-200m	-	-	63012 (14166)

To test the affects that the post-tension forces had on the tower evaluation, the post tensioning forces were reduced in three separate instances. The 150 m tower was used with a post tensioning force 90%, 80% and 70% of the original post tensioning force as noted in Table 3.9. As noted previously, the original post tensioning force used was extrapolated from LaNier [18]. The reduced post tensioning forces are as noted in Table 3.10. The goal of this investigation was to determine any changes to the deflections, stresses, natural frequencies, and load multipliers.

Table 3.10. Reduced post tensioning forces.

Height (m (ft))	**150 (492)**	**150 (492)**	**150 (492)**
Post-Tensioning Force (kN (k))			
Percent P-T Force of original 150 m Tower (%)	90	80	70
0-50m	36695 (8250)	32618 (7333)	28541 (6416)
50-100m	36695 (8250)	32618 (7333)	28541 (6416)
100-150m	56711 (12749)	50410 (11333)	44109 (9916)

A convergence study was performed on the 150 m concrete tower. Peak stress was recorded for different element sizes, as can be seen in Figure 3.13. A mesh size of 0.20 m was determined to be adequate and will be used. As shown in the Figure 3.13. below, the mesh size of 0.20 m is where the peak stress starts to converge. This study uses 0.20 m mesh because any further mesh reduction would significantly increase the run time of the ANSYS model without any real benefit to the solution.

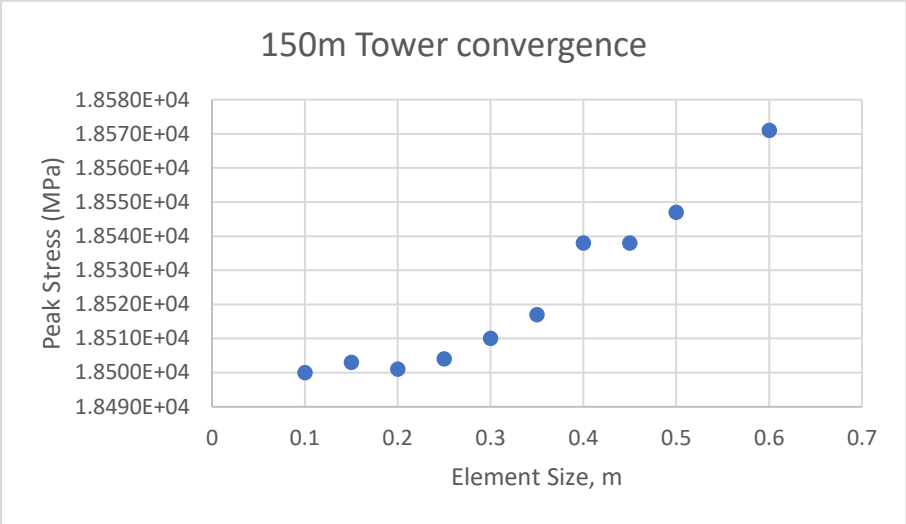

Figure 3.13. Convergence study on 150 m tower.

The model does not account for individual modeling of the duct material or post tensioning steel. The material properties use a composite section to consider the concrete and post tensioning steel with a composite stiffness. The type of tendon (grouted or ungrouted) would also have an impact on the actual stiffness of the section. The model assumes uncracked elastic behavior which is the design requirement for post-tensioned segmental bridge elements. Gross section properties are used for the geometry of cross-section.

Material properties of the 100 m, 150 m, and the 200 m tower are summarized in Table 3.11. Density, Young's Modulus and Poisson's ratio were calculated for each section using composite material equations. An example calculation is detailed below, equations 4-9. The equations combined the material properties from the post-tensioning steel and the concrete. The PT strands in the concrete towers were not discretely modeled with bar elements since the composite material property used in ANSYS should result in an accurate model for our purposes without the additional complexity and computational time.

Table 3.11. Material Properties.

Height (m (ft))	**100 (328)**	**150 (492)**	**200 (656)**
Density (kg/m^3)			
0-50 m	2460.1	2448.8	2434.4
50-100 m	2466.71	2461.4	2448.8
100-150 m	-	2466.7	2461.4
150-200 m	-	-	2466.7
Youngs Modulus (MPa)			
0-50 m	39078.84	38747.3	38329
50-100 m	39271.66	39117.7	38747.3
100-150 m	-	39271.7	39117.7
150-200 m	-	-	39271.7
Poisson's ratio			
0-50 m	0.1433	0.1430	0.1426
50-100 m	0.1436	0.1434	0.1430
100-150 m	-	0.1436	0.1434
150-200 m	-	-	0.1436

Composite Material: 100 m Concrete Tower

Longitudinal Young Modulus (Table 11.1, Ref [17]), $E_1 = \nu_f * E_f + \nu_m * E_m$ (Equation 4)

Longitudinal Poisson Ratio (Table 11.1, Ref [17]), $\nu_{12} = \nu_f * \nu_{f12} + \nu_m * \nu_{m12}$ (Equation 5)

ν_f = Volume fraction of material f (steel)

E_f = Modulus of Elasticity of material f (steel) = 196500 MPa (Ref [18])

ν_m = Volume fraction of material m (concrete)

E_m = Modulus of Elasticity of material m (concrete) = $(w_c^{1.5})*33*\sqrt{f_c'}$ = (150 pcf)$^{1.5}$*33*$\sqrt{8000\ psi}$ = 5379406 psi = 37089.7 MPa (Ref [1].) (Equation 6)

ν_{m12} = Poisson ratio of material (steel) = 0.3 (Ref [37])

ν_{f12} = Poisson ratio of material (concrete) = 0.1414 (Ref [38])

ρ_m = Density of Steel = 7850 kg/m^3 (Ref [37])

ρ_f = Density of Concrete = 2392 kg/m^3 (Ref [1])

Area of Post Tensioning Steel per 50 m section; (24-0.6in 7 wire strands per tendon) A=0.217in^2 (Area per single strand [25])

0-50 m: 28 tendons=28 tendons*(24 strands/tendon)=672 strand*(0.217 in^2/strand)=145.824 in^2=0.094 m^2

50-100 m: 17 tendons=17 tendons*(24 strands/tendon)=408 strand*(0.217 in^2/strand)=88.536 in^2=0.057 m^2

Calculate cross sectional area of tower (xA)
0-50 m: average diameter=6.63 m, average thickness=0.724 m;
$xA=(\frac{\pi}{4})*(d_{outer}^2-d_{inner}^2)=(\frac{\pi}{4})*((6.63+0.724/2)^2-(6.63-0.724/2)^2)=7.54\ m^2$
50-100 m: average diameter=4.65 m, average thickness=0.572 m;
$xA=(\frac{\pi}{4})*(d_{outer}^2-d_{inner}^2)=(\frac{\pi}{4})*((4.65+0.572/2)^2-(4.65-0.572/2)^2)=4.17\ m^2$

Calculate volume fraction (v_f)
Steel:
0-50 m: v_f = area of steel/xA=0.094 m^2/7.54 m^2=0.0125
50-100 m: v_f =0.0571 m^2/4.17 m^2=0.0137
Concrete:
0-50 m: v_m =1-v_f=1-0.0125=0.9875
50-100 m: v_m=1-0.137=0.9863

Composite Modulus of Elasticity
$E=v_{f*}E_f+v_m*E_m$
(Equation 7)
0-50 m: $E=v_{f*}E_f+v_m*E_m$
E=0.0125*196500 MPa+0.9875*37809.7=39078.8 MPa
50-100 m: $E=v_{f*}E_f+v_m*E_m$
E=0.0137*196500 MPa+0.9863*37809.7=39271.7 MPa

Composite Poisson's Ratio
$\nu=v_{f*}\nu_f+v_m*\nu_m$
(Equation 8)
0-50 m: $\nu=v_{f*}\nu_f+v_m*\nu_m$
ν =0.0125*0.3 +0.9875*0.1414=0.1434
50-100 m: $\nu=v_{f*}\nu_f+v_m*\nu_m$
ν =0.0137*0.3 +0.9863*0.1414=0.1436

Composite Density
$\rho=v_{f*}\rho_f+v_m*\rho_m$
(Equation 9)
0-50 m: $\rho=v_{f*}\rho_f+v_m*\rho_m$
ρ =0.0125*7850 +0.9875*2392=2460.1 kg/m^3
50-100 m: $\rho=v_{f*}\rho_f+v_m*\rho_m$
ρ =0.0137*7850 +0.9863*2392=2466.7 kg/m^3

The ANSYS modules used are listed below:

- Static Structural: Von-mises stress, maximum and minimum principal stresses, total deformation.
- Eigenvalue Buckling: load multiplier (safety factor); and

- Modal: natural frequency.

The maximum and minimum principal stress in the concrete, which was compared with the compression and tensile limits, respectively of our specified concrete strength as calculated per ACI 318-19, (Equation 10, 11) [1]. Von-mises stresses were recorded to compare between models. Total deformation was measured in the static structural module to determine the deflection anticipated at the top of the concrete tower. This value was compared to the maximum allowable deflection as calculated in Equation 11. Deflection is of particular interest because too much deflection could cause the turbine blades to strike the tower while in operation. The eigenvalue buckling module provides the load multiplier as the safety factor of the model. The safety factor was recorded and compared for all three tower models. The modal simulation was used to check the natural frequency of the towers. It is important to note that the tower natural frequency in a tower design would typically be checked to be within the 1P and 3P bounds to avoid resonance. This study does not calculate the 1P and 3P frequencies due to the lack of turbine information. Further analysis could be done if tower components were selected. Listed below in Table 3.12. are the limiting parameters for the concrete towers.

Compressive Stress Limit (ACI Table 24.5.3.1 [1])

(Equation 10)

$0.6*f'_c = 0.6*(8\ ksi) = 4.8\ ksi = 3.31E+07\ Pa$

Tensile Stress Limit (ACI Table R24.5.2.1 [1])

(Equation 11)

$7.5*\sqrt{f'c} = 7.5*\sqrt{8000\ psi} = 670.8\ psi = 4.63E+06\ Pa$

Nicholson equation-allowable horizontal drift limit (Ref [23].)

(Equation 12)

$0.125*h=0.125*100\ m = 1.25\ m$

Table 3.12. Concrete Tower Modeling.

Height (m (ft))	100 (328)	150 (492)	200 (656)
PT strands	56	78	100
Maximum Allowable Compressive stress (Pa (ksi)) (Equation 1)	3.31E+07 (4.2)		
Maximum Allowable Tensile stress (Pa (ksi)) (Equation 2)	4.63E+06 (0.627)		
Maximum deflection (m (ft)) – (Equation 3)	1.25 (4.10)	1.875 (6.15)	2.5 (8.20)

4.0 Results and Analysis

4.1 Steel Tower Results

The goal of the steel tower portion was to reproduce the ANSYS model that was created by Wang et al. [37] to verify assumptions from the paper and to apply the assumptions to the concrete model that was developed in this study.

The stated assumptions made by Wang et al. [37], about tower material properties, geometry, and loading that were used in the reproduction of the steel tower are summarized in Section 3.0. Table 4.1. details the findings of the tower modeled in this study as well as the results from Wang et al. [37]. Figure 4.1-4 show images of each analysis performed in ANSYS for the steel tower verification. The ANSYS analyses prepared in this verification study were Static Structural: Von-mises stress, directional deformation, Eigenvalue Buckling: load multiplier (safety factor) and Modal: natural frequency.

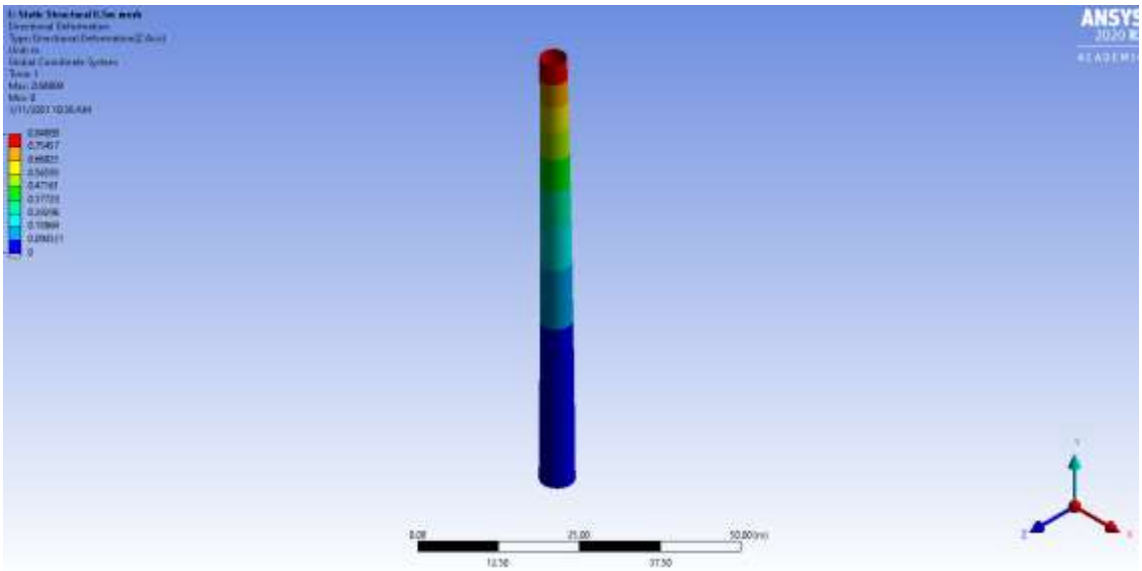

Figure 4.1. Static structural directional deformation.

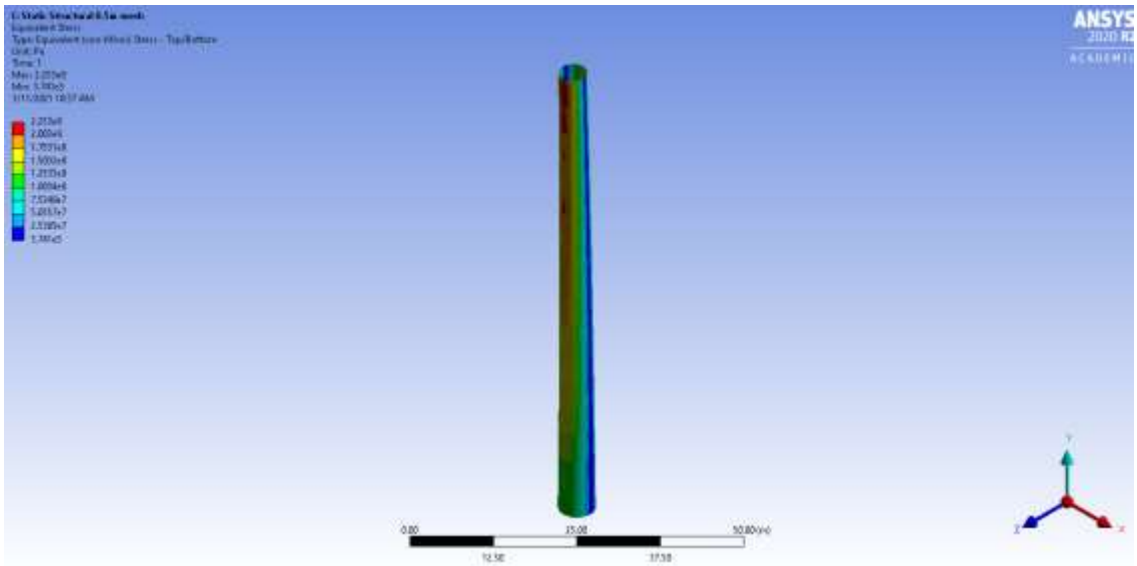

Figure 4.2. Static structural equivalent stress.

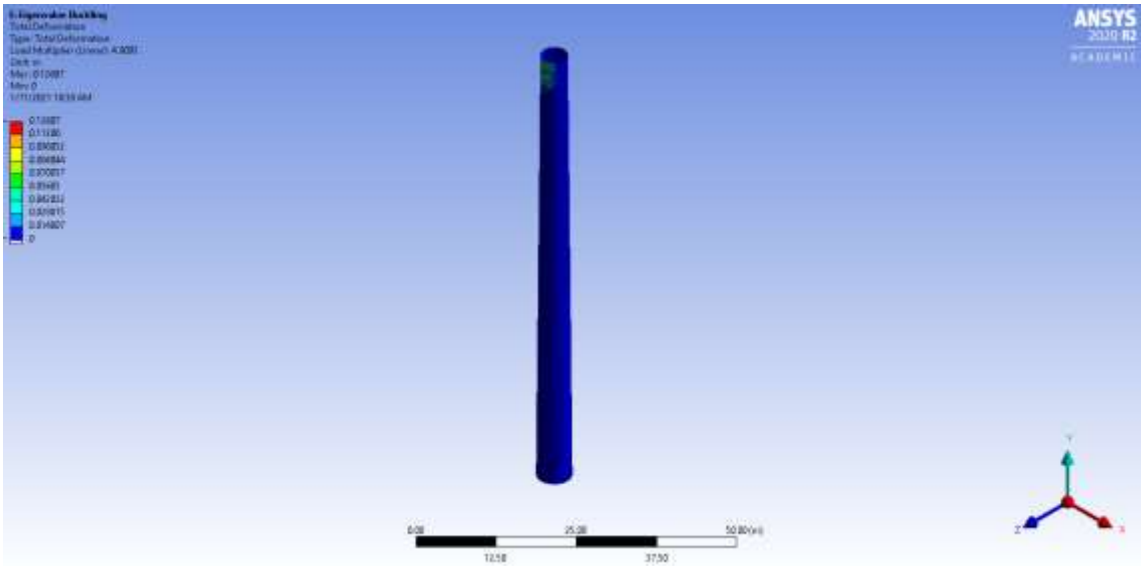

Figure 4.3. Eigenvalue buckling analysis.

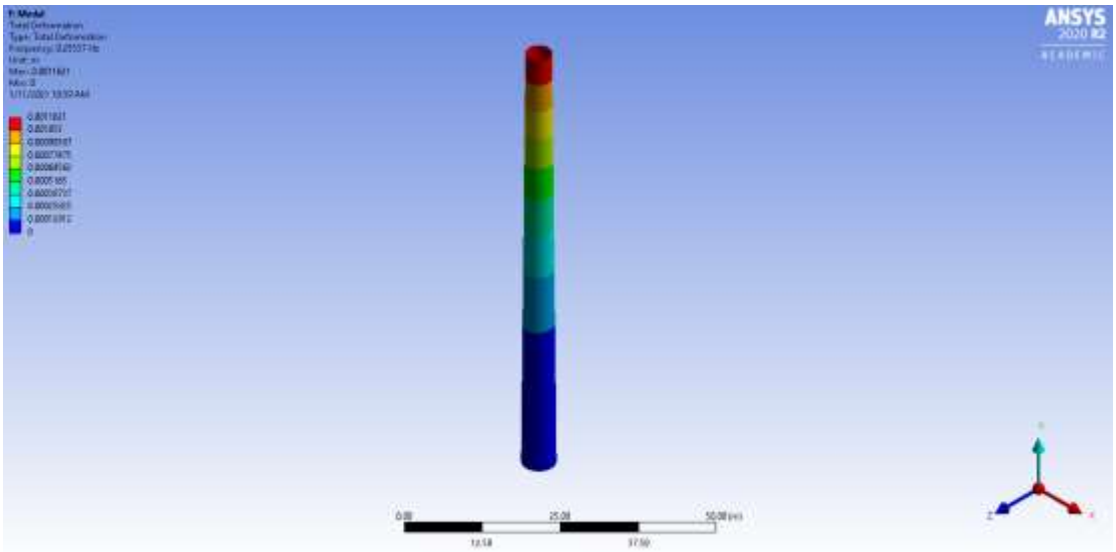

Figure 4.4. Modal Analysis, natural frequency, 1st mode.

Table 4.1. Baseline Steel Tower Verification.

	Maximum (Tomczak)	Maximum (Wang, et. al., 2019)	%Difference
Directional Deformation (m)	0.849	0.965	12.04%
Von-Mises Stress Distribution (Pa)	2.25E+08	2.0487E+08	-9.97%
Frequency (Hz)	0.255	0.298	14.18%
Load Multiplier	4.909	3.329	-47.79%

Listed above in Table 3.1. is the comparison between Wang et al. [37] and the reproduction steel tower. Directional deformation was measured using Static Structural Analysis. The maximum recorded deformation from the reproduction steel tower was 0.84889 m, with a difference of 12% in comparison. Von-mises stress was also measured using Static Structural, with a difference of 10% from Wang et al. [37]. Natural frequencies of the two towers were within 14.2% difference. The primary results of the stress and the natural frequency resulting from the static structural is in the range of Wang et al. [37]. These three measurements are within 15% difference which is reasonable given that it is assumed that not all the information was outlined in the paper for reproducing the model.

The only large difference is between the load multiplier calculated in ANSYS module Eigenvalue Buckling. There is a 48% difference between the two models. The results of the findings raise some questions for some of the parameters. This could be a result of inconsistent geometry or material properties between the reproduction model and Wang et al. [37] model. Some of the assumptions that were made based on having no information in Wang et al. [37] that may have induced differences include: loading conditions, fixed joint conditions between segments, geometry and the ANSYS analysis process. Overall, the verification study is in the range of Wang et al. [37].

4.2 Concrete Tower Results

The loading on the three concrete towers is discussed in Section 3 and reported in Table 3.5 Tower geometries, material properties and forces have been reported in Section 3.2.

The results of the concrete tower analysis are summarized in Table 4.2 below. Figure 4.5-10 show a graphical representation of Table 4.2. Shown in Table 4.2. below, the directional deformation shows increases with an increase in the tower height, which is expected. The same loading is applied to the towers with the height as the only variable; it can be assumed that the deflection will be increased, as the results show. The tower natural frequency and load multiplier decreased as tower height increased which is also expected.

The minimum principal stress increased as tower height increased. The results are showing that the 150 m and 200 m towers are very similar in minimum and maximum principal stresses and von-mises stress. This could be caused by the fact that the post tensioning forces were extrapolated from the base 100 m tower. The towers should have similar stresses since the post tension loads vs. height is similar. Another thing to note is that the turbine loading on the towers are the same for all three towers, in real life this would be unlikely to occur. As towers increase in height, the towers would be able to accommodate larger turbine blade diameters, increasing the loads on the tower, thus increasing the stresses in the tower. As stated previously, the industry has been moving

towards increasing the energy generation of turbines, with the increase in tower height, it is attractive to also increase the turbine size to produce more energy, consequently increasing the tower loading. The tower cross-section in this study has the space to add additional post tensioning tendons to accommodate additional loads from future larger turbines.

Table 4.2. Concrete Turbine Tower Results.

Tower	**100**	**150**	**200**
Directional Deformation (m)	0.22548	0.2787	0.34264
Minimum Principle (Compressive) stress (Pa)	-1.77E+07	-1.84E+07	-1.85E+07
Maximum Principle (Tensile) Stress (Pa)	2.88E+05	2.27E+05	2.28E+05
Von-Mises Stress Distribution (Pa)	1.98E+07	1.85E+07	1.85E+07
Frequency (Hz)	0.40241	0.34149	0.27485
Load Multiplier	6.557	5.3008	4.6347

Table 4.4. lists the maximum values for the concrete towers based on stress and deflection limits. The maximum allowable deflection was implemented based on the concern that excessive tower deflection could result in the turbine blades impacting the turbine tower. The equation used is detailed in the equation section, used by Nicholson [23], which was obtained from the ACI 307 [2]. Maximum compressive and maximum tensile stress was calculated based on ACI 318-19, section 24.5 [1] to make sure the concrete would be able to handle the stresses placed on the tower by the turbine loading. Comparing the results with the design constraints laid out in Table 3.3, the results are within the constraints of the analysis and are an adequate preliminary design for our purposes.

In addition, all three PT concrete towers were analyzed in ANSYS with nonlinear affects (P-Delta affects) as shown in Table 4.3. P-delta affects consider additional stresses due to the lateral displacement occurring at the top of a tower or column. Lateral displacement causes the vertical point load to act with an eccentricity, offset from the center of the column, adding additional moment to the column.

As shown below in Table 4.3, all the towers analyzed with p-delta affects have a higher directional deformation than the towers that do not consider p-delta affects. This trend is reasonable since it is caused by the additional stresses on the tower when a vertical point load acts on a tower that has deflected. Minimum principal stress all shows slight increases with p-delta towers over the non p-delta towers. Maximum principal stress shows a decrease in the p-delta towers in comparison to the non p-delta towers. The von-mises stresses showed a slight increase in the 150 m and 200 m towers, while the 100 m tower showed a slight decrease. This could be caused by the much higher rate of deflection change coming from the 150 m and 200 m towers. The load multipliers for the p-delta towers decrease in comparison to the non-p-delta towers. The rate of decrease is dependent on the tower height. In general frequency also decreases with the p-delta towers analyzed. The frequency for the 100 m tower is very similar for both towers analyzed with and without p-delta affects. This could be since deflection did not change nearly as much as the 150 m and 200 m towers.

Table 4.3. Concrete Turbine Tower Results.

Tower	**100**	**100 P-delta**	**150**	**150 P-delta**	**200**	**200 P-delta**
Directional Deformation (m)	0.22548	0.26614	0.2787	0.3436	0.34264	0.43691
Minimum Principle (Compressive) stress (Pa)	1.77E+07	1.80E+07	1.84E+07	1.87E+07	1.85E+07	1.87E+07
Maximum Principle (Tensile) Stress (Pa)	2.88E+05	*2.06E+05	2.27E+05	2.10E+05	2.28E+05	2.09E+05
Von-Mises Stress Distribution (Pa)	1.98E+07	1.79E+07	1.85E+07	1.87E+07	1.85E+07	1.87E+07
Frequency (Hz)	0.40241	0.40257	0.34149	0.31009	0.27485	0.24637
Load Multiplier	6.557	5.5602	5.3008	4.3034	4.6347	3.6369

*Maximum tensile stress occurs at the tower midspan as opposed to the tower top.

Table 4.4. Constraints

Tower	**100**	**150**	**200**
Maximum allowable deflection (Ref. [20])	1.25	1.875	2.5
Maximum Compressive stress (Pa)	2.90E+07	2.90E+07	2.90E+07
Maximum Tensile Stress (Pa)	4.33E+06	4.33E+06	4.33E+06

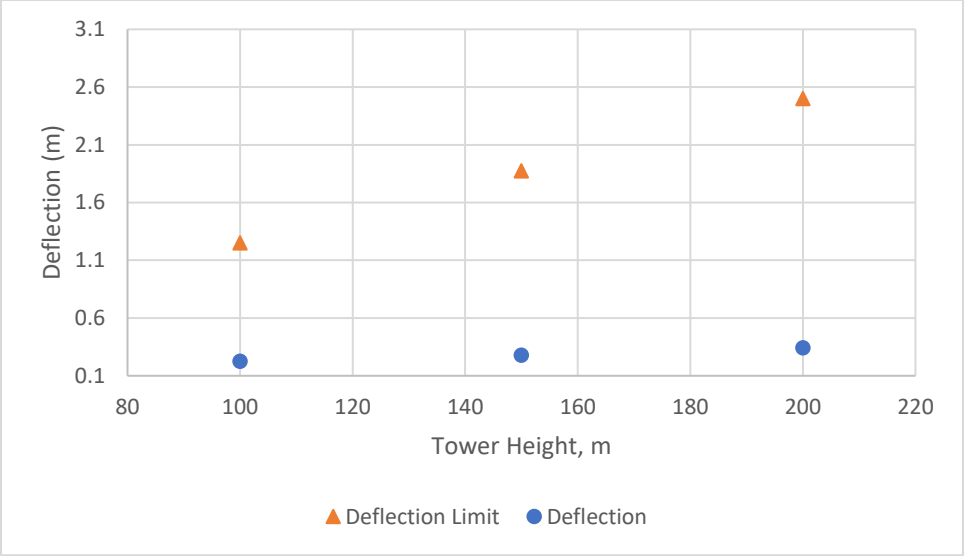

Figure 4.5. Deflection vs. Tower Height.

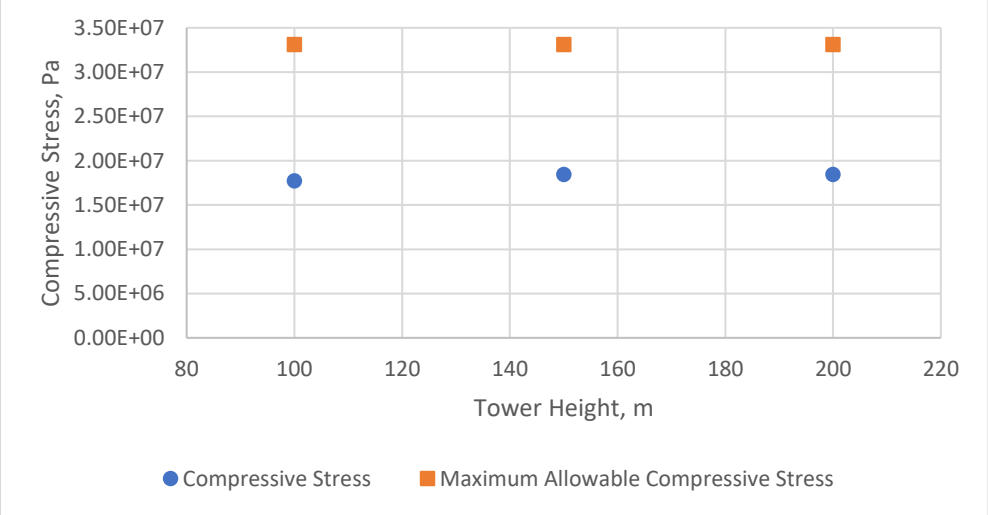

Figure 4.6. Compressive Stress vs. Tower Height.

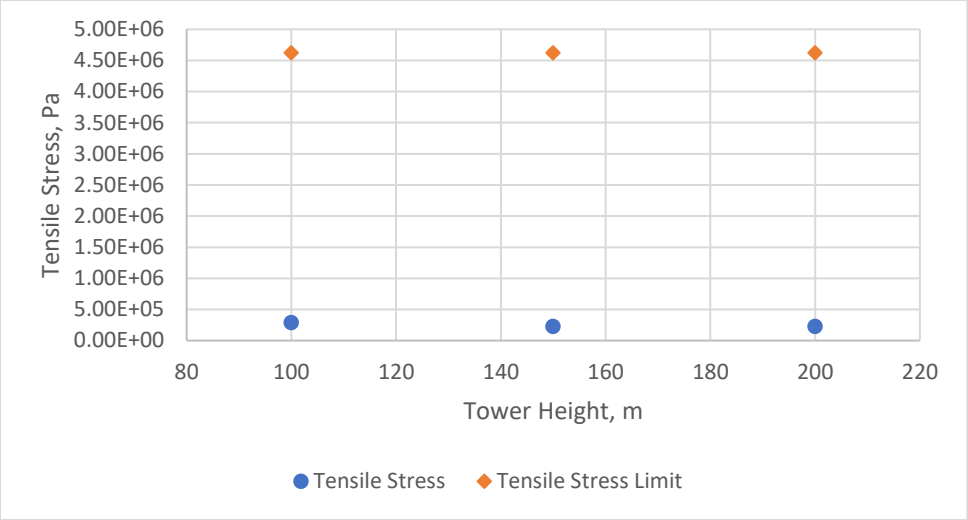

Figure 4.7. Tensile Stress vs. Tower Height.

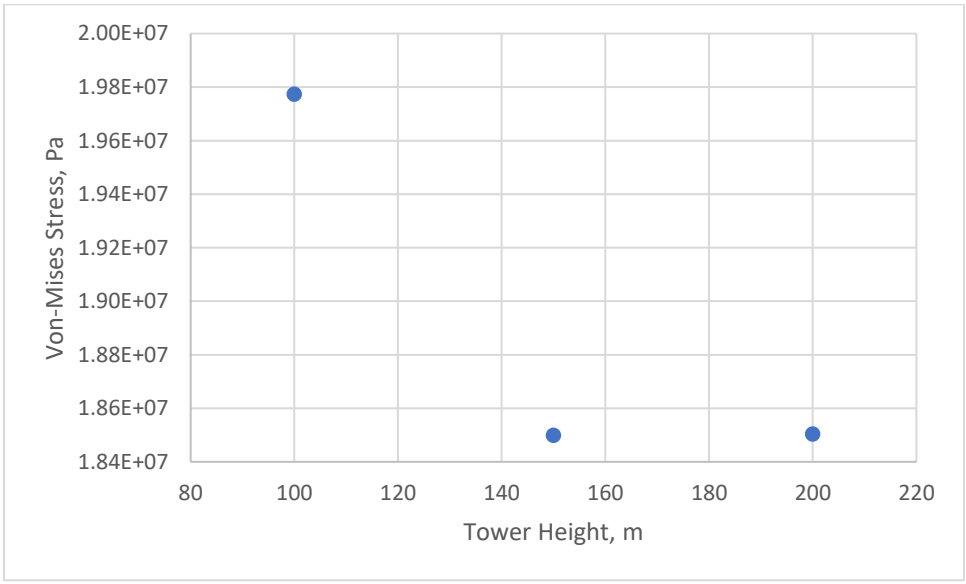

Figure 4.8. Von-Mises Stress vs. Tower Height.

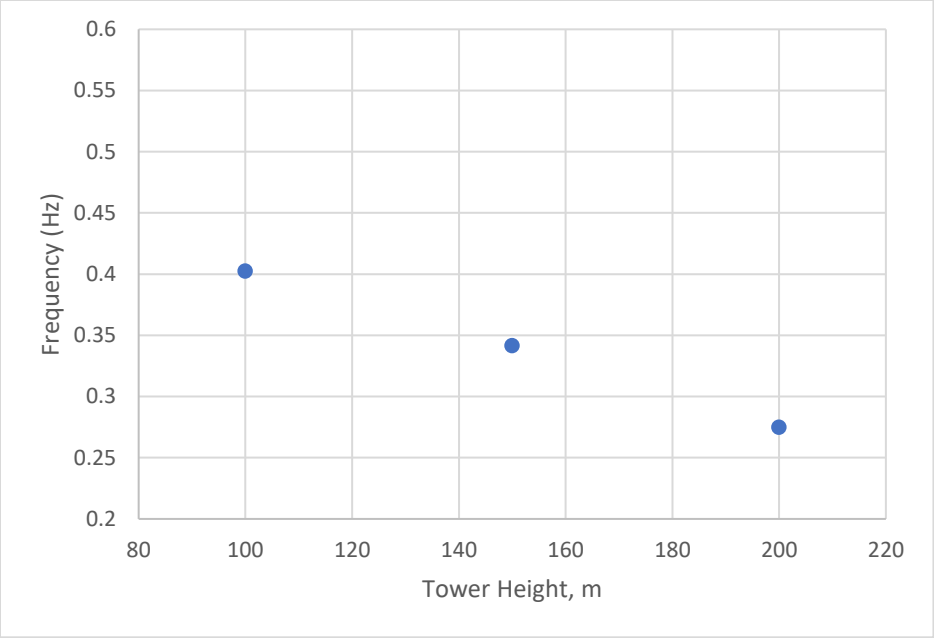

Figure 4.9. Frequency vs. Tower Height.

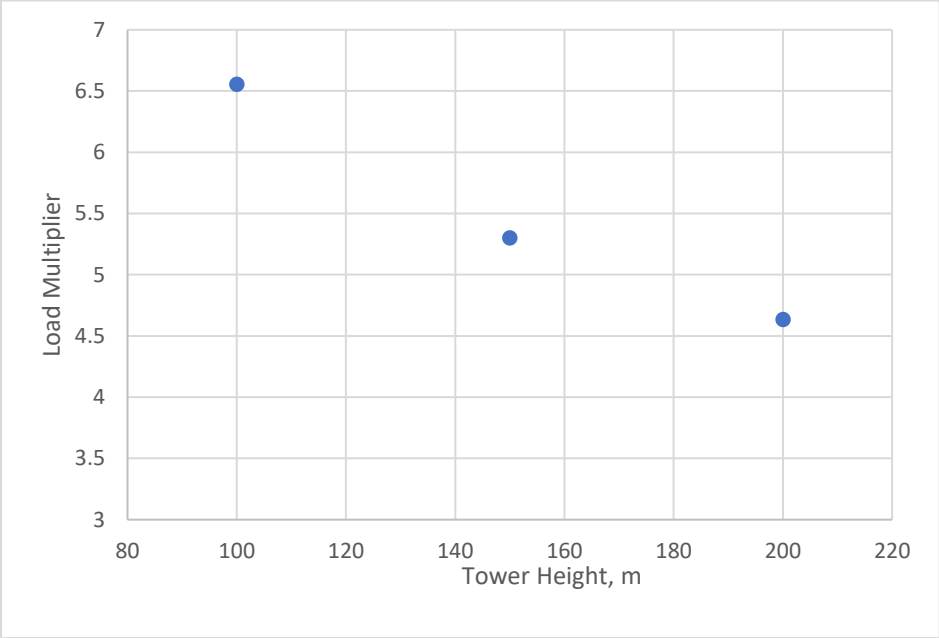

Figure 4.10. Load Multiplier vs. Tower Height.

To verify tower models a hand calculation was performed for the natural frequency of the 100 m tower (Equation 4). The results of the process are summarized below in Table 4.5.

The difference between the hand calculated natural frequency and the ANSYS reported value was 10.8%, leading to additional confidence in the model results.

Table 4.5. Hand calculated Natural Frequency, concrete tower 100 m.

Tower Diameter	**Equation 12 (Hz)**	**ANSYS Reported (Hz)**	**%Difference**
Minimum (Top)	0.289		
Average	0.446	0.40241	10.8%
Maximum (Base)	0.602		

Natural Frequency Hand Calculations

Average natural frequency was calculated using the average tower diameter and wall thickness of the 100 m tower. Equation 12 obtained from Ref. [32] was used to estimate the natural frequency.

$$\omega = 1.875^2 * \sqrt{\frac{E*I}{\rho*A*L^4}}$$

(Equation 12)

E=Modulus of Elasticity composite tower = 3915.25 MPa (composite over 100m tower, Equation 6 for procedure)
I=Moment of Inertia=22.75 m^4
A=5.705 m^2
L=100 m
ρ=density, see composite=2463.4 kg/m^3

$$\omega=1.875^2 * \sqrt{\frac{3.92E+10\ Pa*22.75\ m^4}{2463.4\ \frac{kg}{m^3}*5.705m^2*100m^4}}=0.446\ \text{Hz}$$

The results for the reduced post tensioning force towers are listed below in Table 4.6. The 150 m concrete tower was used in the analysis of the reduced post tension forces. The post tensioned forces were reduced to 90%, 80% and 70% of the original post tension force. Graphical representation of the results is shown in Figures 4.11-16.

As expected, concrete stresses varied with post tensioning force. The directional deformation was unaffected by the reduction of the post tensioning force, but this is a result of modeling the post tensioning force as a single, centered vertical force. Future

models may discretely model the individual tendons. However, for evaluation of basic stresses in a stiff tower, the model used in this study provides the basic information needed for design.

The minimum principal stress and von mises stress decreased with the decrease in post tension force, as expected. While the maximum principal stress increased with the decrease in the post tension force. The reason for this pattern is that as the axial force decreased, the compressive stress will decrease while the tensile stress will increase. The tower natural frequency remained the same. Frequency is not affected by any changes in loading. Frequency is controlled through modulus of elasticity and geometry properties. An increase in the load multiplier (factor of safety) is also noted. Additionally, one thing to note is that the tensile stress increased parabolically as the post tensioning force decreased linearly, as illustrated in Figures 4.13. The only variable that changes with the reduced post tensioned towers are the axial post tensioning forces.

Another benefit to running the towers with a reduced post tensioned force is that it will help determine if the tower analyzed was overdesigned. Comparison between the 70% P-T force and the constraints show that the 70% still meets the requirements. This points to the conclusion that the tower has more post tensioning than is needed and further refinement is suggested for future work once specific location and foundation requirements are known.

Table 4.6. Concrete Turbine Tower Results-Reduced P-T Force Comparison.

Tower Post-Tensioning Force (%)	**100**	**90**	**80**	**70**
Tower Height (m)	150	150	150	150
Directional Deformation (m)	0.2787	0.2787	0.2787	0.2787

Minimum Principal (Compressive) stress (Pa)	-1.84E+07	-1.75E+07	-1.66E+07	-1.57E+07
Maximum Principal (Tensile) Stress (Pa)	2.27E+05	2.23E+07	2.72E+07	4.17E+07
Von-Mises Stress Distribution (Pa)	1.85E+07	1.77E+07	1.67E+07	1.57E+07
Frequency (Hz)	0.34149	0.34149	0.34149	0.34149
Load Multiplier	5.3008	5.7624	6.3121	6.9775

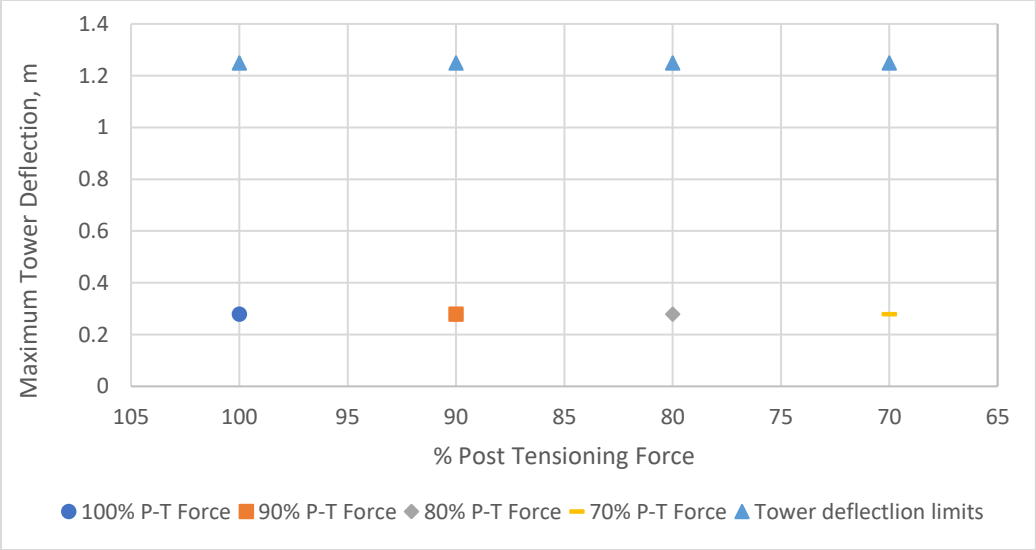

Figure 4.11. Deflection vs. Post Tensioning Force.

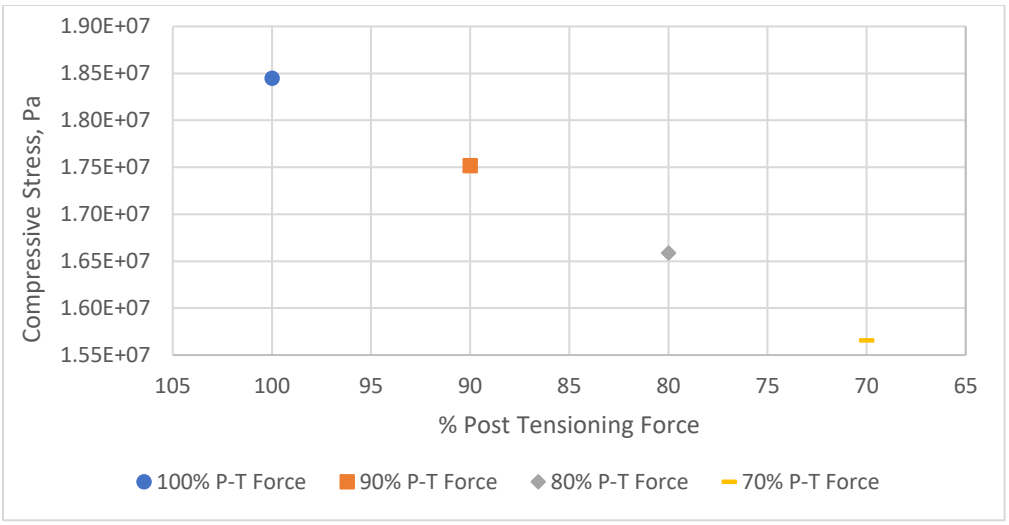

Figure 4.12. Compressive Stress vs. Post Tensioning Force.

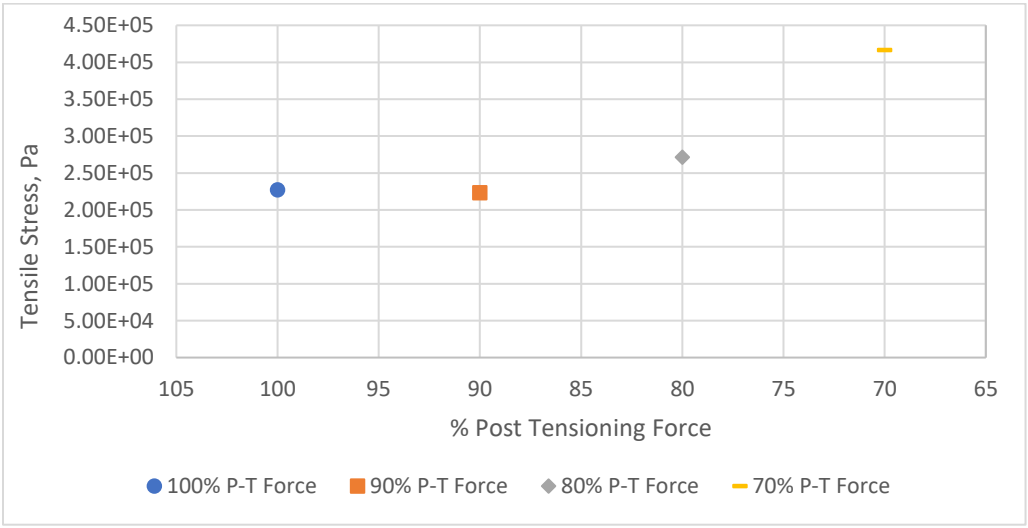

Figure 4.13. Tensile Stress vs. Post Tensioning Force.

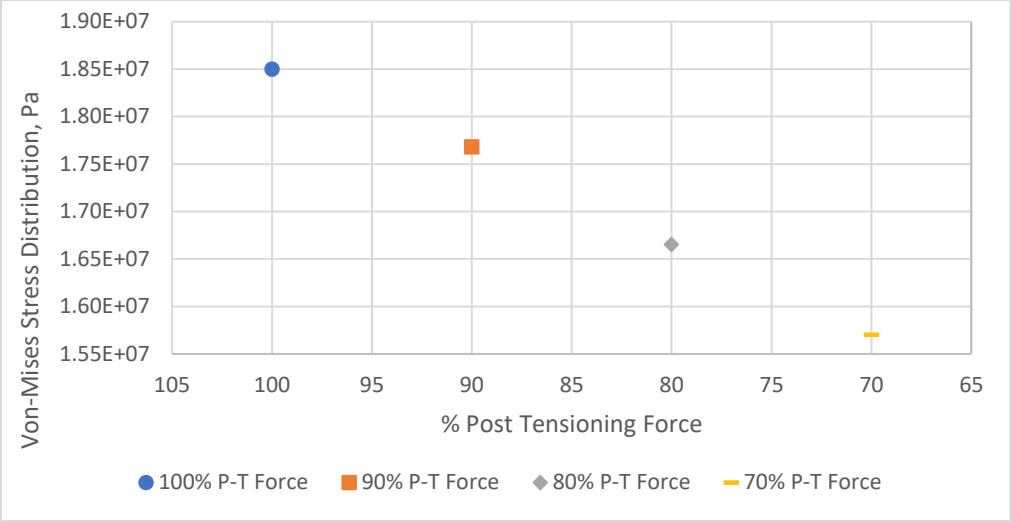

Figure 4.14. Von-Mises Stress vs. Post Tensioning Force.

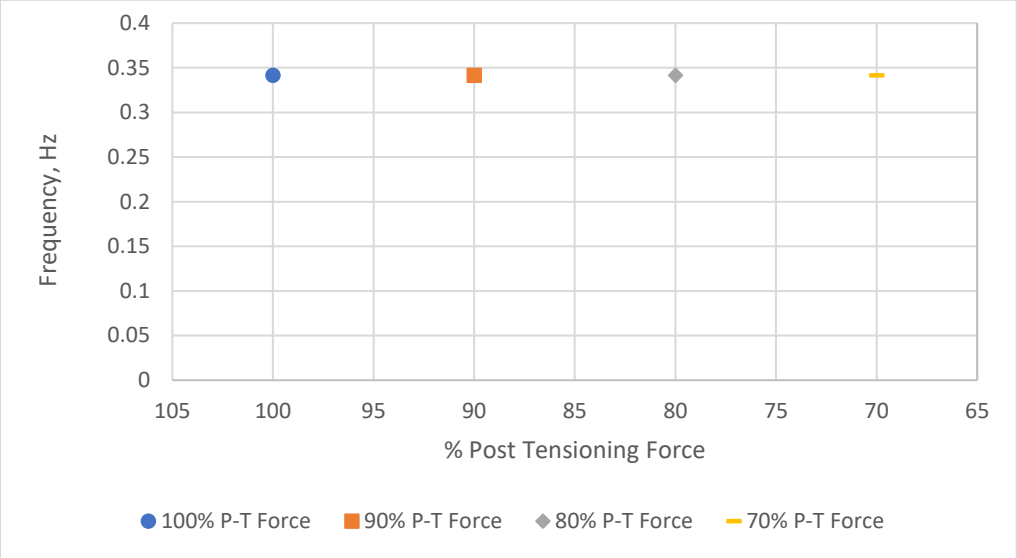

Figure 4.15. Frequency vs. P-T Force.

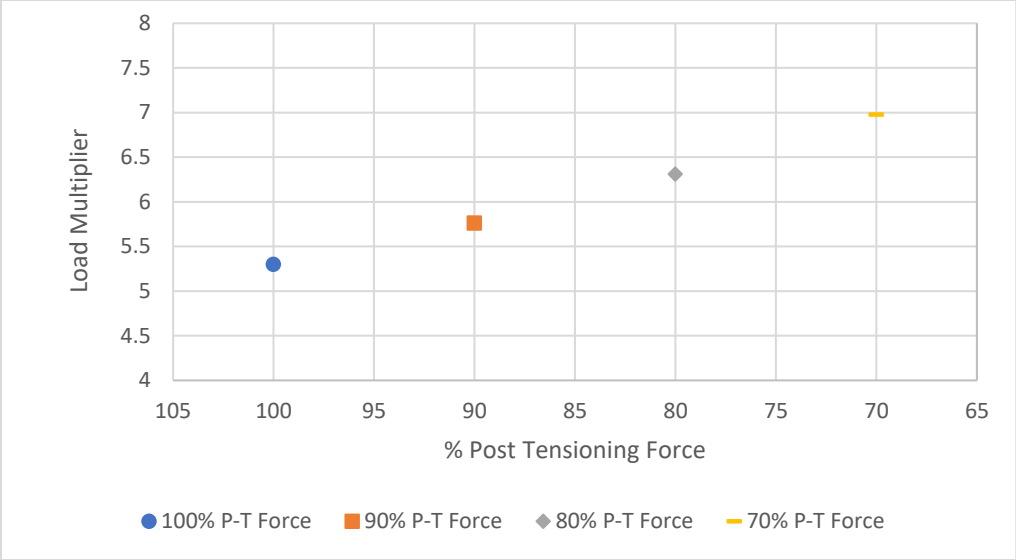

Figure 4.16. Load Multiplier vs. P-T Force.

Based on the above tables, the concrete towers modeled in this study are adequate to support the assumed loading. Further refinement of the turbine loading, and base constraints based on a determined site and turbine model would be the next step for a full design. Refinement would include location selection and wind studies to determine the most extreme wind loading on the turbines at the specific location of interest. Increasing turbine blade length should be considered for taller wind turbines to meet market demand. As stated earlier, the market is transitioning to larger turbine blades along with taller towers to produce more energy. The tower design used in this study would then be further refined to be more efficient with materials including post tensioning quantities and layout.

5.0 Summary and Conclusions

Recent market trends have shown that the wind energy industry has been moving towards taller towers with larger turbine blades to increase the wind energy potential. The more traditionally used steel towers are not economically feasible for towers taller than 80 m due to the increased cost in the transportation and field fabrication of larger steel segments. At approximately 80 m, concrete towers begin to become economical, constructable and efficient compared to steel towers.

The use of post-tensioned concrete in wind turbine towers is a new and developing market for high wind turbine towers. The use of tall wind turbines can be utilized in areas where there is little or no wind resource at low hub heights. Using taller towers can allow developers to produce wind energy in areas that were not feasible at low hub heights (i.e., south-eastern United States).

This research has analyzed a steel tower by performing a verification study that matched well with the source research. Additionally, this research has evaluated the feasibility of using post-tensioned concrete in wind turbine tower applications.

Multiple concrete towers of different heights (100 m, 150 m, 200 m) were modeled in ANSYS to measure the von-mises, maximum and minimum principal stress, total deformation (using Static Structural ANSYS module) and total deformation (Eigenvalue buckling and Modal ANSYS module).

The concrete tower models showed a feasible base for the constraints of interest. The models presented in this research all show that concrete is a viable option for tall turbine tower materials. Additionally, the model developed provides baseline information needed for evaluating general post-tensioning tendon layouts and capacities. Further research is required for specific locations of interest. Tower design optimization should also be done

on a case-by-case basis since conditions (soil, wind speed, and many others) at each tower location vary.

6.0 Bibliography

[1] ACI Committee 318, 2019. Building Code Requirements for Structural Concrete (ACI 318-19): An ACI Standard; Commentary on Building Code Requirements for Structural Concrete (ACI 318R-19). American Concrete Institute.

[2] ACI 307, 'Code Requirements for Reinforced Concrete Chimneys (ACI 307-08) and Commentary, American Concrete Institute, 2008.

[3] ASCE and AWEA, 2011. Recommended practice for compliance of large land-based wind turbine support structures.

[4] ASCE/SEI (ASCE/Structural Engineering Institute). (2016). "Minimum design loads for buildings and other structures." *ASCE/SEI 7-16*, Reston, VA.

[5] Camargo, E.A., Ulfkjaer, J.P., Brincker, R., Nøergaard, J. and Gadegaard, S.S., 2019. Operational Modal Analysis and Finite-Element Model Updating of Pilot Concrete Wind Turbine Tower. Journal of Structural Engineering, 145(2), p.05018003.

[6] Dillon, L. (2018, September 10). California to rely on 100% clean electricity by 2045 under bill signed by Gov. Jerry Brown. *Los Angeles Times.*

[7] Dolan, C. W., Morgan, K. B., & Kuchma, D. A. (2016). *Report on Design of Concrete Wind Turbine Towers*. Farmington Hills, MI: American Concrete Institute.

[8] Eller, Donnelle. (2016, June 28). Watch MidAmerican build tallest wind turbine in the U.S. *Desmoinesregister.*

[9] (2020, February 11). FINITE ELEMENT ANALYSIS SOFTWARE (FEA SOFTWARE). *Autodesk.com.* https://www.autodesk.com/solutions/finite-element-analysis

[10] Global Wind Energy Council. (2017). Global Wind Report: Annual Market Update 2017.

[11] Harte, R. and Van Zijl, G.P., 2007. Structural stability of concrete wind turbines and solar chimney towers exposed to dynamic wind action. *Journal of Wind engineering and industrial aerodynamics*, *95*(9-11), pp.1079-1096.

[12] History of Wind Energy. *Energy.gov.* https://www.energy.gov/maps/map-projected-growth-wind-industry-now-until-2050

[13] IEC. (2021, June 6). IEC 61400. https://webstore.iec.ch/searchform&q=IEC%2061400

[14] Jin, Q. and Li, V.C., 2019. Structural and durability assessment of ECC/concrete dual-layer system for tall wind turbine towers. Engineering Structures, 196, p.109338.

[15] Kenna, A. and Basu, B., 2015. A finite element model for pre-stressed or post-tensioned concrete wind turbine towers. *Wind Energy*, *18*(9), pp.1593-1610.

[16] Kim, B.J., Plodpradit, P., Kim, K.D. and Kim, H.G., 2018. Three-dimensional analysis of prestressed concrete offshore wind turbine structure under environmental and 5-MW turbine loads. Journal of Marine Science and Application, 17(4), pp.625-637.

[17] Knoll, F., Prosser, M.J. and Otter, J., 1976. Prestressing the CN Tower. Prestressed Concrete Institute Journal, 21(3), pp.84-111.

[18] LaNier, M.W., 2005. *LWST Phase I project conceptual design study: Evaluation of design and construction approaches for economical hybrid steel/concrete wind turbine towers; June 28, 2002--July 31, 2004* (No. NREL/SR-500-36777). National Renewable Energy Lab., Golden, CO (US).

[19] Lantz, E.J., Roberts, J.O., Nunemaker, J., DeMeo, E., Dykes, K.L. and Scott, G.N., 2019. Increasing wind turbine tower heights: Opportunities and challenges (No. NREL/TP-5000-73629). National Renewable Energy Lab.(NREL), Golden, CO (United States).

[20] Laszlo P. Kollar, George S. Springer. *Mechanics of Composite Structures.* Cambridge University Press, 2009.

[21] Lotfy, I., 2012. Prestressed concrete wind turbine supporting system.

[22] Ma, H. and Meng, R., 2014. Optimization design of prestressed concrete wind-turbine tower. Science China Technological Sciences, 57(2), pp.414-422.

[23] Nicholson, John Corbett. "Design of wind turbine tower and foundation systems: optimization approach." MS (Master of Science) thesis, University of Iowa, 2011. https://doi.org/10.17077/etb.bhnu76gr

[24] *North American Annual Average Wind Speed at 100-Meter above Surface Level*, NREL 2017, https://www.nrel.gov/gis/assets/images/wtk-100-north-america-50-nm-01.jpg

[25] PCI Design Handbook, 8th Edition.

[26] Peggar, R., 2017. Design and structural testing of tall Hexcrete wind turbine towers.

[27] Roberts, D. (2019, May 20). These huge new wind turbines are a marvel. They're also the future. *Vox* https://www.energy.gov/eere/wind/history-us-wind-energy

[28] Roberts, D. (2016, June 1). The tallest wind power tower in the US, assembled in one hypnotizing video. *Vox.*

[29] Rycroft, Mike. (2017, January 11). Concrete towers lift wind turbines to new heights. *EE Publishers* https://www.ee.co.za/article/concrete-towers-lift-wind-turbines-new-heights.html

[30] *U.S. Wind Speed at 200-Meter above Surface Level*, NREL 2017, https://www.nrel.gov/gis/assets/images/wtk-200m-2017-01.jpg

[31] Van Zyl, W.S. and Van Zijl, G.P.A.G., 2015. Dynamic behaviour of normally reinforced concrete wind turbine support structures. Journal of the South African Institution of Civil Engineering, 57(4), pp.38-44.

[32] Veritas, N., 2002. *Guidelines for design of wind turbines*. Det Norske Veritas: Wind Energy Department, Ris National Laboratory.

[33] vlab.amrita.edu,. (2011). Free Vibration of a Cantilever Beam (Continuous System). Retrieved 16 January 2021, from vlab.amrita.edu/?sub=3&brch=175&sim=1080&cnt=1

[34] VSL (03/2013). VSL POST-TENSIONING SOLUTIONS.

[35] Sunshine Skyway Bridge: Construction, History & Facts. *Study.com.* https://study.com/academy/lesson/sunshine-skyway-bridge-construction-history-facts.html

[36] Sritharan, Sri. (2011, June 2). Wind Turbine Systems – Soils, Foundation and Tower. Wilson Engineering.11

[37] Wang, L., Kolios, A., Luengo, M.M. and Liu, X., 2016. Structural optimisation of wind turbine towers based on finite element analysis and genetic algorithm. *Wind Energy Sci. Discuss*.

[38] Wight, J. K., 2016. Reinforced Concrete Mechanics and Design. Pearson.

Appendix A

Table Appendix A-1.1. Envelope Forces for wind turbine Ref [4].

The Envelope Force for Wind Turbine Loads at 100m Hub Height					
		No SafetyFactor			
		Thrust	Moment	Vertical	Torsion
		Fh(kN)	Mh(kNm)	Fz(kN)	Mz(kN)
1.5 MW	EWM50	384	3,805	832	1,966
	EOG50	403	1,468	832	232
	Fat. Load	57	567		551
3.6 MW	EWM50	1,086	16,767	3,155	5,961
	EOG50	1,199	9,913	3,129	1,597
	Fat. Load	143	2,213		2,220
5.0 MW	EWM50	578	28,568	4,998	5,834
	EOG50	1,065	19,337	4,879	3,714
	Fat. Load	197	3,687		3,483
	Including	SafetyFactor	1.35		
		Thrust	Moment	Vertical	Torsion
		Fh(kN)	Mh(kNm)	Fz(kN)	Mz(kN)
1.5 MW	EWM50	518	5,137	1,123	2,654
	EOG50	544	1,982	1,123	313
3.6 MW	EWM50	1,466	22,635	4,259	8,048
	EOG50	1,619	13,382	4,224	2,156
5.0 MW	EWM50	781	38,567	6,747	7,876
	EOG50	1,437	26,105	6,587	5,014
	GE Load	SafetyFactor	1.35		
		Thrust	Moment	Vertical	Torsion
		Fh(kN)	Mh(kNm)	Fz(kN)	Mz(kN)
1.5 MW	EWM50	514	4,358	1320	3,310
	Diff.(%)	-0.84%	-15.17%	17.52%	24.71%
	Fat. Load	52	550		
	Diff.(%)	-8.77%	-3.01%		
3.6 MW	EWM50	1,245	14,413	3,406	13,879
	Diff.(%)	-15.13%	-36.32%	-20.03%	72.46%
	Fat. Load	148	2355		
	Diff.(%)	3.85%	6.40%		
5.0 MW	EWM50	1,693	22,244	4,685	22,110
	Diff.(%)	116.85%	-42.32%	-30.56%	180.73%
	Fat. Load	207	3760		
	Diff.(%)	5.08%	1.97%		

Envelope Forces for Wind Turbine Loads
100 m Hub Height
(after Reference 26)

Table J-6

Table Appendix A-1.2. 100 m Concrete Tower Dimensions.

Segment	Location of Segment	Height (m)	Thickness (m)	Diameter (m)
1	Base	0	0.724	7.62
2	Base	5	0.724	7.4219
3	Base	10	0.724	7.2238
4	Base	15	0.724	7.0257
5	Base	20	0.724	6.8276
6	Base	25	0.724	6.6295
7	Base	30	0.724	6.4314
8	Base	35	0.724	6.2333
9	Base	40	0.724	6.0352
10	Base	45	0.724	5.8371
11	Base	50	0.5715	5.639
12	Base	55	0.5715	5.4409
13	Base	60	0.5715	5.2428
14	Base	65	0.5715	5.0447
15	Base	70	0.5715	4.8466
16	Base	75	0.5715	4.6485
17	Base	80	0.5715	4.4504
18	Base	85	0.5715	4.2523
19	Base	90	0.5715	4.0542
20	Base	95	0.5715	3.8561
20	Top	100	0.5715	3.658

Table Appendix A-1.3. 150 m Concrete Tower Dimensions.

Segment		Height	Thickness	Diameter
1	**Base**	0	0.9525	9.601
2	**Base**	5	0.9525	9.4029
3	**Base**	10	0.9525	9.2048
4	**Base**	15	0.9525	9.0067
5	**Base**	20	0.9525	8.8086
6	**Base**	25	0.9525	8.6105
7	**Base**	30	0.9525	8.4124
8	**Base**	35	0.9525	8.2143
9	**Base**	40	0.9525	8.0162
10	**Base**	45	0.9525	7.8181
11	**Base**	50	0.724	7.62
12	**Base**	55	0.724	7.4219
13	**Base**	60	0.724	7.2238
14	**Base**	65	0.724	7.0257
15	**Base**	70	0.724	6.8276
16	**Base**	75	0.724	6.6295
17	**Base**	80	0.724	6.4314
18	**Base**	85	0.724	6.2333
19	**Base**	90	0.724	6.0352
20	**Base**	95	0.724	5.8371
21	**Base**	100	0.5715	5.639
22	**Base**	105	0.5715	5.4409
23	**Base**	110	0.5715	5.2428
24	**Base**	115	0.5715	5.0447
25	**Base**	120	0.5715	4.8466
26	**Base**	125	0.5715	4.6485
27	**Base**	130	0.5715	4.4504
28	**Base**	135	0.5715	4.2523
29	**Base**	140	0.5715	4.0542
30	**Base**	145	0.5715	3.8561
31	**Top**	150	0.5715	3.658

Table Appendix A-1.4. 200 m Concrete Tower Dimensions.

Segment		Height	Thickness	Diameter
1	Base	0	1.3335	11.582
2	Base	5	1.3335	11.3839
3	Base	10	1.3335	11.1858
4	Base	15	1.3335	10.9877
5	Base	20	1.3335	10.7896
6	Base	25	1.3335	10.5915
7	Base	30	1.3335	10.3934
8	Base	35	1.3335	10.1953
9	Base	40	1.3335	9.9972
10	Base	45	1.3335	9.7991
11	Base	50	0.9525	9.601
12	Base	55	0.9525	9.4029
13	Base	60	0.9525	9.2048
14	Base	65	0.9525	9.0067
15	Base	70	0.9525	8.8086
16	Base	75	0.9525	8.6105
17	Base	80	0.9525	8.4124
18	Base	85	0.9525	8.2143
19	Base	90	0.9525	8.0162
20	Base	95	0.9525	7.8181
21	Base	100	0.724	7.62
22	Base	105	0.724	7.4219
23	Base	110	0.724	7.2238
24	Base	115	0.724	7.0257
25	Base	120	0.724	6.8276
26	Base	125	0.724	6.6295
27	Base	130	0.724	6.4314
28	Base	135	0.724	6.2333
29	Base	140	0.724	6.0352
30	Base	145	0.724	5.8371
31	Base	150	0.5715	5.639
32	Base	155	0.5715	5.4409
33	Base	160	0.5715	5.2428
34	Base	165	0.5715	5.0447
35	Base	170	0.5715	4.8466
36	Base	175	0.5715	4.6485
37	Base	180	0.5715	4.4504

38	Base	185	0.5715	4.2523
39	Base	190	0.5715	4.0542
40	Base	195	0.5715	3.8561
41	Top	200	0.5715	3.658

Table Appendix A-1.5. 100m Concrete Tower Composite Material Properties.

				Steel properties						
	Number of PT Tendons	Area of Strands (in^2)	average d (m)	avg. t (m)	xarea of tube (m2)	poisson ratio	Area of strands (m^2)	vf (volume fraction of strand)	Ef (Mpa)	Steel Density (kg/m^3)
0-50m	56	145.824	6.6295	0.724	7.539442236	0.3	0.09407981	0.012478	196500	7850
50-100	34	88.536	4.6485	0.5715	4.173005403	0.3	0.05711989	0.013688	196500	7850

	Concrete Properties				composite properties			
	Vm (volume fraction of matrix)	Em (psi) (concrete) (in ANSYS)	Em (MPa) (concrete) (in ANSYS)	Concrete poisson ratio	Concrete Density (kg/m^3)	Young's Modulus (Mpa)	poisson's ratio	density (kg/m^3)
0-50m	0.987521648	5.38E+06	37089.65738	0.1414	2392	39078.84	0.14337907	2460.107
50-100	0.986312051	5.38E+06	37089.65738	0.1414	2392	39271.66	0.14357091	2466.709

Table Appendix A-1.6. 150m Concrete Tower Composite Material Properties.

				Steel properties					
	Number of PT Strands	Area of Strands (in^2)	averaged (m)	avg. t (m)	Xarea of tube (m2)	poisson ratio	Area of strands (m^2)	vf (volume fraction of strand)	Steel Density (kg/m^3)
0-50m	78	203.112	8.6105	0.931727	12.60193	0.3	0.13104	0.010398	7850
50-100	56	145.824	6.6295	0.710136	7.395072	0.3	0.09408	0.012722	7850
100-150	34	88.536	4.6485	0.5715	4.173005	0.3	0.05712	0.013688	7850

	Concrete Properties						composite properties		
	Ef (Mpa)	Vm (volume fraction of matrix)	Em (psi) (concrete) (in ANSYS)	Em (MPa) (concrete) (in ANSYS)	Concrete poisson ratio	Concrete Density (kg/m^3)	Young's Modulus (Mpa)	poisson's ratio	density (kg/m^3)
0-50m	196500	0.989602	5.38E+06	37089.66	0.1414	2392	38747.27	0.143049	2448.754
50-100	196500	0.987278	5.38E+06	37089.66	0.1414	2392	39117.67	0.143418	2461.436
100-150	196500	0.986312	5.38E+06	37089.66	0.1414	2392	39271.66	0.143571	2466.709

Table Appendix A-1.7. 200m Concrete Tower Composite Material Properties.

				Steel properties						
	average d (m)	Number of PT Strands	Area of Strands (in^2)	avg. t (m)	xarea of tube (m2)	*poisson ratio	Area of strands (m^2)	vf (volume fraction of strand)	Ef (Mpa)	Steel Density (kg/m^3)
0-50m	10.5915	100	260.4	1.298864	21.60931	0.3	0.168	0.007774	196500	7850
50-100	8.6105	78	203.112	0.931727	12.60193	0.3	0.13104	0.010398	196500	7850
100-150	6.6295	56	145.824	0.710136	7.395072	0.3	0.09408	0.012722	196500	7850
150-200	4.6485	34	88.536	0.5715	4.173005	0.3	0.05712	0.013688	196500	7850

	Concrete Properties					composite properties		
	Vm (volume fraction of matrix)	Em (psi) (concrete) (in ANSYS)	Em (MPa) (concrete) (in ANSYS)	Concrete poisson ratio	Concrete Density (kg/m^3)	Young's Modulus (Mpa)	poisson's ratio	density (kg/m^3)
0-50m	0.992225589	5.38E+06	37089.66	0.1414	2392	38328.98	0.142633	2434.433
50-100	0.989601613	5.38E+06	37089.66	0.1414	2392	38747.27	0.143049	2448.754
100-150	0.98727804	5.38E+06	37089.66	0.1414	2392	39117.67	0.143418	2461.436
150-200	0.986312051	5.38E+06	37089.66	0.1414	2392	39271.66	0.143571	2466.709

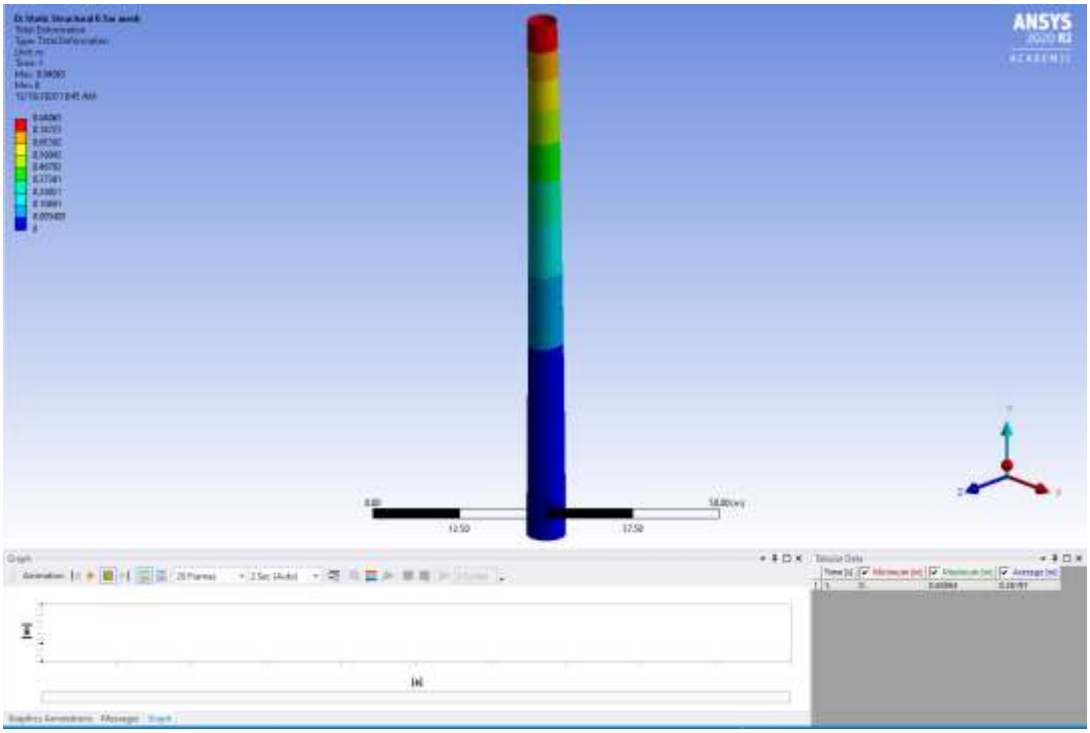

Figure Appendix A-1.1. Steel Tower Total Deformation (Static Structural).

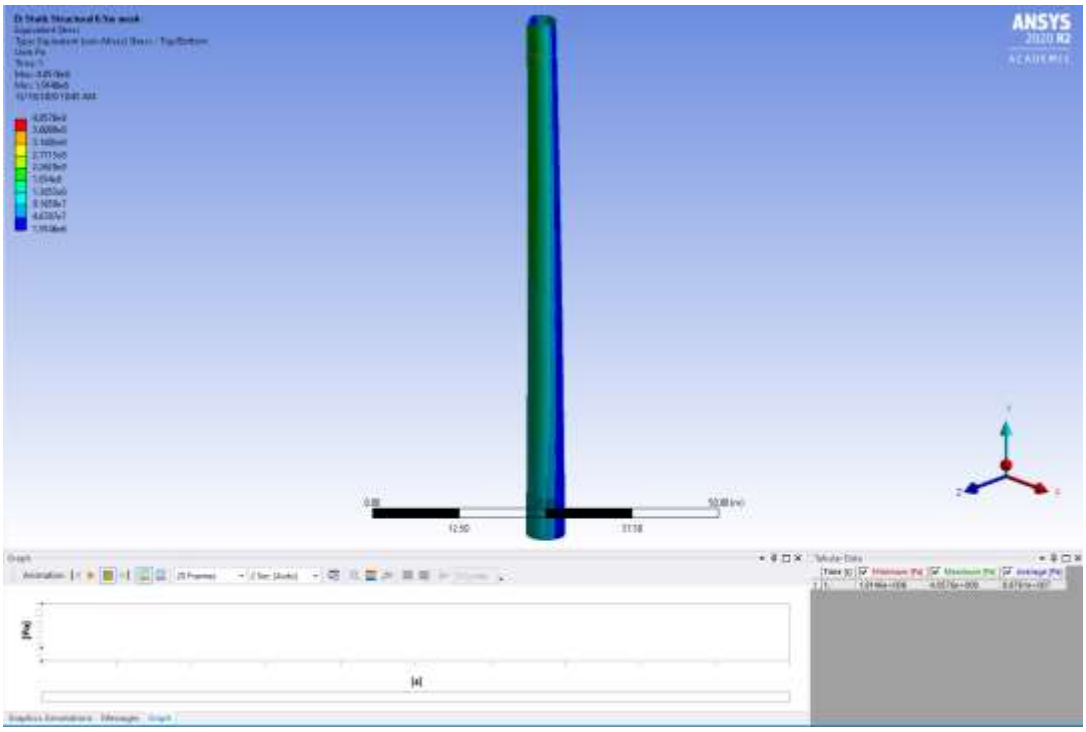

Figure Appendix A-1.2 Steel Tower Equivalent Stress (Static Structural).

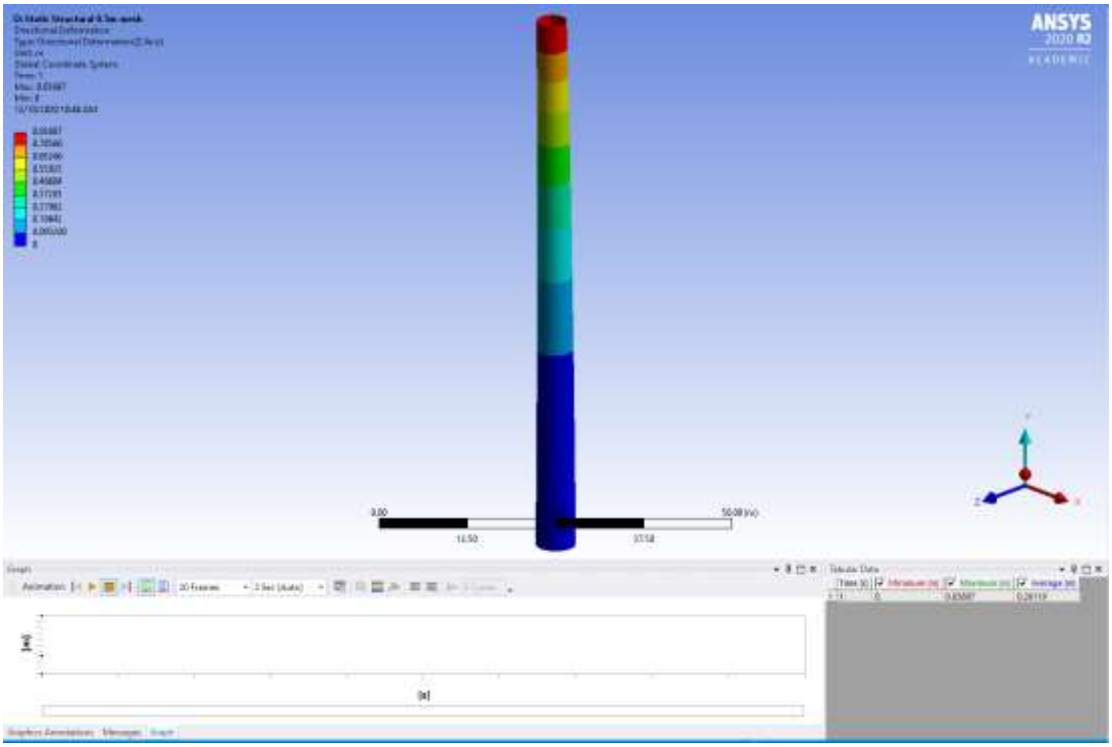

Figure Appendix A-1.3. Steel Tower Directional Deformation (Static Structural).

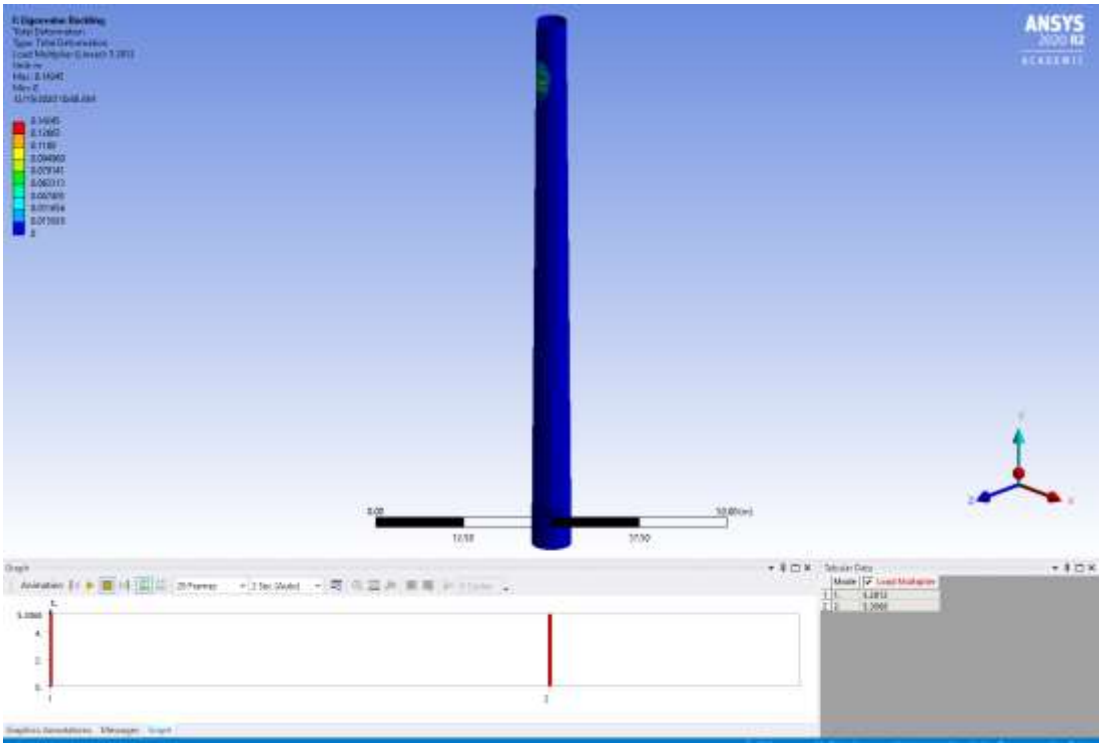

Figure Appendix A-1.4. Steel Tower Load Multiplier (Eigenvalue Buckling).

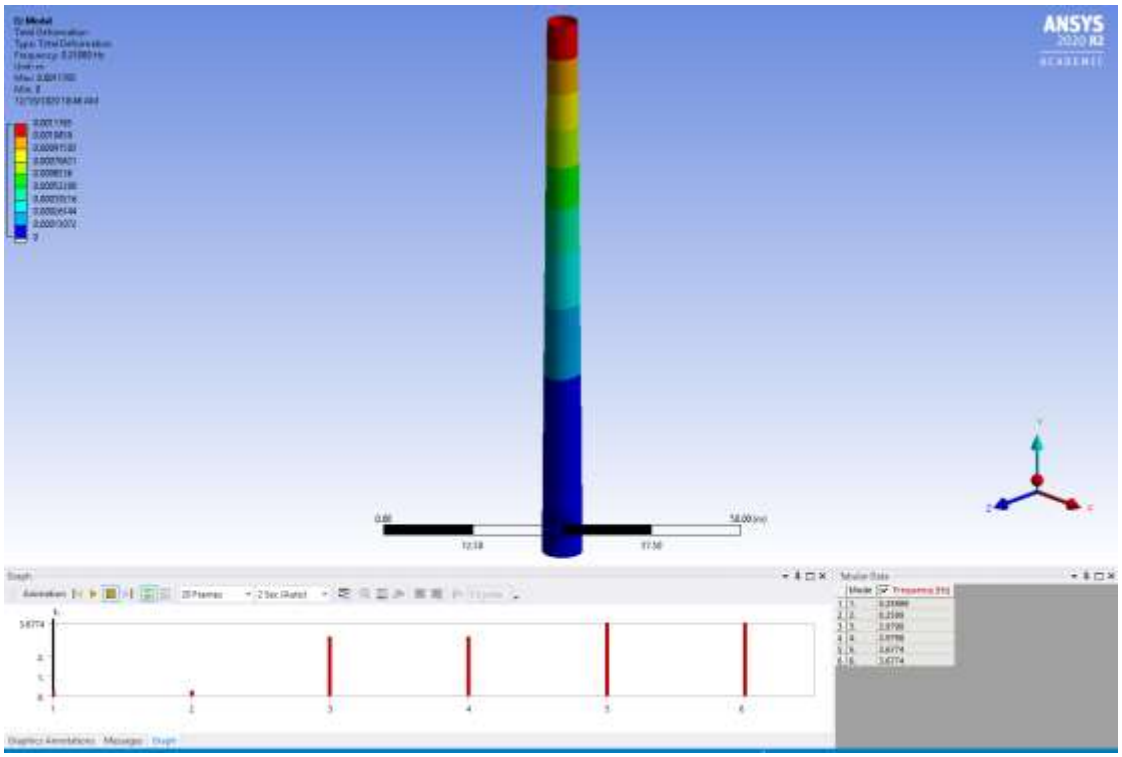

Figure Appendix A-1.5. Steel Tower Modal (Frequency).

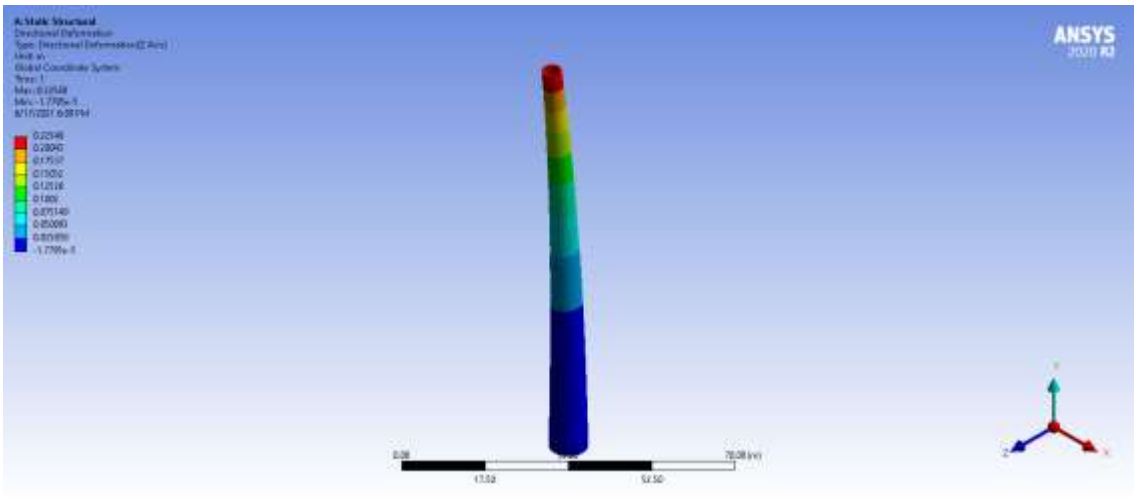

Figure Appendix A-1.6. 100m Concrete Tower Total Deformation (Static Structural).

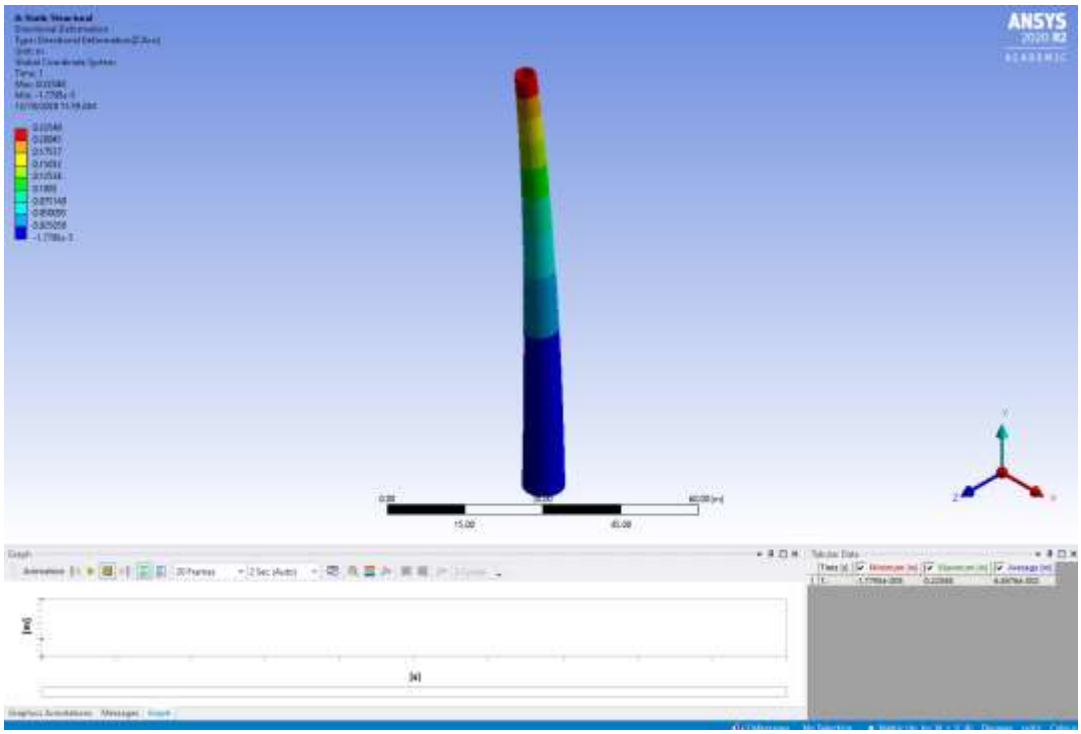

Figure Appendix A-1.7. 100m Concrete Tower Directional Deformation (Static Structural).

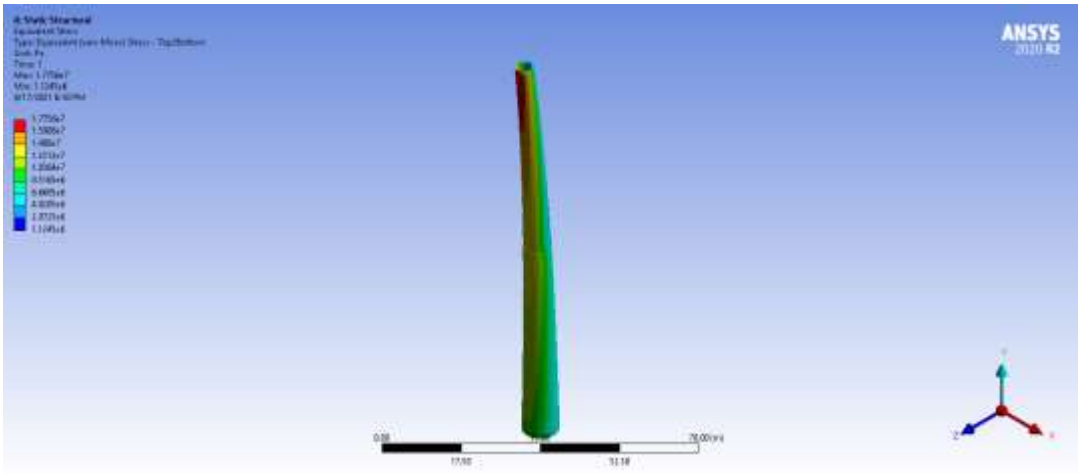

Figure Appendix A-1.8. 100m Concrete Tower Equivalent Stress (Static Structural).

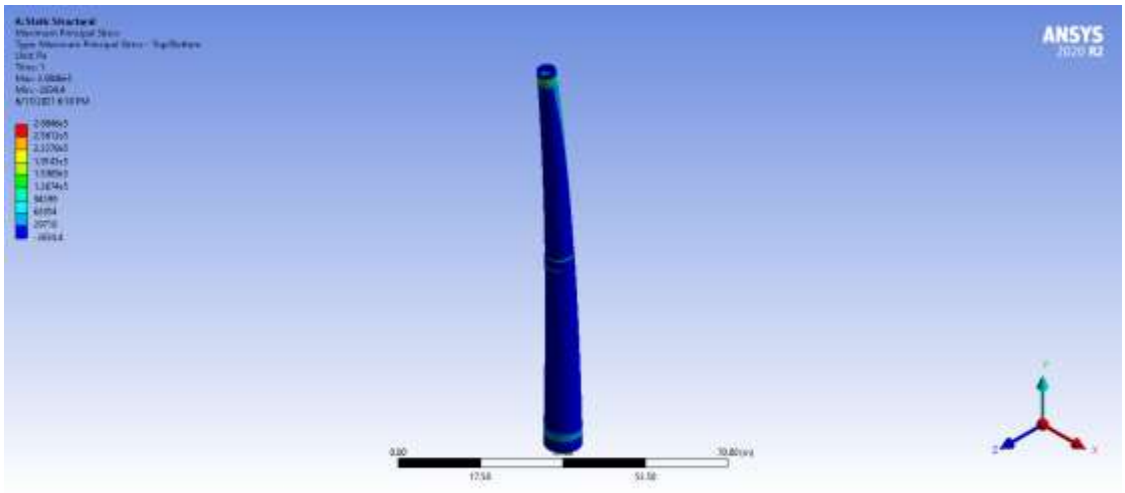

Figure Appendix A-1.9. 100m Concrete Tower Maximum Principal Stress (Static Structural).

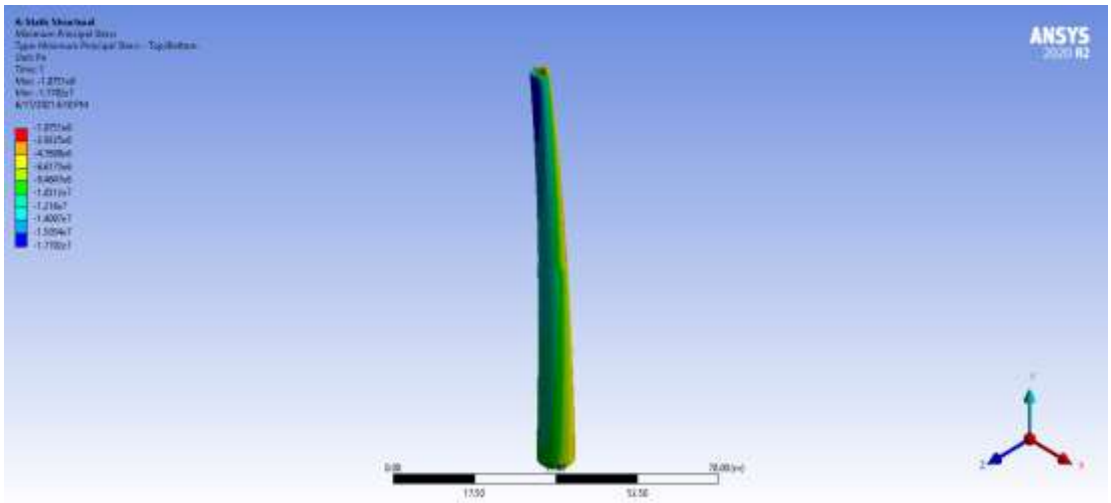

Figure Appendix A-1.10. 100m Concrete Tower Minimum Principal Stress (Static Structural).

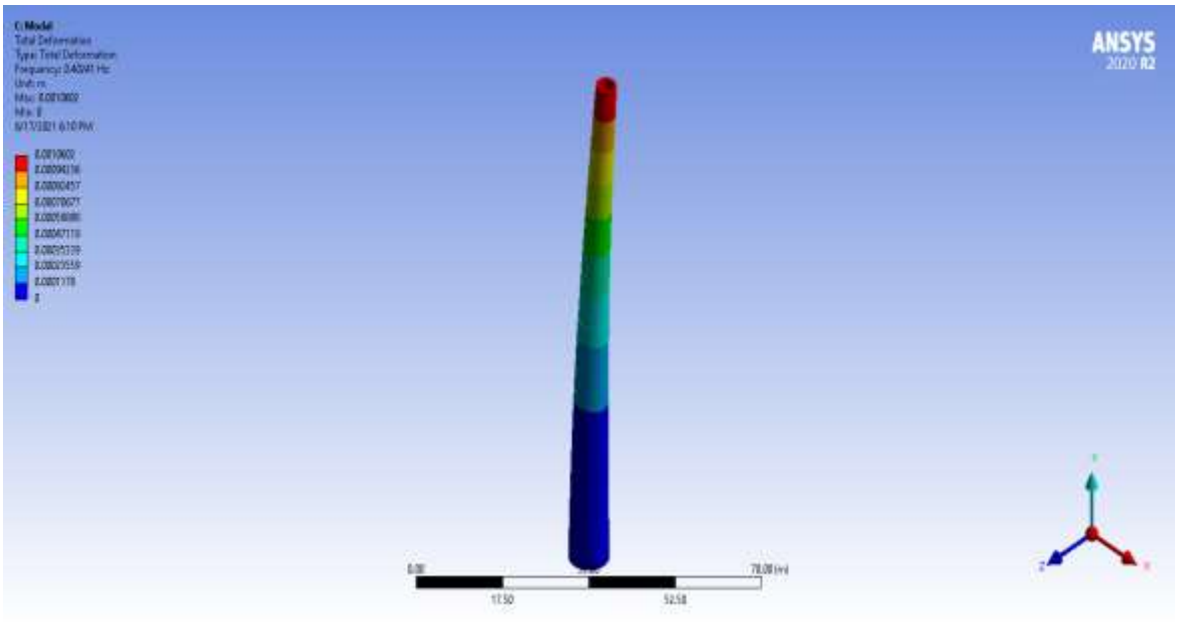

Figure Appendix A-1.11. 100m Concrete Tower Natural Frequency (Modal Analysis).

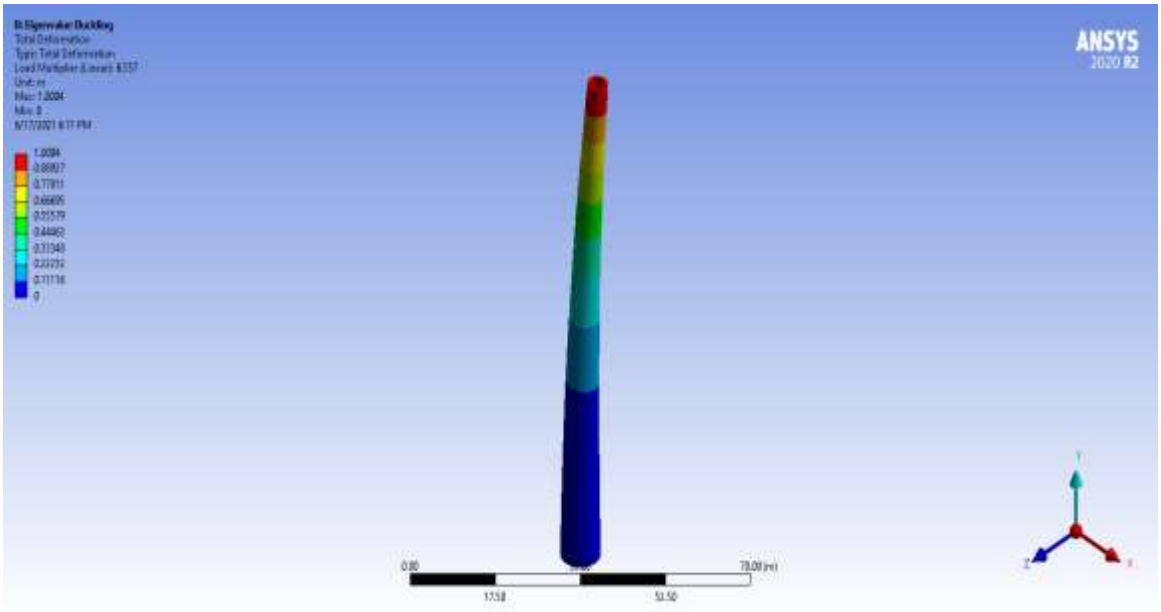

Figure Appendix A-1.12. 100m Concrete Tower Load Multiplier (Eigenvalue Buckling Analysis).

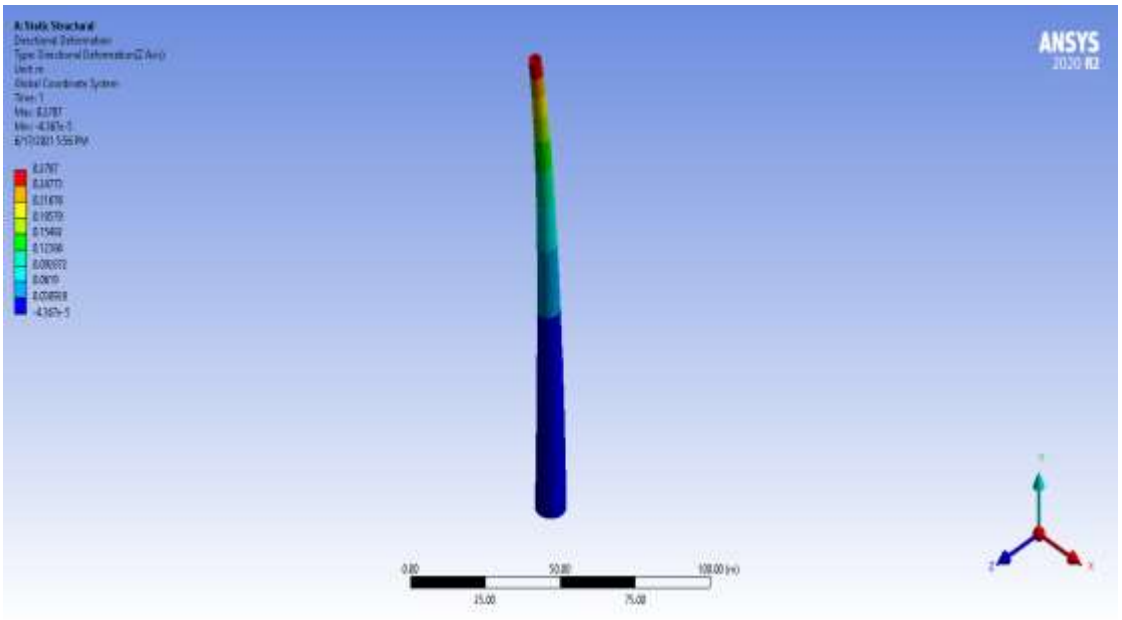

Figure Appendix A-1.13. 150m Concrete Tower Directional Deformation (Static Structural).

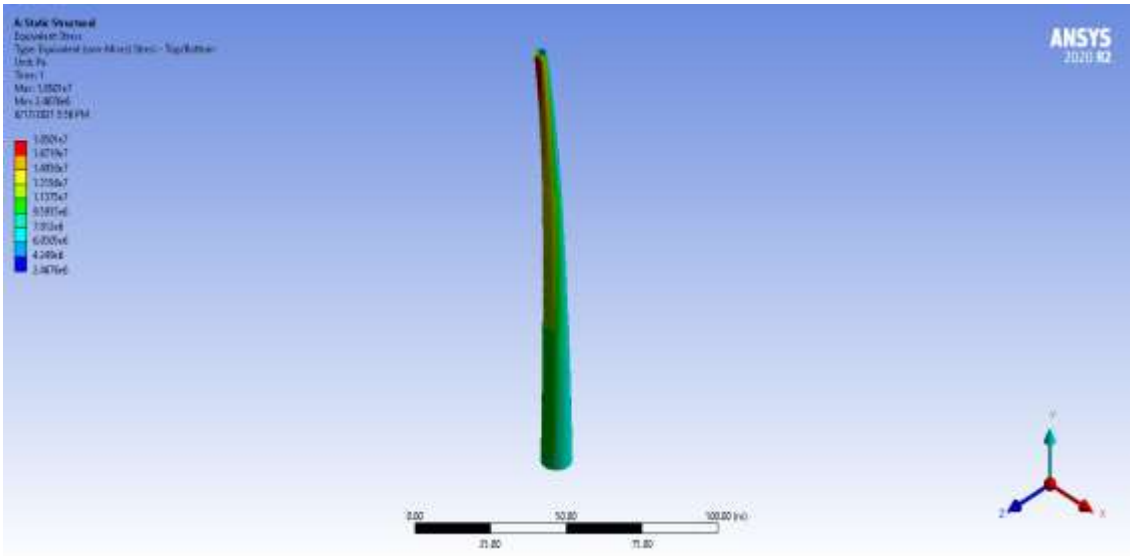

Figure Appendix A-1.14. 150m Concrete Tower Equivalent Stress (Static Structural).

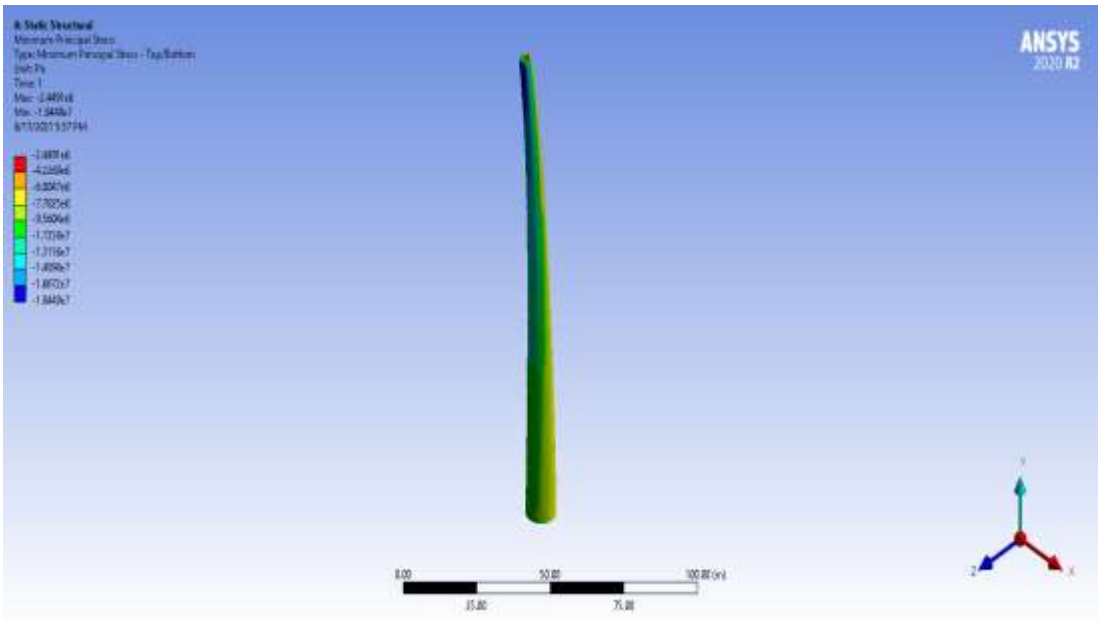

Figure Appendix A-1.15. 150m Concrete Tower Maximum Principal Stress (Static Structural).

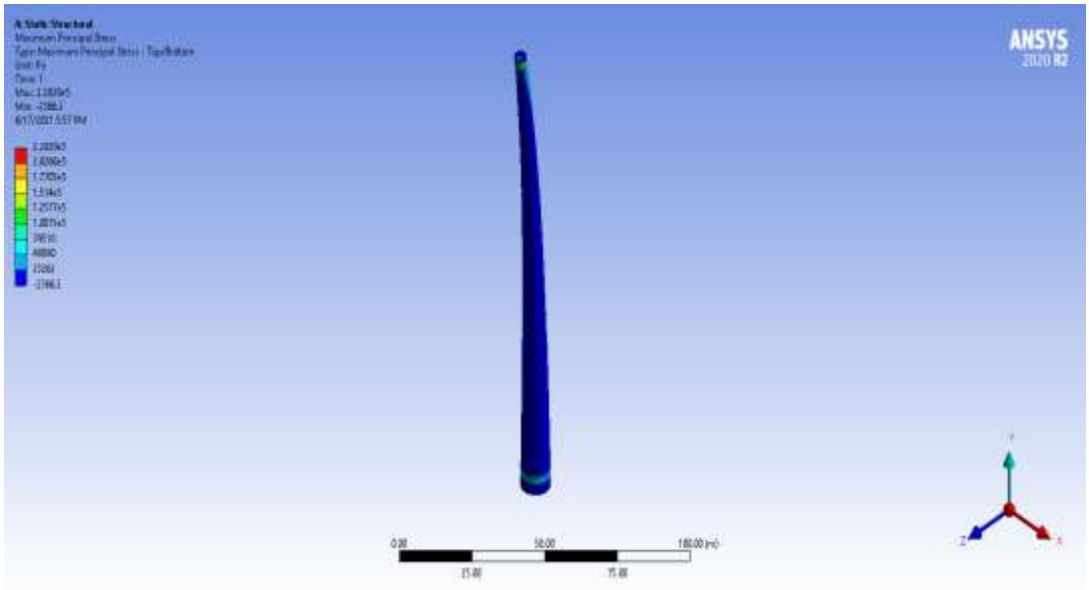

Figure Appendix A-1.16. 150m Concrete Tower Minimum Principal Stress (Static Structural).

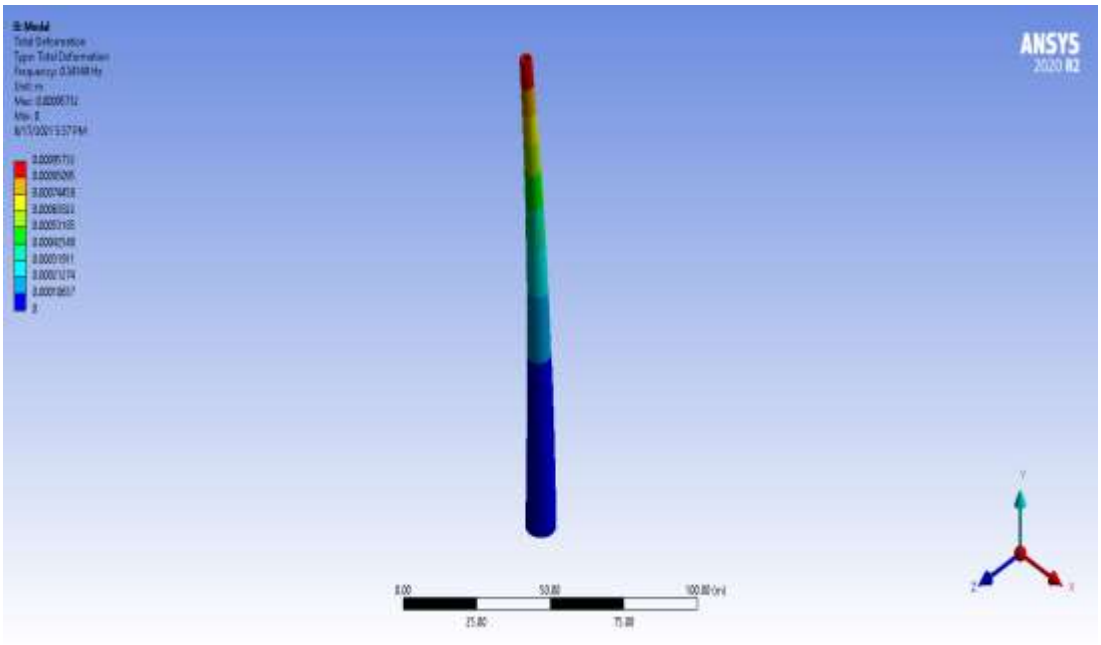

Figure Appendix A-1.17. 150m Concrete Tower Natural Frequency (Modal Analysis).

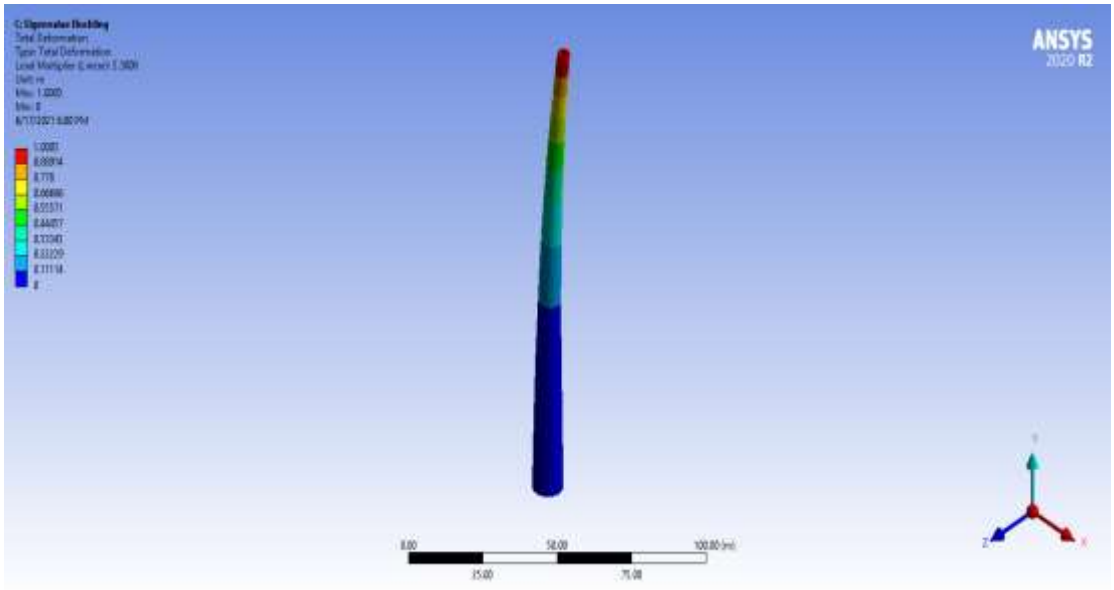

Figure Appendix A-1.18. 150m Concrete Tower Load Multiplier (Eigenvalue Buckling Analysis).

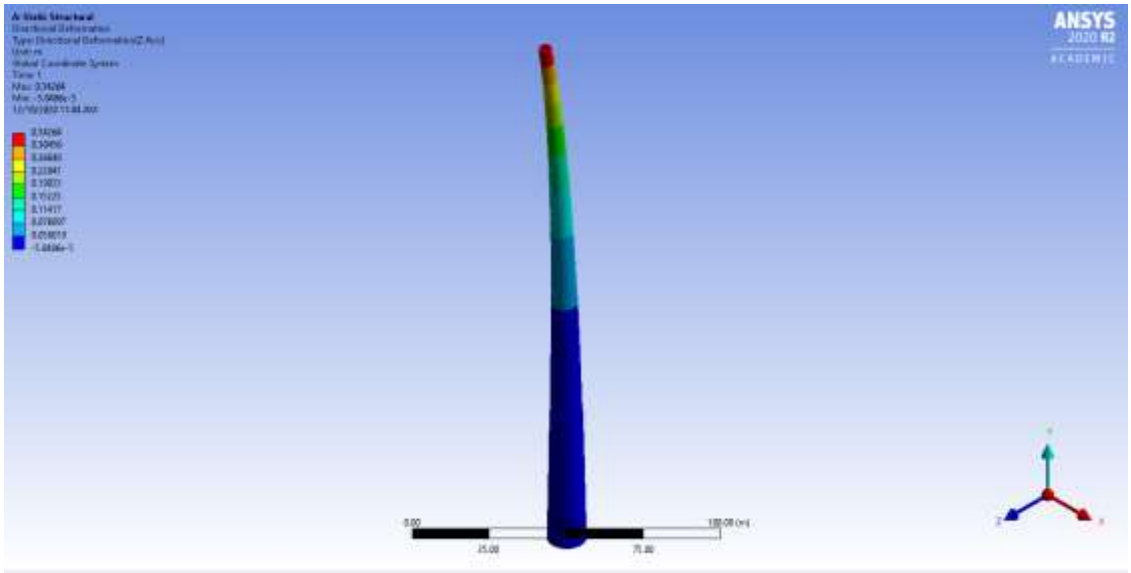

Figure Appendix A-1.19. 200m Concrete Tower Directional Deformation (Static Structural).

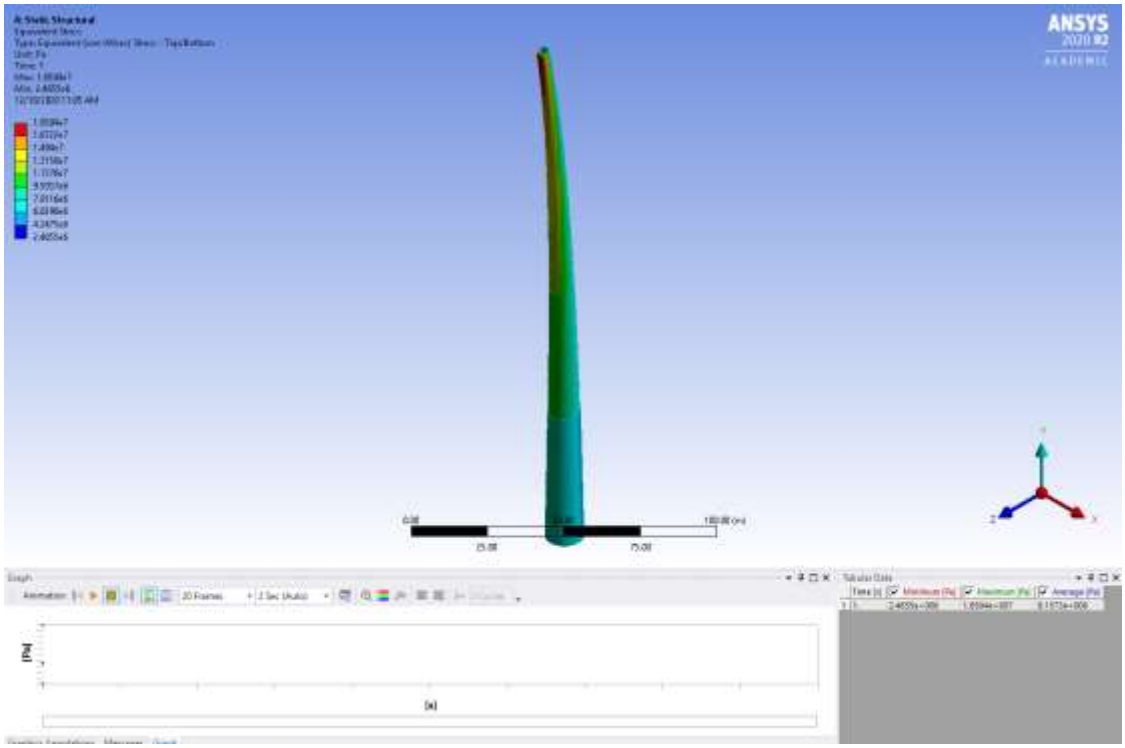

Figure Appendix A-1.20. 200m Concrete Tower Equivalent Stress (Static Structural).

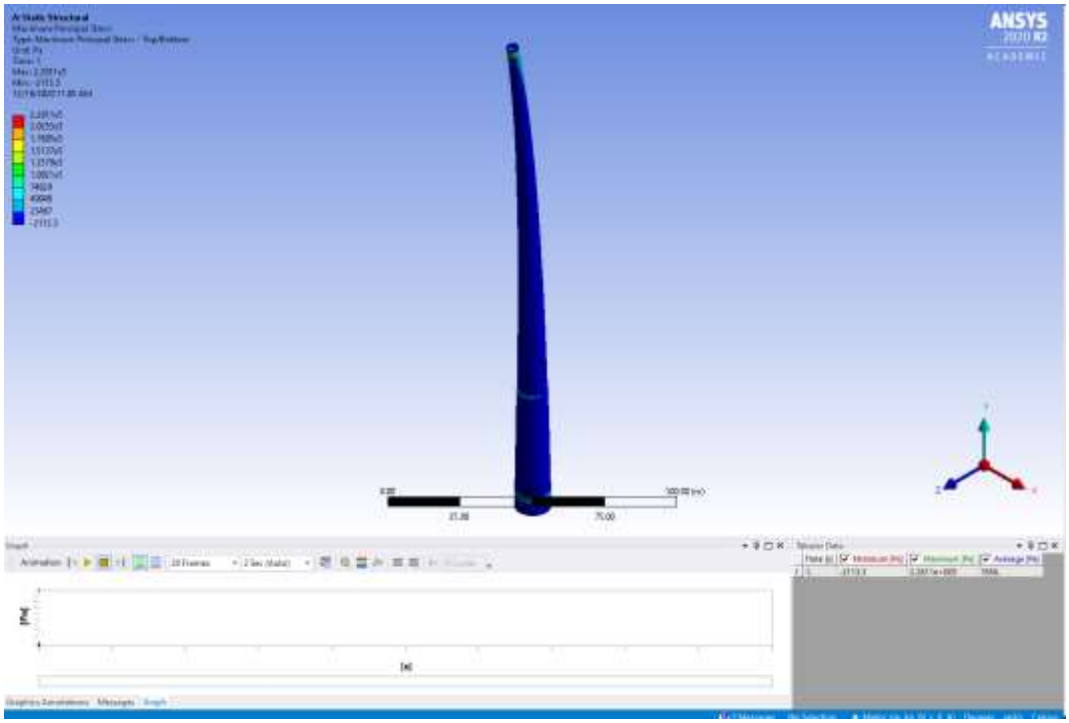

Figure Appendix A-1.21. 200m Concrete Tower Maximum Principal Stress (Static Structural).

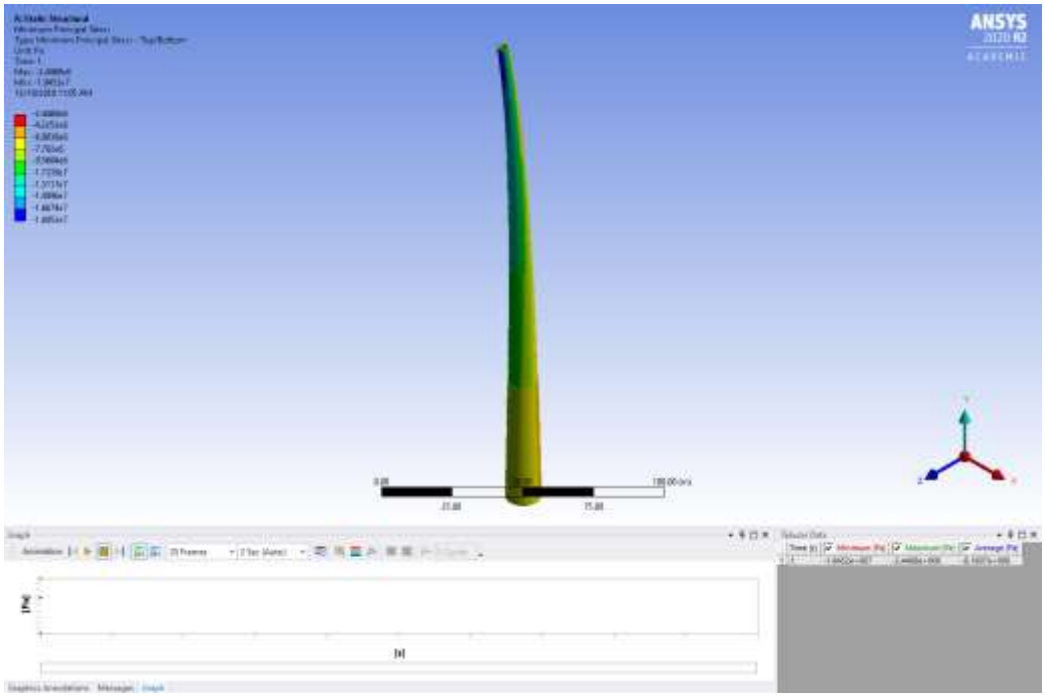

Figure Appendix A-1.22. 200m Concrete Tower Minimum Principal Stress (Static Structural).

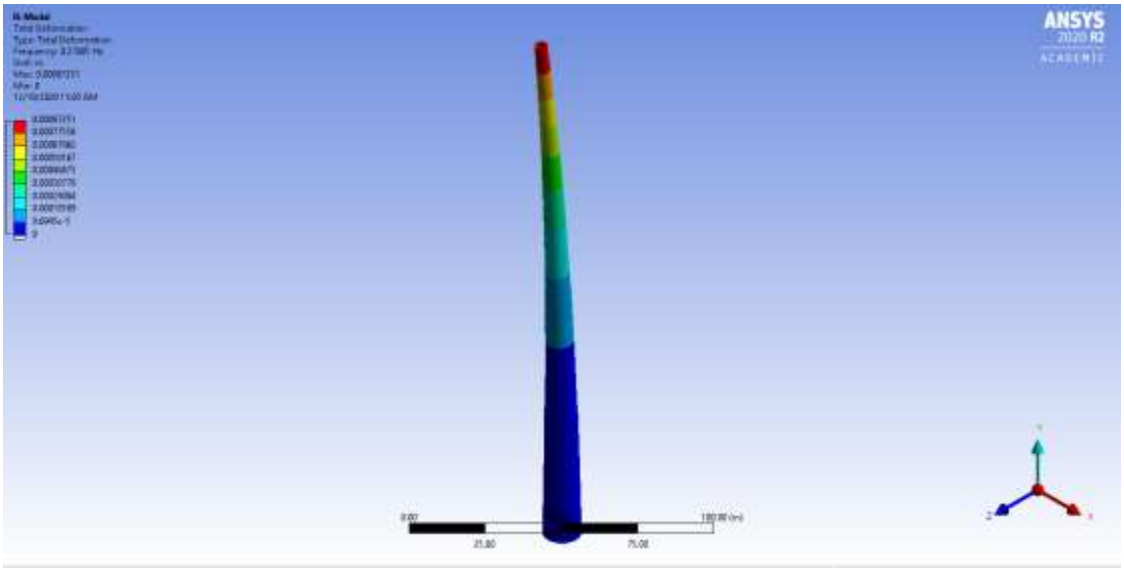

Figure Appendix A-1.23. 200m Concrete Tower Natural Frequency (Modal Analysis).

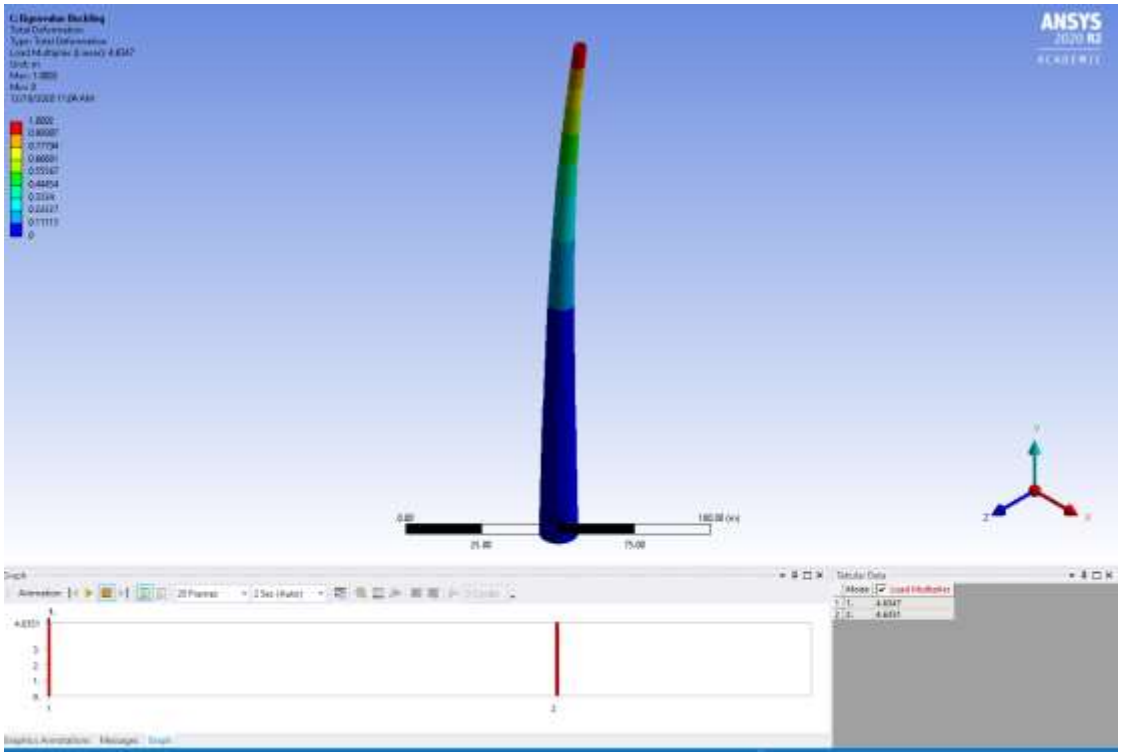

Figure Appendix A-1.24. 200m Concrete Tower Load Multiplier (Eigenvalue Buckling Analysis).

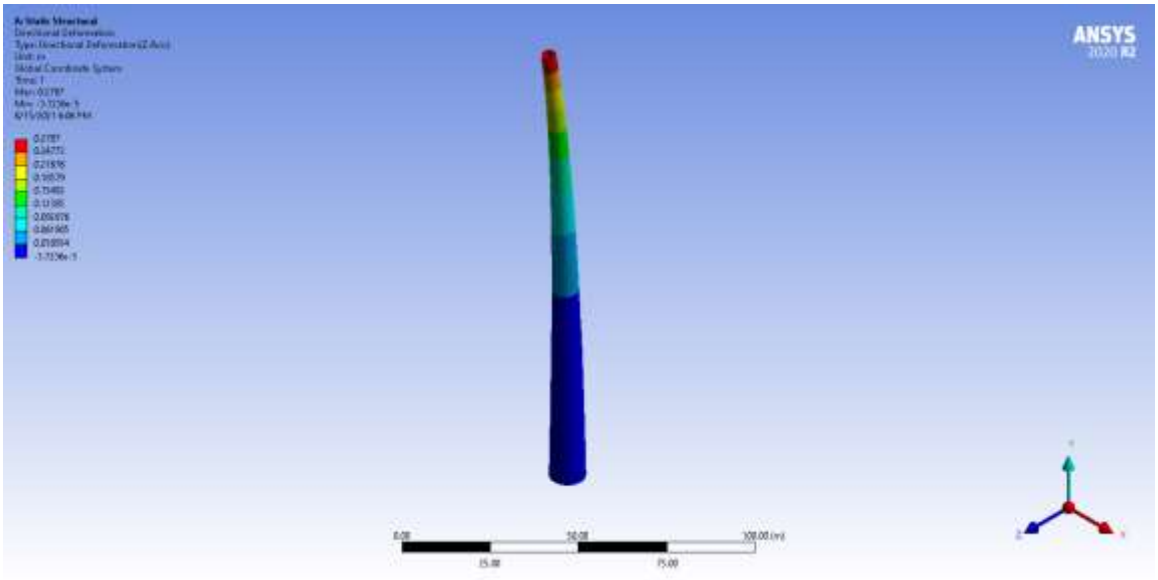

Figure Appendix A-1.25. 150m (90% P-T Force) Concrete Tower Directional Deformation (Static Structural).

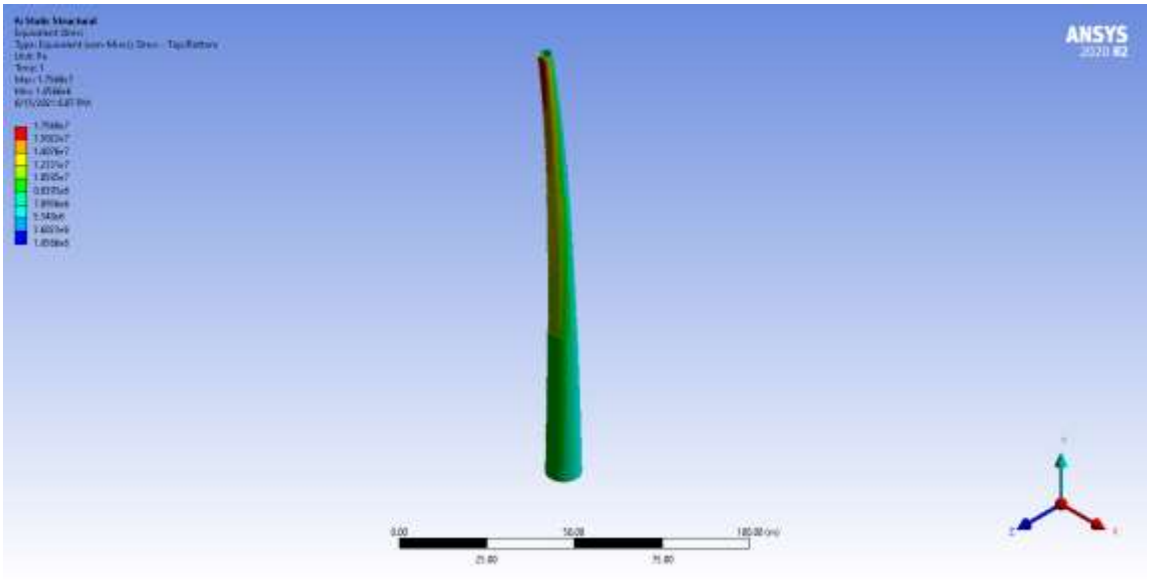

Figure Appendix A-1.26. 150m (90% P-T Force) Concrete Tower Von-Mises Stress (Static Structural).

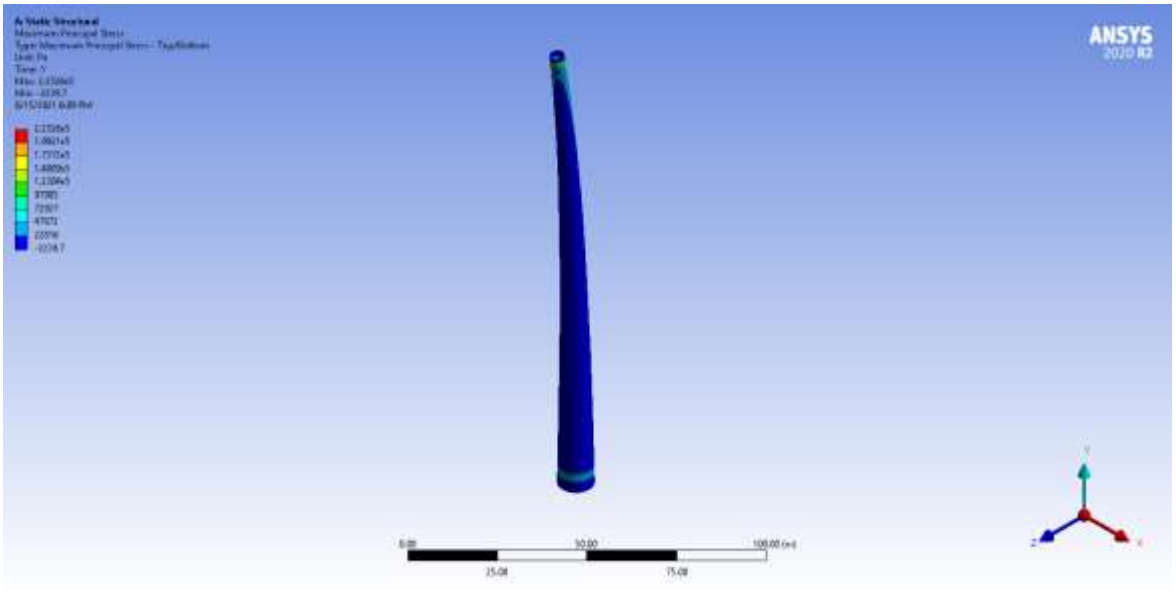

Figure Appendix A-1.27. 150m (90% P-T Force) Concrete Tower Maximum Principal Stress (Static Structural).

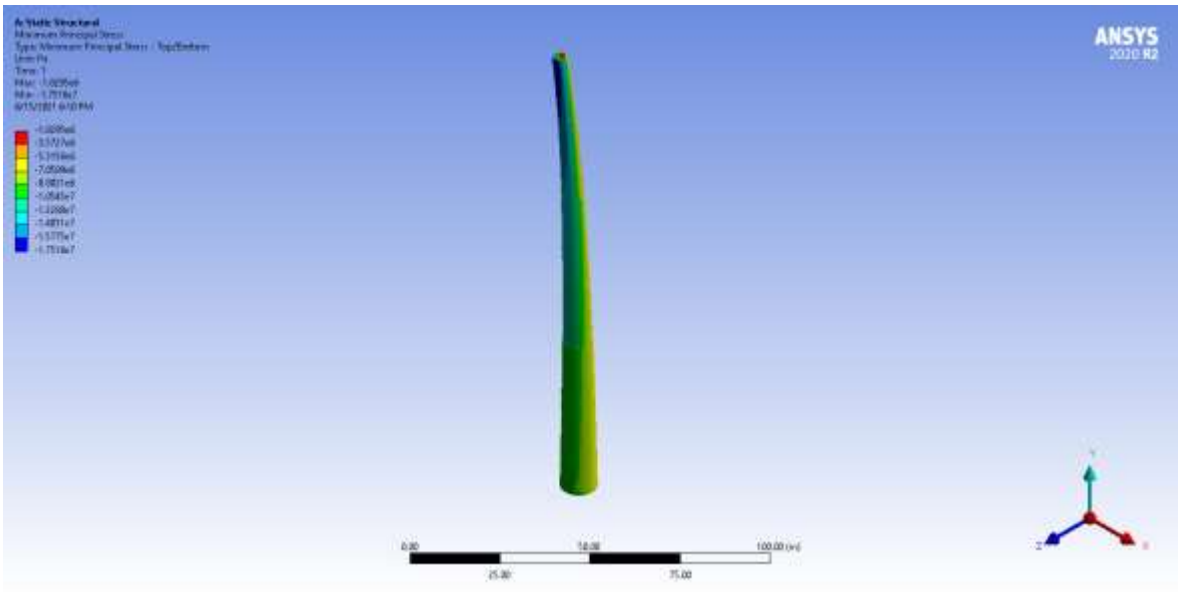

Figure Appendix A-1.28. 150m (90% P-T Force) Concrete Tower Minimum Principal Stress (Static Structural).

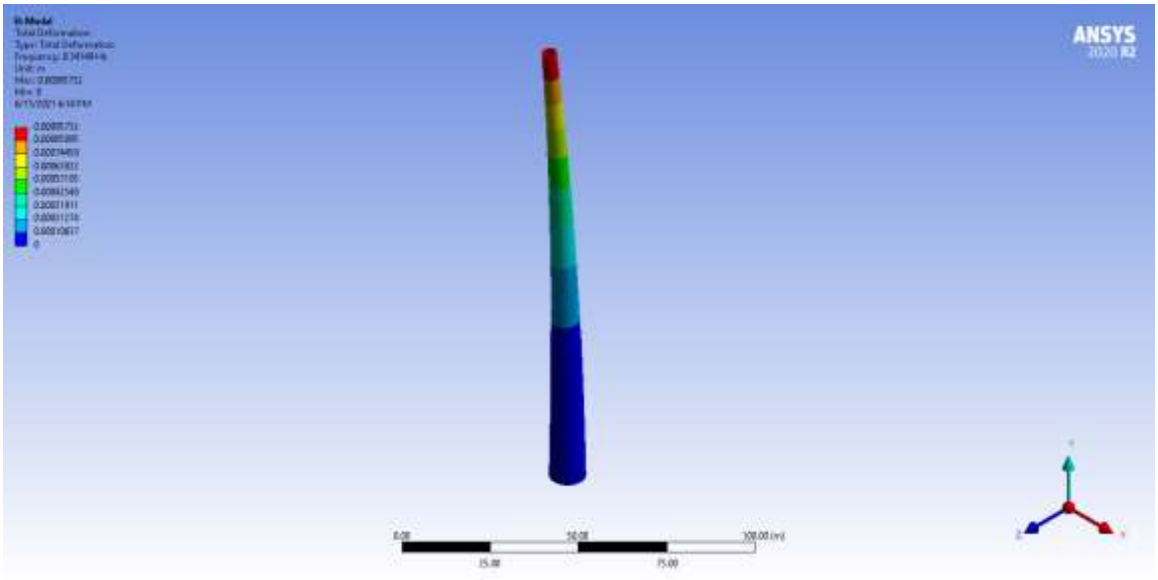

Figure Appendix A-1.29. 150m (90% P-T Force) Concrete Tower Natural Frequency (Modal Analysis).

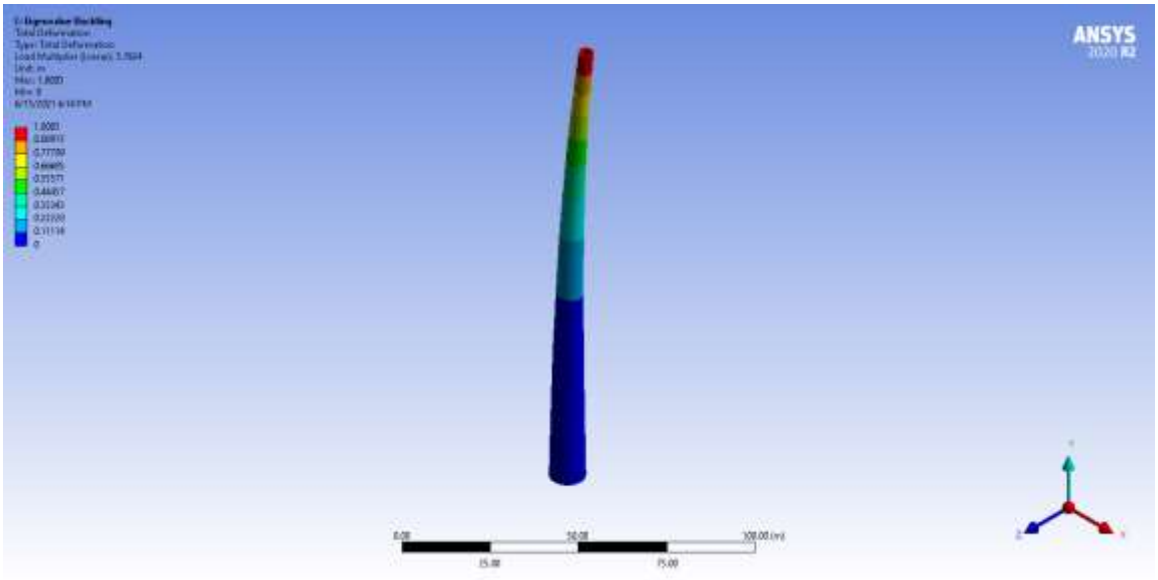

Figure Appendix A-1.30. 150m (90% P-T Force) Concrete Tower Load Multiplier (Eigenvalue Buckling Analysis).

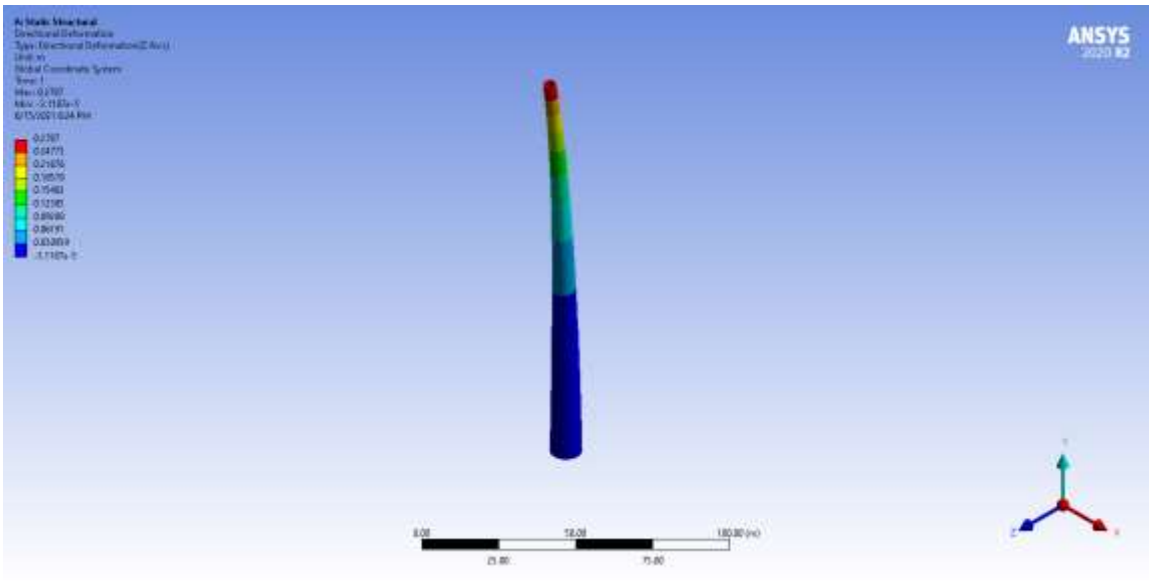

Figure Appendix A-1.31. 150m (80% P-T Force) Concrete Tower Directional Deformation (Static Structural).

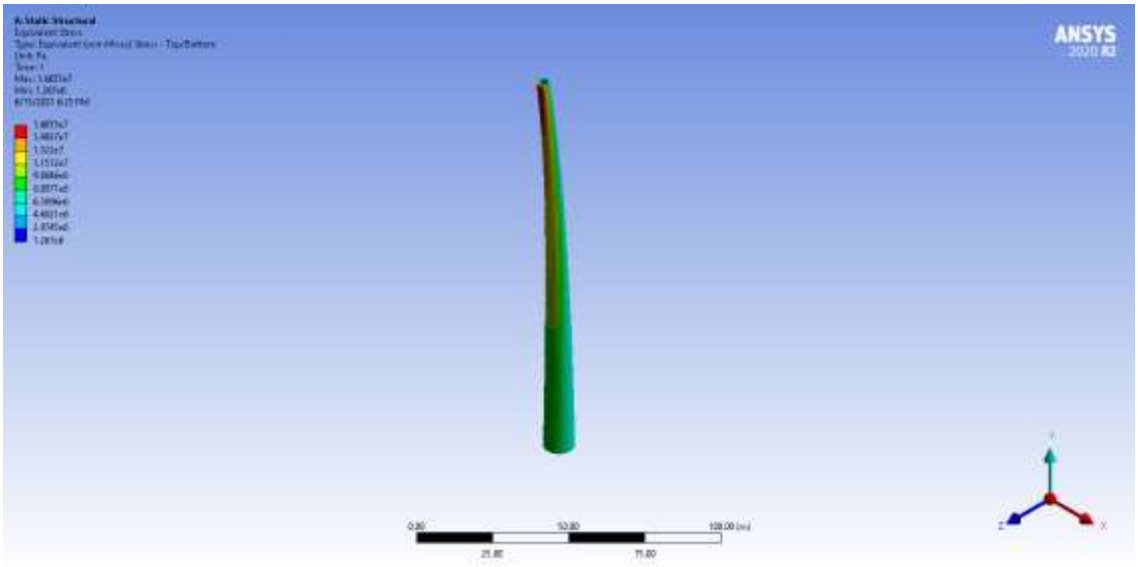

Figure Appendix A-1.32. 150m (80% P-T Force) Concrete Tower Von-Mises Stress (Static Structural).

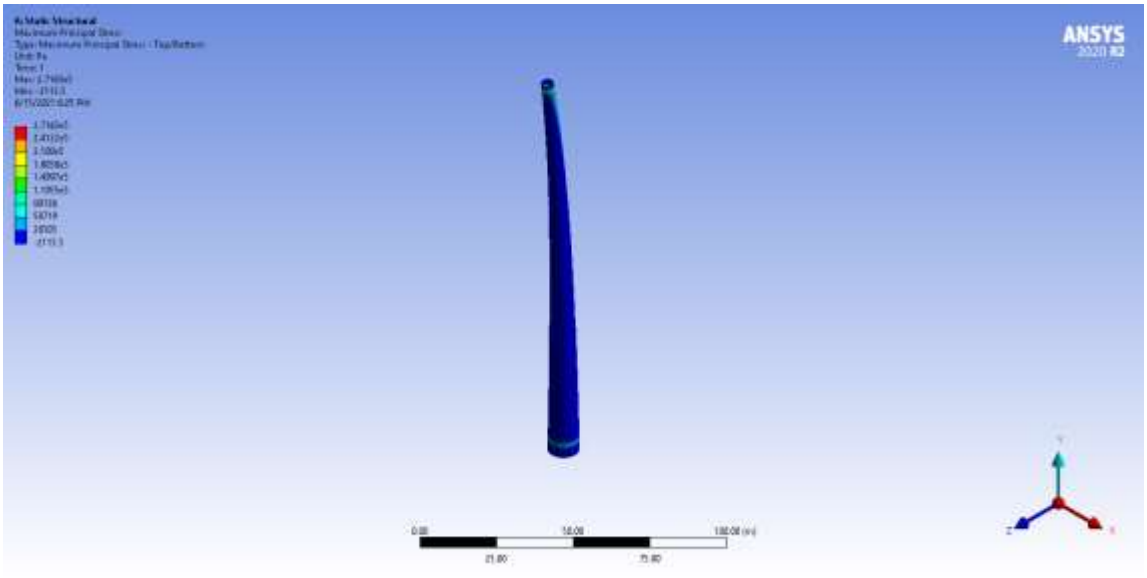

Figure Appendix A-1.33. 150m (80% P-T Force) Concrete Tower Maximum Principal Stress (Static Structural).

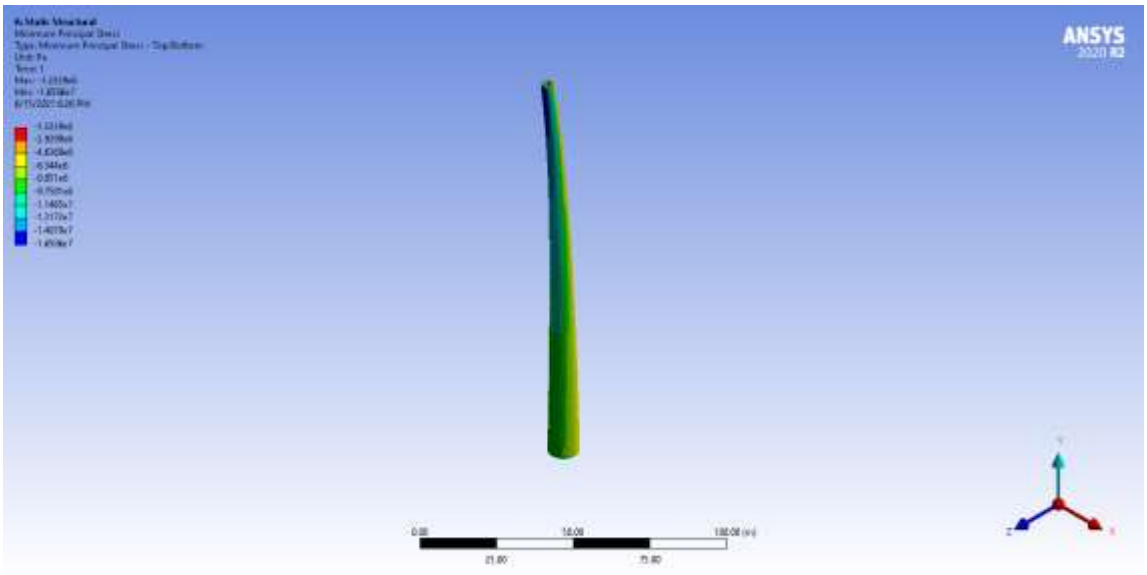

Figure Appendix A-1.34. 150m (80% P-T Force) Concrete Tower Minimum Principal Stress (Static Structural).

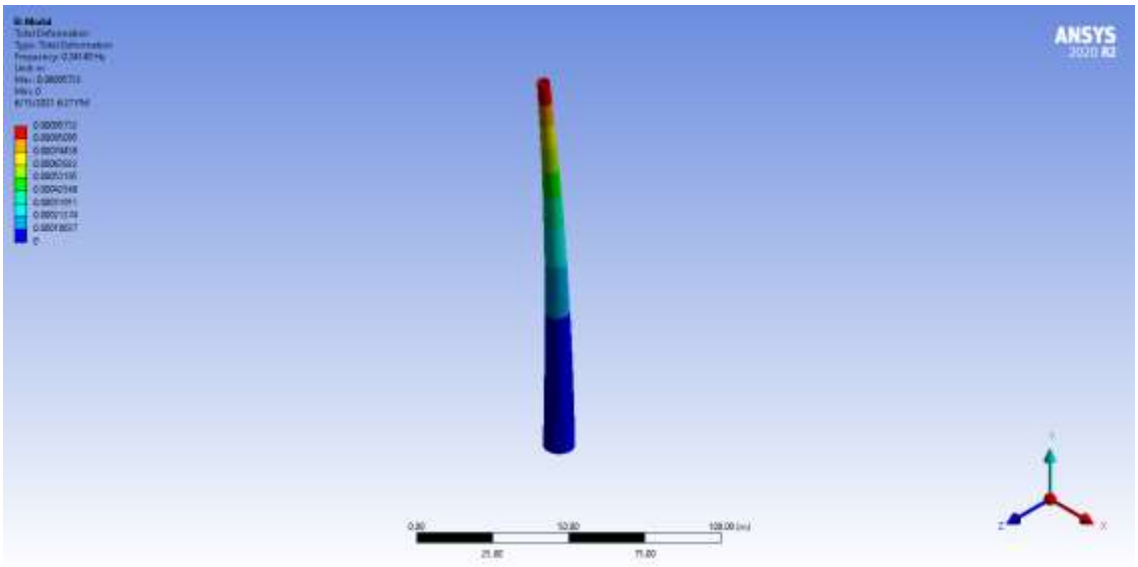

Figure Appendix A-1.35. 150m (80% P-T Force) Concrete Tower Natural Frequency (Modal Analysis).

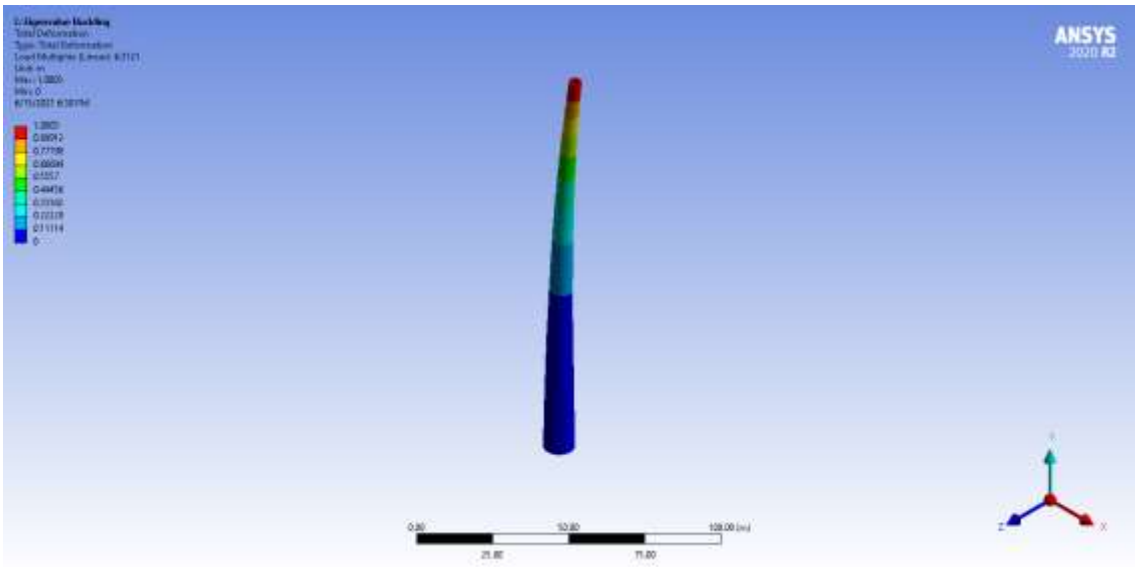

Figure Appendix A-1.36. 150m (80% P-T Force) Concrete Tower Load Multiplier (Eigenvalue Buckling Analysis).

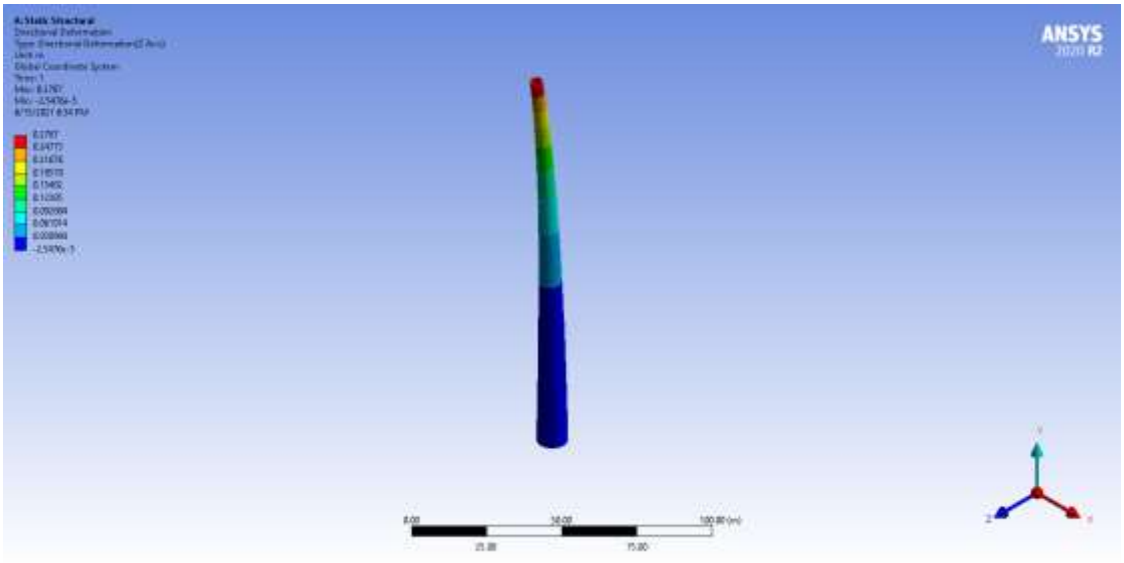

Figure Appendix A-1.37. 150m (70% P-T Force) Concrete Tower Directional Deformation (Static Structural).

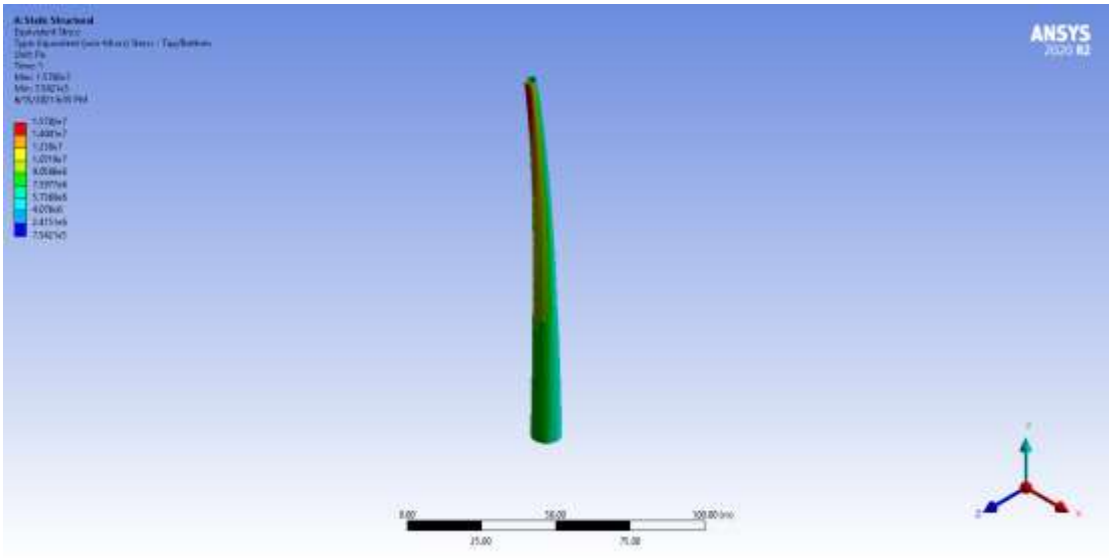

Figure Appendix A-1.38. 150m (70% P-T Force) Concrete Tower Von-Mises Stress (Static Structural).

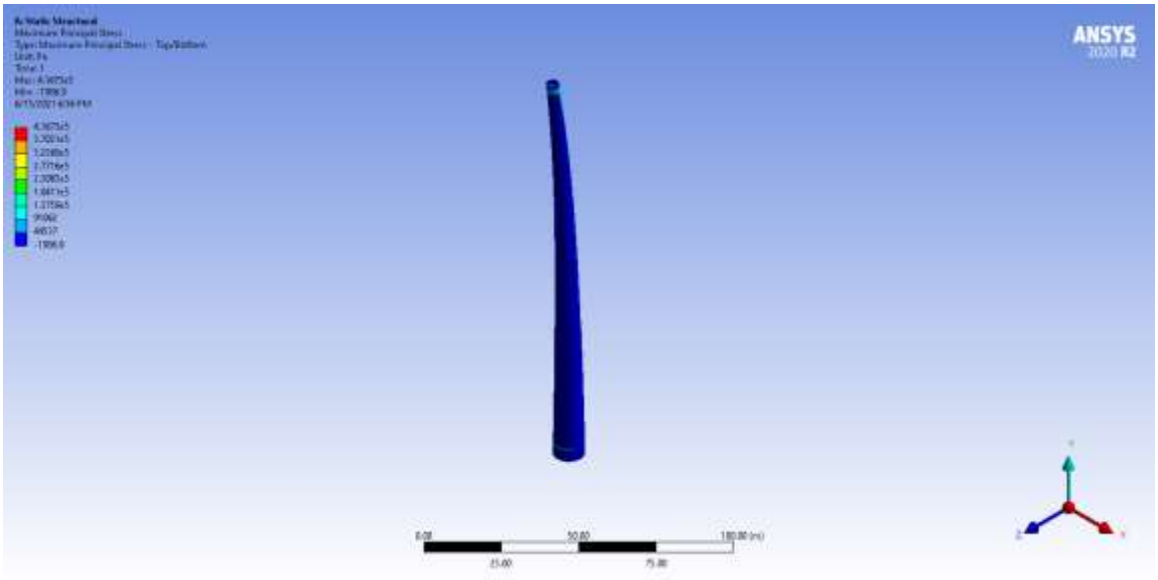

Figure Appendix A-1.39. 150m (70% P-T Force) Concrete Tower Maximum Principal Stress (Static Structural).

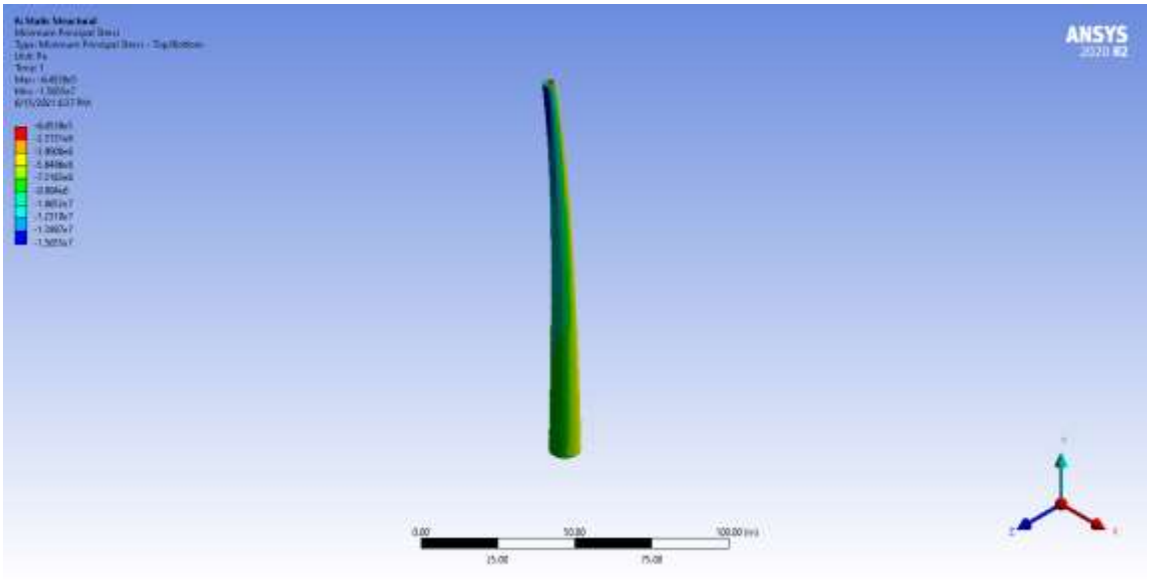

Figure Appendix A-1.40. 150m (70% P-T Force) Concrete Tower Minimum Principal Stress (Static Structural).

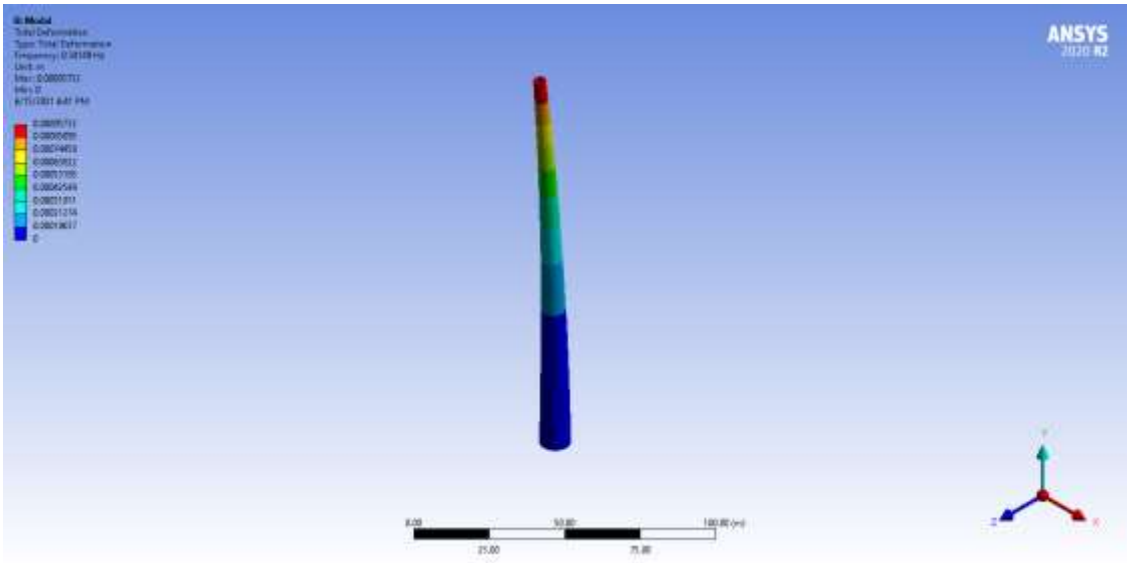

Figure Appendix A-1.41. 150m (70% P-T Force) Concrete Tower Natural Frequency (Modal Analysis).

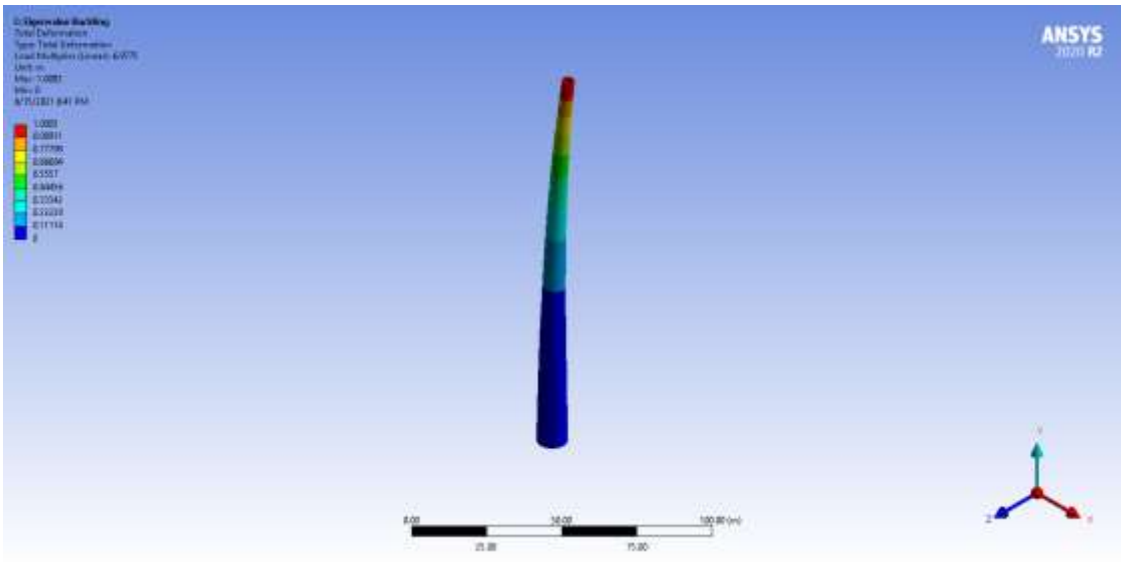

Figure Appendix A-1.42. 150m (70% P-T Force) Concrete Tower Load Multiplier (Eigenvalue Buckling Analysis).

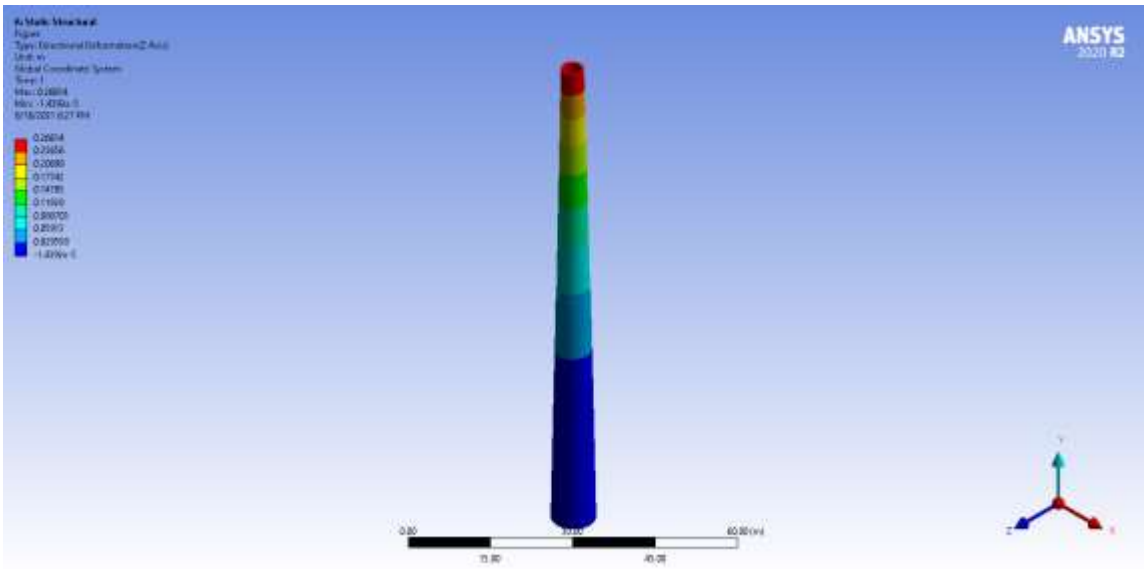

Figure Appendix A-1.43. 100m P-delta Concrete Tower Directional Deformation (Static Structural).

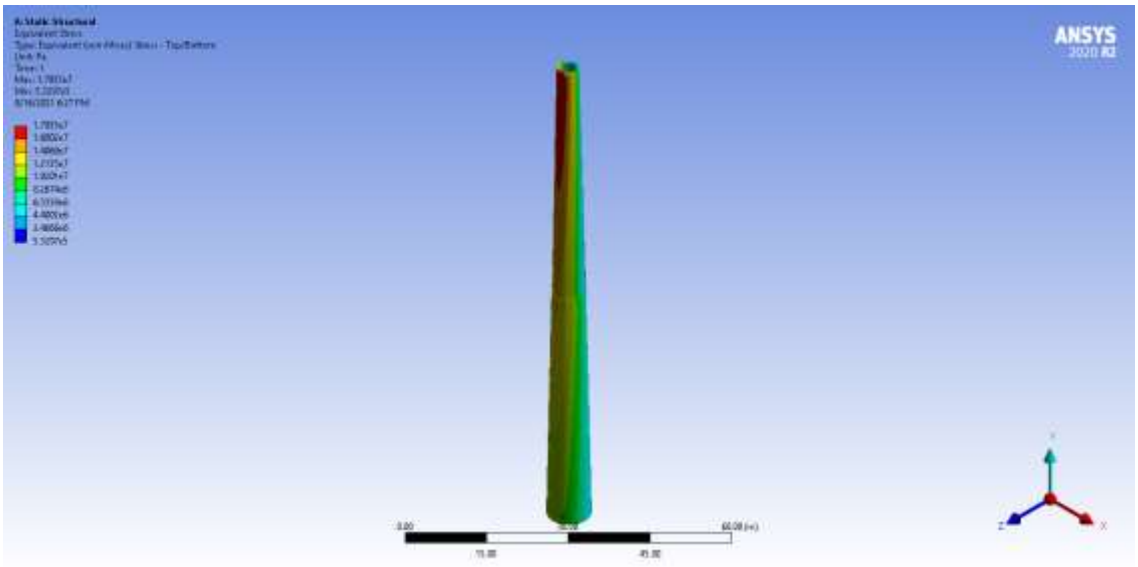

Figure Appendix A-1.44. 100m P-delta Concrete Tower Von-Mises Stress (Static Structural).

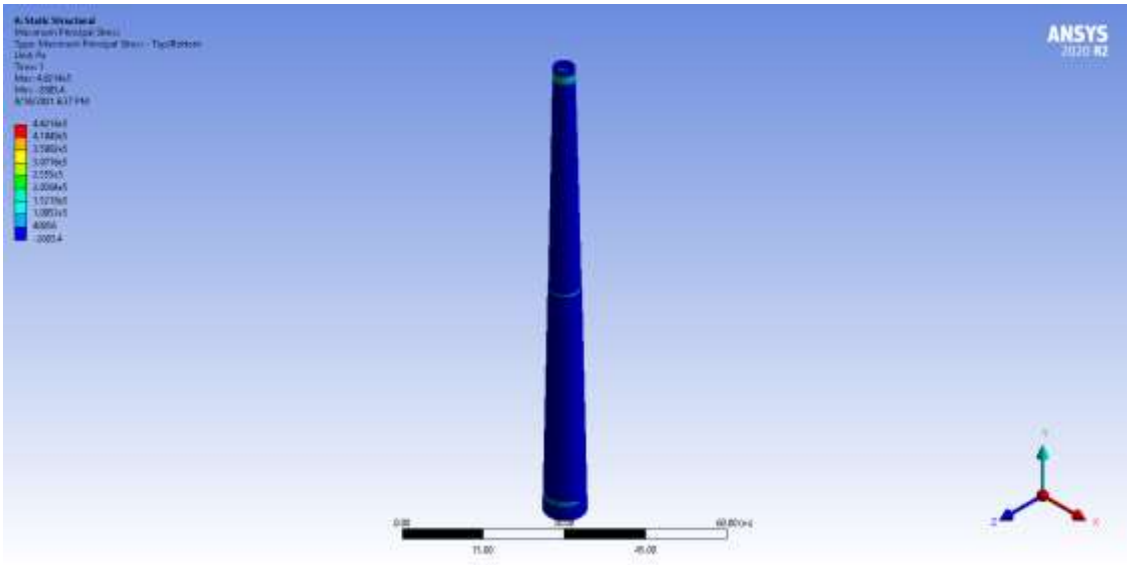

Figure Appendix A-1.45. 100m P-delta Concrete Tower Maximum Principal Stress (Static Structural).

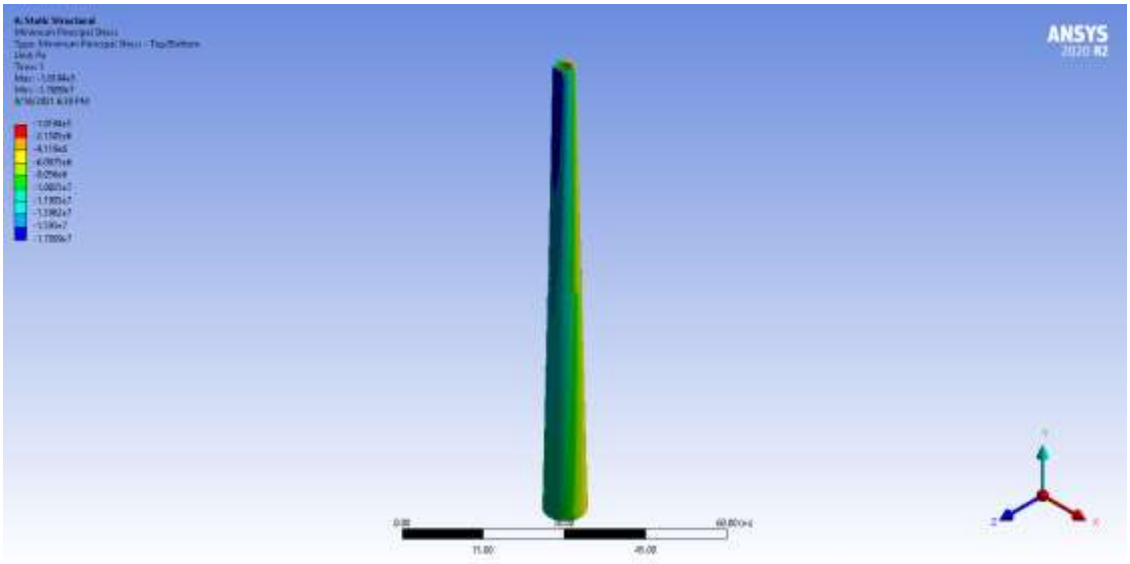

Figure Appendix A-1.46. 100m P-delta Concrete Tower Minimum Principal Stress (Static Structural).

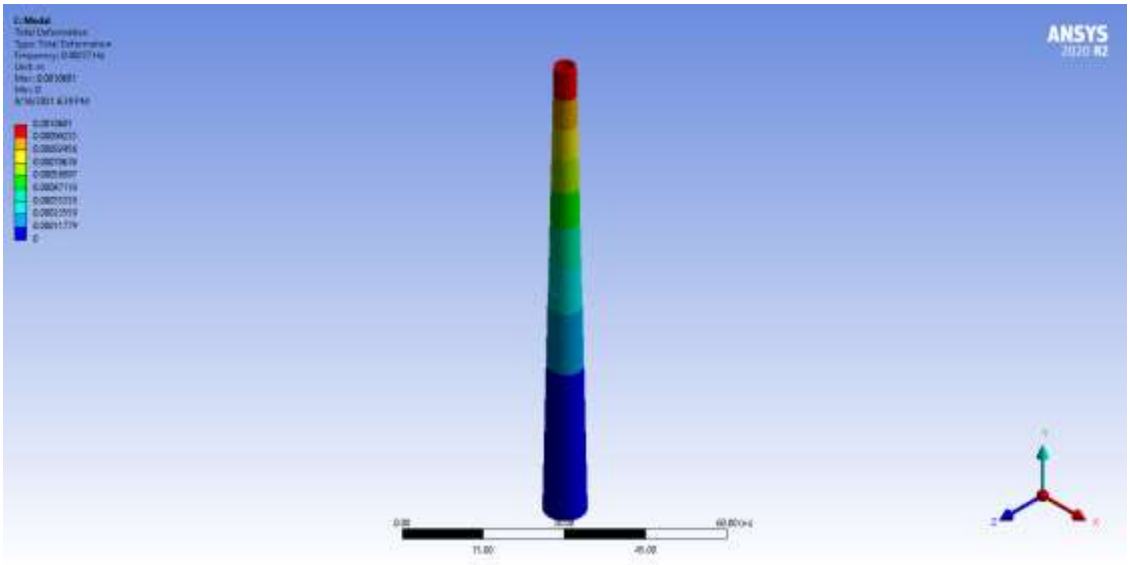

Figure Appendix A-1.47. 100m P-delta Concrete Tower Natural Frequency (Modal Analysis).

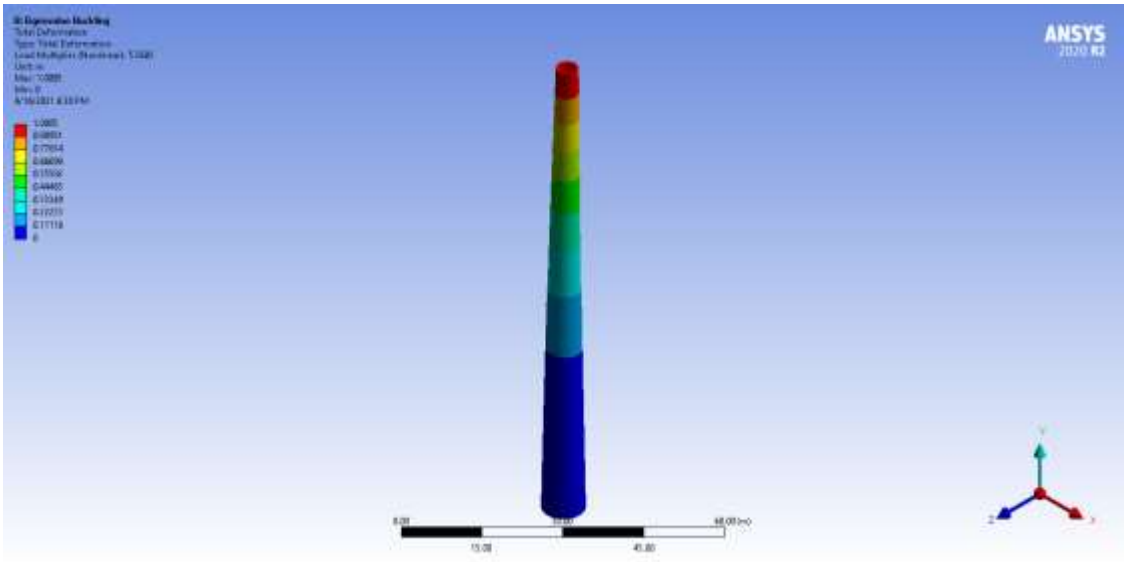

Figure Appendix A-1.48. 100m P-delta Concrete Tower Load Multiplier (Eigenvalue Buckling Analysis).

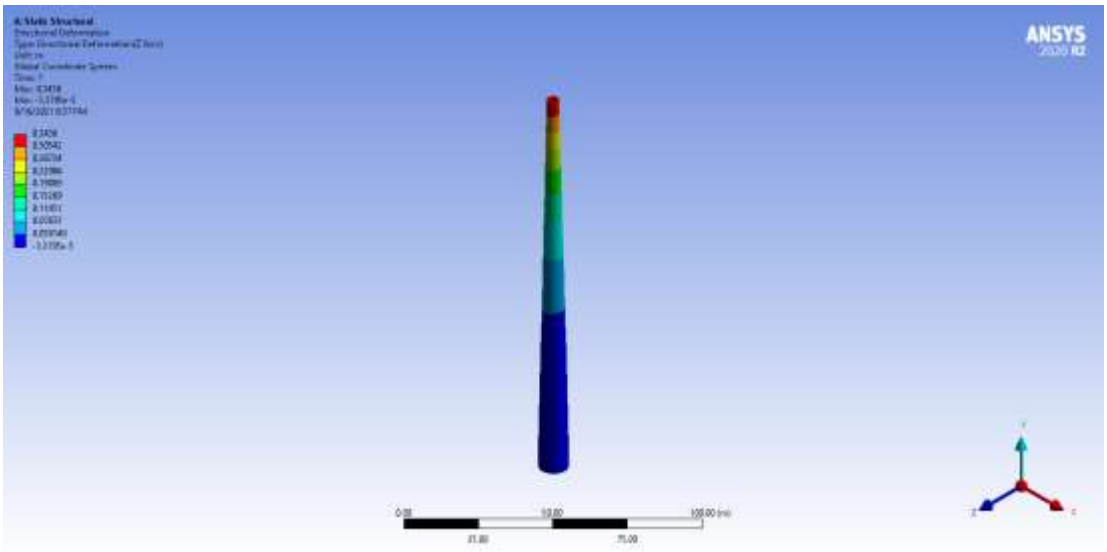

Figure Appendix A-1.49. 150m P-delta Concrete Tower Directional Deformation (Static Structural).

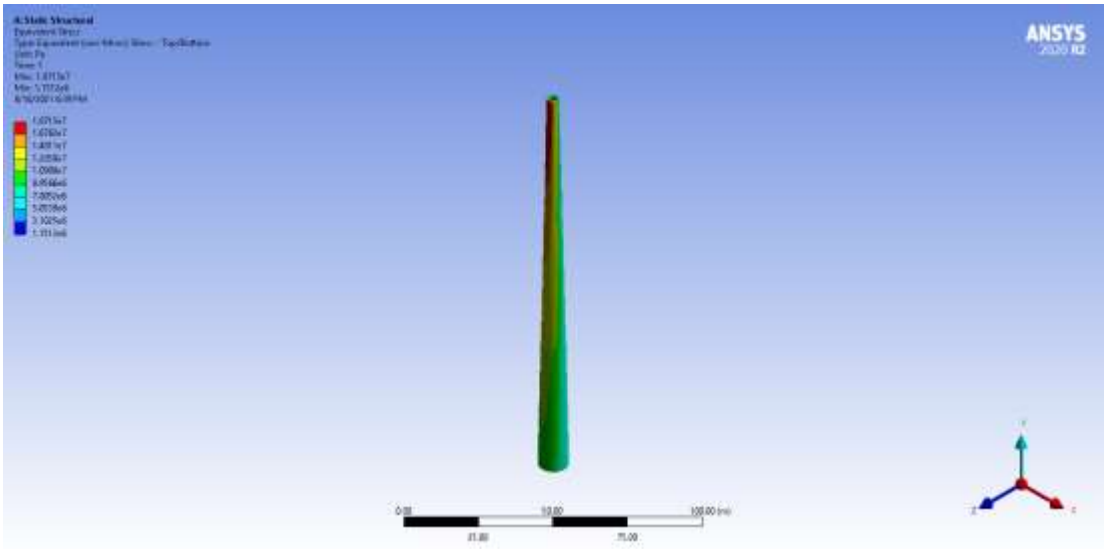

Figure Appendix A-1.50. 150m P-delta Concrete Tower Von-Mises Stress (Static Structural).

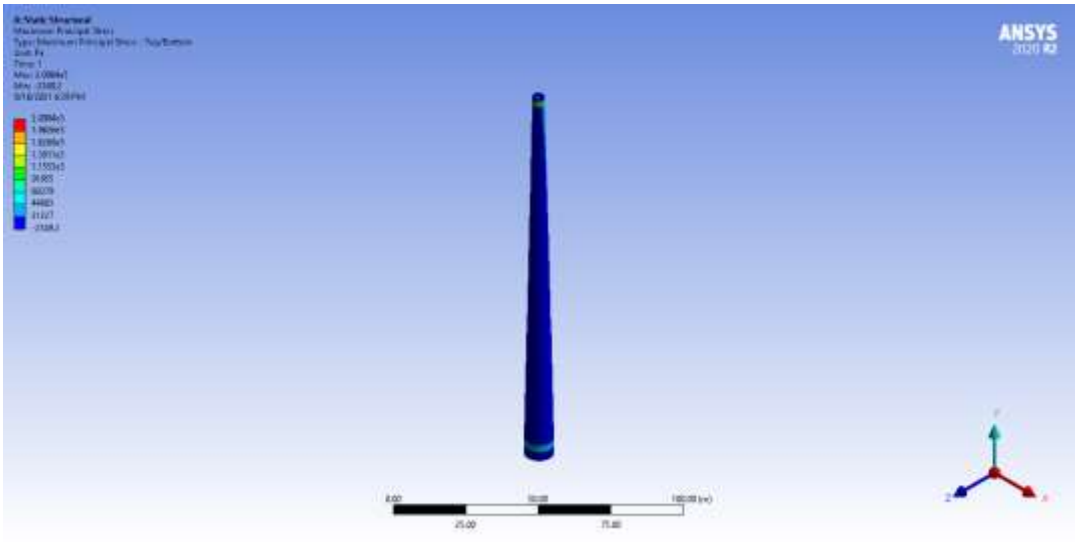

Figure Appendix A-1.51. 150m P-delta Concrete Tower Maximum Principal Stress (Static Structural).

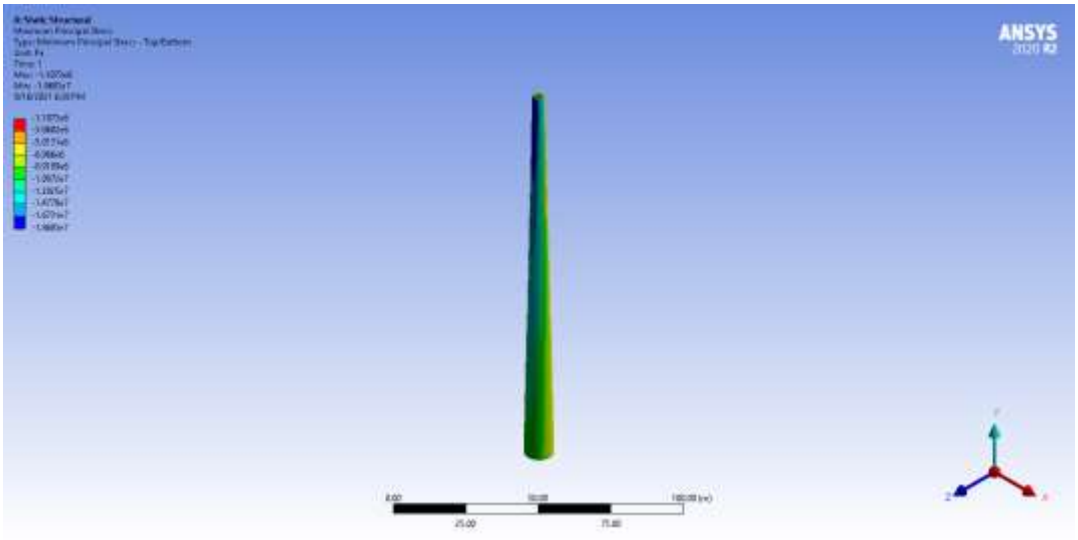

Figure Appendix A-1.52. 150m P-delta Concrete Tower Minimum Principal Stress (Static Structural).

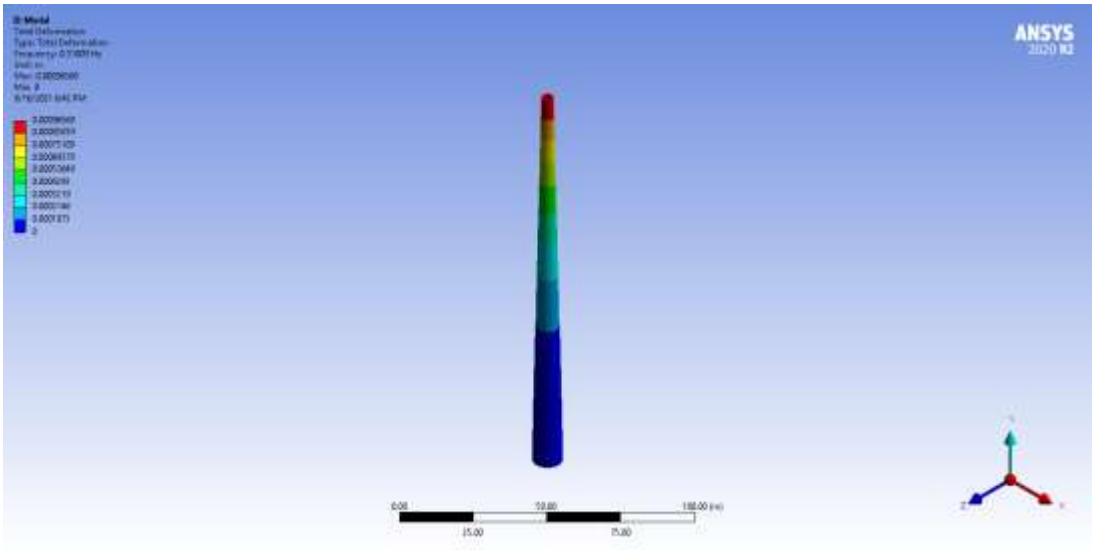

Figure Appendix A-1.53. 150m P-delta Concrete Tower Natural Frequency (Modal Analysis).

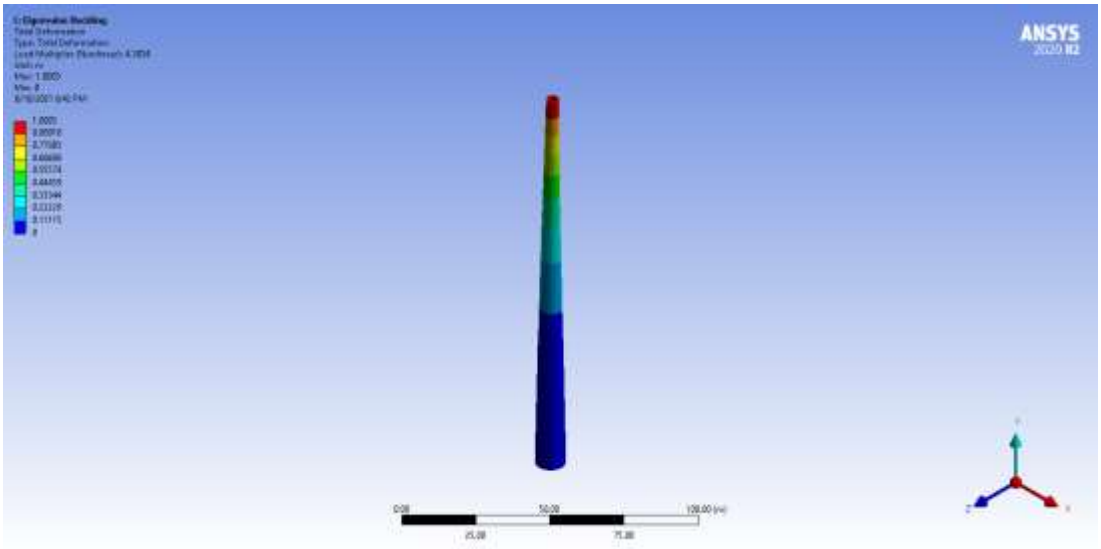

Figure Appendix A-1.54. 150m P-delta Concrete Tower Load Multiplier (Eigenvalue Buckling Analysis).

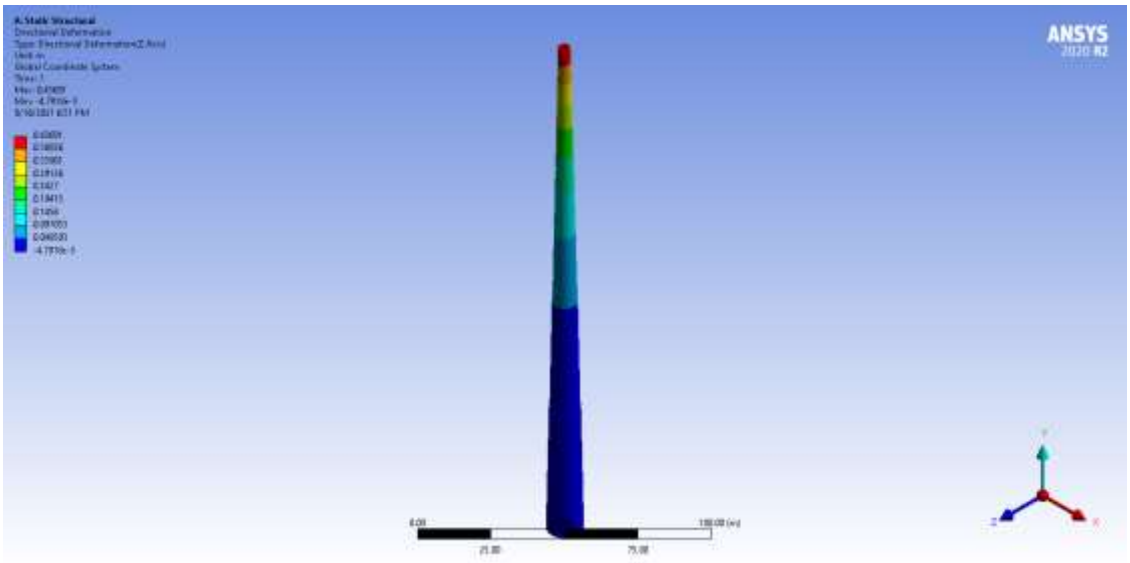

Figure Appendix A-1.55. 200m P-delta Concrete Tower Directional Deformation (Static Structural).

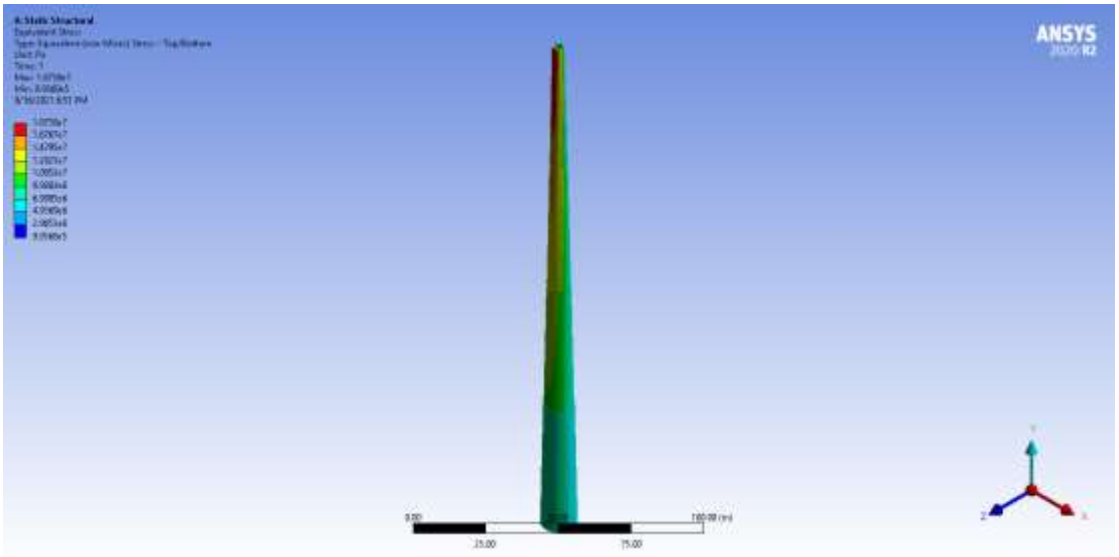

Figure Appendix A-1.56. 200m P-delta Concrete Tower Von-Mises Stress (Static Structural).

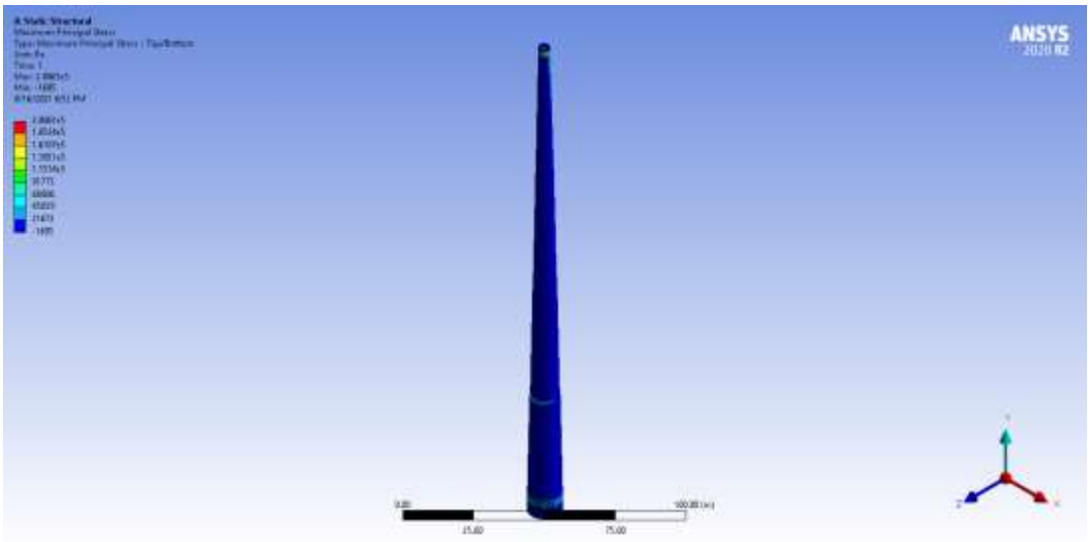

Figure Appendix A-1.57. 200m P-delta Concrete Tower Maximum Principal Stress (Static Structural).

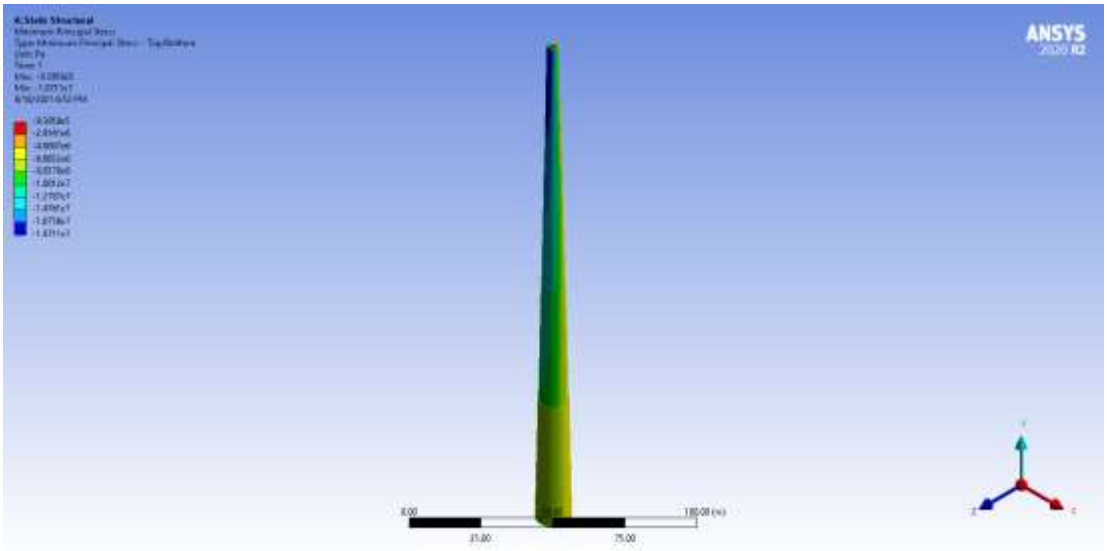

Figure Appendix A-1.58. 200m P-delta Concrete Tower Minimum Principal Stress (Static Structural).

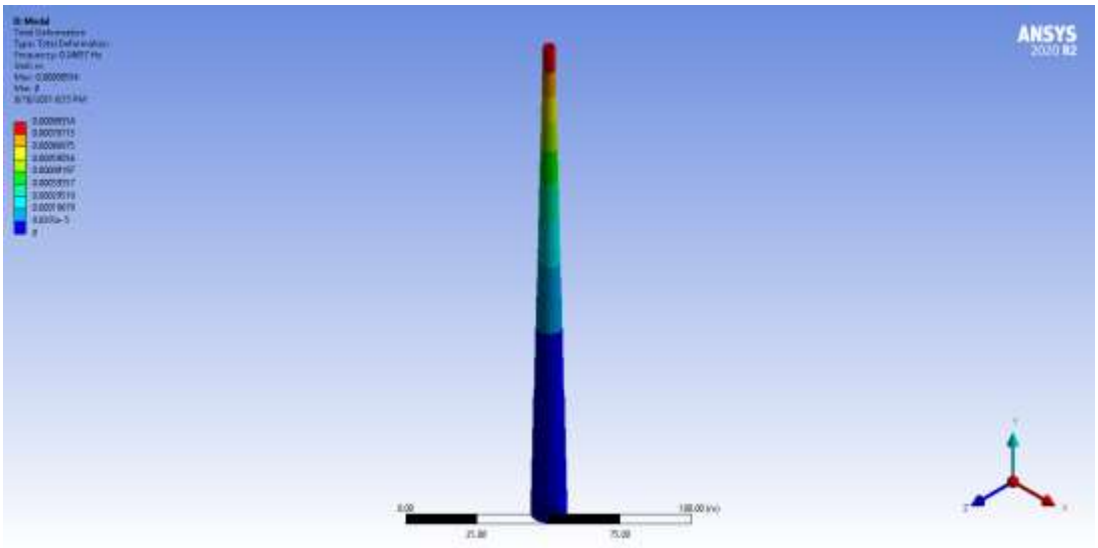

Figure Appendix A-1.59. 200m P-delta Concrete Tower Natural Frequency (Modal Analysis).

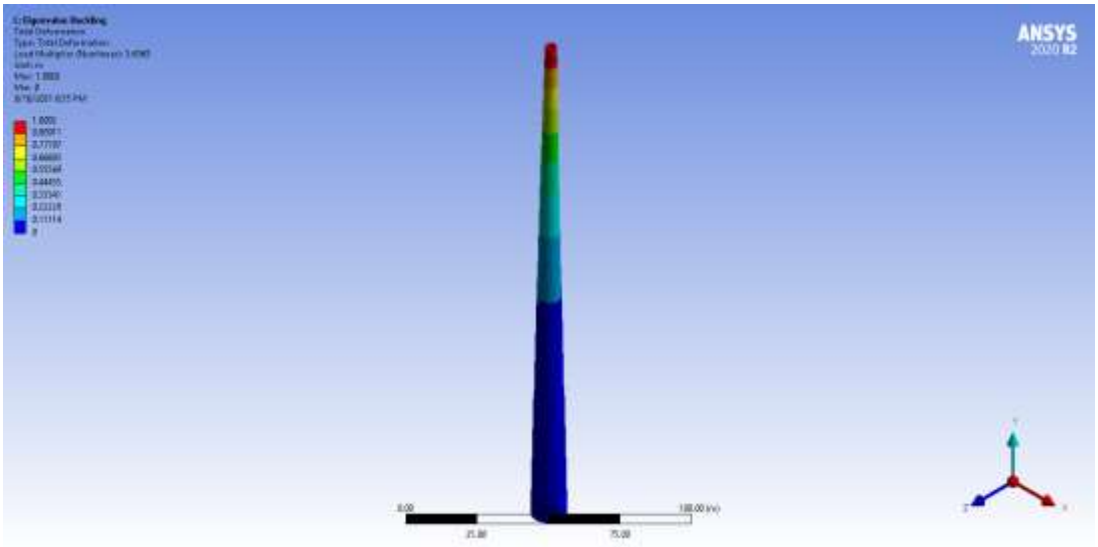

Figure Appendix A-1.60. 200m P-delta Concrete Tower Load Multiplier (Eigenvalue Buckling Analysis).